MECHANICAL PROPERTIES OF

FIBROUS COMPOSITES

Annual Report
July 30, 1963
Contract NASw 470
GE Requisition 214-F59

Prepared for:
National Aeronautics and Space Administration
Washington, D. C.

Prepared by:
B. Walter Rosen, Norris F. Dow and Zvi Hashin*
Space Sciences Laboratory
Missle and Space Division
General Electric Company
Philadelphia, Pennsylvania

*Towne School of Engineering
University of Pennsylvania

ABSTRACT

Relationships between the properties of fibrous composites and the properties of their constituents are evaluated. Bounds and expressions for the effective elastic moduli of materials reinforced by hollow circular fibers are derived by a variational method. Exact results are obtained for hexagonal arrays of identical fibers and approximate results for random arrays of fibers, which may have unequal cross sections. Typical numerical results are obtained for technically important elastic moduli. The tensile strength of composite materials consisting of a ductile matrix uniaxially reinforced by high strength, high stiffness fibers are analyzed. The fibers are treated as having a statistical distribution of imperfections which result in fiber failure under applied stress. The statistical accumulation of such flaws results in failure of the composite. The application of the analysis is demonstrated by using glass fiber strength data in an evaluation of glass fiber reinforced composites. Supporting experimental studies are described. These include measurements of strength and stiffness of particle reinforced matrix materials and the development of an experimental procedure for tensile testing of thin fibrous composites containing only a single layer of fibers. Microscopic observation of the latter specimens indicated random fiber fractures at loads significantly below the ultimate composite strength level.

TABLE OF CONTENTS

I. INTRODUCTION

The studies described in this report are directed toward the attainment of advanced composite structural materials for aerospace vehicle applications. The approach is through the enhancement of understanding of the mechanics of deformation and failure of composites, and of the influence thereon of the properties of, and interactions between, the constituents.

The current availability and development of a variety of high strength and high stiffness fibers and the rapidly growing technology of filament winding have motivated the initial studies in the area of fiber reinforced composites. The initial tasks of evaluating effective elastic constants and ultimate tensile strength of such materials are treated herein. These problems have been studied previously, to a certain extent, and the relationship of the previous work to the present studies are described in the appropriate locations in the text.

The elastic constants are treated using the variational principals of elasticity to establish bounds or approximate expressions for the five elastic constants of a uniaxially reinforced fibrous composite. These results indicate the relative effects of changes in matrix and fiber characteristics and have motivated experimental studies of the effect of particulate additives to the matrix and of changing the cross-sectional shape of the fiber. The control of material density and the effect of biaxial stiffening are also considered and the elastic constants for biaxially oriented voids in place of fibers is studied. The results of

these studies are presented in section II.

The tensile strength of a fibrous composite is treated with a statistical failure model, which is applicable to brittle fibers. The analytical results are applied to glass-plastic composites to determine the direction of desired improvement in matrix characteristics. An experimental program was undertaken to qualify the analysis. The test specimens contained a single layer of glass fibers which enabled microscopic evaluation, by transmitted light, of the internal failure process. The results of the tensile strength program are described in section III.

Once the basic relations between the composite and constituent properties are established, it becomes necessary to determine the relative importance of the various properties. Thus, a structural efficiency study which considers generalized structures and load environments must be performed. As examples of this approach, the stability of a flat plate, containing oriented voids, under in plane compressive loads is treated. As a second problem of this type the shear stresses associated with the biaxial stiffening present in laminates are studied. Studies of this type utilizing the previously described analyses can provide guidelines for the development of improved composites. These structural application studies are described in section IV.

II. ELASTIC CONSTANTS

One of the initial requirements for the definition of composite material characteristics is for the effective elastic constants of the material. In the case of a uniaxial fiber array, the material may be treated as a transversely isotropic medium characterized by five elastic constants. The evaluation of these constants for both solid and hollow fibers is presented in section A. With these constants available, the elastic behavior of laminates of uniaxially stiffened layers can be studied in a straight forward fashion. Elastic constants for plates with biaxially oriented voids are described in section B. The experimental studies motivated by the results of these analyses are described in section C.

A. FIBER REINFORCED MATERIALS

1. Introduction

In continuing search for lightweight materials of great strength and stiffness, considerable effort has been made in recent years in the technological development of fiber reinforced materials. Such materials consist of a relatively soft binder in which much stiffer fibers are embedded. The present work is concerned with the theoretical study of the elastic properties of such materials containing circular hollow or solid fibers which are all oriented in one direction. It is here assumed that the binder and fiber materials are linearly elastic, isotropic, and homogeneous. Because of fiber orientation the reinforced material is anisotropic.

Two cases are here considered. In the first, the fibers are of identical cross section and form an hexagonal array in the transverse plane, and in the second the fibers may have different diameters, but with same ratio of inner to outer diameter and are randomly located in the transverse plane. In both cases the composite is macroscopically homogeneous and transversely isotropic (these concepts will be discussed below) and has five elastic moduli. The problem then is to find expressions for the effective elastic moduli of the reinforced materials in terms of the elastic moduli and the geometric parameters of its constituents.

The problem of the prediction of elastic moduli of macroscopically isotropic composites has recently been treated by bounding techniques, using variational principles of the theory of elasticity. Methods suitable

for arbitrary phase geometry have been given by Paul [1] and Hashin and Shtrikman [2, 3] and for specified (spherical inclusions) phase geometry by Hashin [4]. Methods for arbitrary phase geometry, although in principle applicable, are of little value for the present problem since they cannot distinguish between the present specified geometry and an arbitrary mixture of binder, fiber material and voids, possessing the same elastic symmetry as the fiber reinforced material. Because of the void phase these methods would give zero lower bounds for the effective elastic moduli. In the present paper a variational bounding method closely related to the one employed in [4] is used. The analysis is based on the principles of minimum potential and minimum complementary energy and makes use of the present specific geometry.

There has been little previous theoretical work in the present specific subject. It has been assumed by Dietz [5] and others that the Young's modulus in fiber direction can be evaluated by the "law of mixtures". The effect of discontinuous fibers upon this longitudinal modulus has been studied in an approximate fashion by Outwater [6] and Rosen, Ketler & Hashin [7]. A problem related to the present one has been treated by Hill and Crossley [8] who investigated the elastic behavior of an elastic material containing long fibers, of identical square cross sections, arranged in a square array. The anisotropic composite has in this case six elastic moduli. Rigorously valid bounds for five of these were derived by variational methods, using piecewise constant admissible fields.

The five elastic moduli of the reinforced material here considered are rigorously bounded (except for the insignificant error involved in fulfilment of fiber end conditions in the St. Venant sense) for the case of identical fibers arranged in an hexagonal array. For random fiber arrangement a geometric approximation is involved. The bounding method in this case yields coincident bounds, and thus approximate expressions, for four of the moduli and non-coincident bounds for a remaining modulus. First, the general method of applying variational principles is described and then the method is applied to each of the moduli. Typical numerical results are presented for several of the more commonly used moduli. Required solutions to certain boundary value problems for composite circular cylinders are presented. The analyses of the transverse plane strain bulk and shear moduli originally appeared in [7]. They are repeated here for clarity and completeness.

2. General Method

The general definition of effective elastic moduli of heterogeneous materials has been discussed in [8] and [9]. For the purpose of self consistency a short discussion, specific to the problem here treated, will now be given.

In fiber reinforced materials the ratio of length to fiber diameter is usually very large. Accordingly, fiber end conditions will only be considered here in the St. Venant sense. Consequently it is sufficient to consider a very large cylindrical specimen of reinforced material, with fibers in the generator direction extending from base to base.

(In reality the fibers terminate at random heights.) The specimen is referred to a cartesian coordinate system $x_1x_2x_3$ whose x_1 axis points in the fiber direction while x_2x_3 are in the transverse plane.

Let the specimen be subjected to one of the boundary conditions

$$u^o_i(S) = \epsilon^o_{ij} x_j \tag{2.1}$$

$$T^o_i(S) = \sigma^o_{ij} n_j \tag{2.2}$$

over its entire bounding surface S. Here u^o_i and T^o_i are displacement and stress vector components respectively, x_j are surface coordinates and n_j the components of the outward normal to S. The range of subscripts is 1, 2, 3 and a repeated subscript indicates summation.

For boundary condition (2.1) it can be shown that the average strains over the specimen are ϵ^o_{ij} and for (2.2) that the average stresses are σ^o_{ij}. The specimen is assumed to be <u>macroscopically homogeneous</u> by which is meant that for either one of boundary conditions (2.1) or (2.2) strain <u>and</u> stress averages taken over large enough subregions of the specimen are the same for any such subregion. Such a subregion will be referred to as a <u>representative volume element</u> (RVE) and will here be chosen as a cylinder whose generators are in x_1 direction and its bases parts of the specimen bases. For an hexagonal array the RVE is an hexagonal prism, surrounding one central fiber. Apart from a narrow specimen boundary layer, stress and strain average invariance in a RVE is then exactly fulfilled. For random placement of fibers the RVE is taken as a cylinder in x_1 direction, con-

taining many fibers and stress and strain average invariance are fulfilled in the limit with increasing transverse section size of RVE.

The effective Hooke's law for the composite is defined as

$$\bar{\sigma}_{ij} = C^*_{ijkl} \bar{\epsilon}_{kl} \qquad (2.3)$$

where the overbar denotes average over RVE, which by hypothesis is also the average over the whole specimen. The C^*_{ijkl} are effective elastic moduli whose number is determined by elastic symmetry. When (2.1) is prescribed the average strains are ϵ^o_{ij} and $\bar{\sigma}_{ij}$ have to be found. Conversely when (2.2) is prescribed the average stresses are known and the average strains are sought.

The definition of effective elastic moduli by (2.3) is physically plausible; it is, however, not very useful because, in order to find averages, a field solution has first to be found, which in general is a hopelessly complex task. An equivalent and more fruitful approach is to define the effective elastic moduli in terms of strain energy and to bound the strain energy for simple applied average stress or strain fields, thus also bounding the $C^*_{ijk;}$. It can be shown that when either (2.1) or (2.2) are prescribed the strain energy W stored in a RVE is given by:

$$W = \frac{1}{2} \bar{\sigma}_{ij} \bar{\epsilon}_{ij} \quad (+)$$

Thus, when (2.1) is prescribed, (2.3) is equivalent to

(+) For discussion related to such energy formulae see for example, Bishop and Hill [10].

$$W^{\epsilon} = \frac{1}{2} C^{*}_{ijkl} \epsilon^{o}_{ij} \epsilon^{o}_{kl} \tag{2.4}$$

and when (2.2) is prescribed, to

$$W^{\sigma} = \frac{1}{2} S^{*}_{ijkl} \sigma^{o}_{ij} \sigma^{o}_{kl} \tag{2.5}$$

where S^{*}_{ijkl} are the effective elastic compliances associated with C^{*}_{ijkl}. Strictly speaking the equivalence of moduli defined by strain energy or by average stress and average strain, for random geometry, holds rigorously only for averages taken over the whole specimen, with (2.1) or (2.2) prescribed. For a large RVE the equivalence is approached in the limit, for a statistically homogeneous material. For the hexagonal array the equivalence is rigorous for the RVE used in that case.

The general elastic features of the material here treated will now be discussed. For the hexagonal fiber array the reinforced material has hexagonal symmetry and is thus also transversely isotropic (compare, e.g. Love [11] p. 160). For random fiber arrangement, transverse isotropy is assumed. The stress-strain relation (2.3) for a transversely isotropic material may be written in terms of five elastic module in the form

$$\bar{\sigma}_{11} = C^{*}_{11} \bar{\epsilon}_{11} + C^{*}_{12} \bar{\epsilon}_{22} + C^{*}_{12} \bar{\epsilon}_{33} \tag{2.6}$$

$$\bar{\sigma}_{22} = C^{*}_{12} \bar{\epsilon}_{11} + C^{*}_{22} \bar{\epsilon}_{22} + C^{*}_{23} \bar{\epsilon}_{33} \tag{2.7}$$

$$\bar{\sigma}_{33} = C^{*}_{12} \bar{\epsilon}_{11} + C^{*}_{23} \bar{\epsilon}_{22} + C^{*}_{22} \bar{\epsilon}_{33} \tag{2.8}$$

$$\bar{\sigma}_{12} = 2C^{*}_{44} \bar{\epsilon}_{12} \tag{2.9}$$

$$\bar{\sigma}_{13} = 2C^*_{44}\,\bar{\epsilon}_{13} \tag{2.10}$$

$$\bar{\sigma}_{23} = (C^*_{22} - C^*_{23})\,\bar{\epsilon}_{23} \tag{2.11}$$

where the usual six by six matrix notation has been used for the elastic moduli.

It is possible to select five independent moduli which are combinations of the above elastic moduli, such that for specified states of stress and strain only one of these moduli will appear in the strain energy function. Thus, the bounds on strain energy can be used directly to yield bounds on the elastic moduli. The moduli so chosen are:

$$K^*_{23} = \frac{1}{2}(C^*_{22} + C^*_{23}) \tag{2.12}$$

$$G^*_{23} = \frac{1}{2}(C^*_{22} - C^*_{23}) \tag{2.13}$$

$$G^*_{12} = G^*_{13} = G^*_{1} = C^*_{44} \tag{2.14}$$

$$E^*_{1} = C^*_{11} - \frac{2C^{*2}_{12}}{C^*_{22} + C^*_{23}} \tag{2.15}$$

and C^*_{11}. Here K^*_{23} and G^*_{23} are a bulk and shear modulus, respectively, governing plane strain deformation in the x_2x_3 plane; G^*_1 is a shear modulus governing shear in any plane normal to the transverse x_2x_3 plane; E^*_1 is the longitudinal Young's modulus and C^*_{11} is associated with axial stress or strain in x_1 direction, while lateral deformation is prevented by a rigid enclosure. From these five elastic

moduli any desired elastic constant can be obtained. Important derived constants are:

$$\nu^*_{21} = \nu^*_{31} = \nu^*_1 = \frac{1}{2}\sqrt{\frac{C^*_{11} - E^*_1}{K^*_{23}}} \tag{2.16}$$

$$E^*_2 = E^*_3 = \frac{4G^*_{23}K^*_{23}}{K^*_{23} + \psi G^*_{23}} \tag{2.17}$$

$$\nu^*_{23} = \frac{K^*_{23} - \psi G^*_{23}}{K^*_{23} + \psi G^*_{23}} \tag{2.18}$$

where

$$\psi = 1 + \frac{4K^*_{23}\nu^{*2}_1}{E^*_1}$$

Here ν^*_1 is the Poisson's ratio for unaxial stress in x_1 direction, $E^*_2 = E^*_3$ is the transverse Young's modulus in the x_2x_3 plane and ν^*_{23} - the transverse Poisson's ratio in the same plane.

The variational bounding method used for the hexagonal array will now be outlined. Let all fibers be surrounded by the largest possible non overlapping equal circular cylindrical surfaces. The radii r_b of these cylinders are defined by the geometry of the array (Fig. 1_a). Let the volumes enclosed within these cylindrical surfaces be denoted by V_1 and the remaining volume by V_2. The cylinder consisting of a fiber of radius r_f and a concentric binder shell of outer radius r_b will in the following be referred to as composite cylinder

(Fig. 2). Assume that the specimen cylindrical surface is wholly in V_2 (it is immaterial whether this condition is really fulfilled as the RVE is a very small fraction of the specimen). For a particular state of strain, defining any one of the elastic moduli given above, the associated linear displacement (2.1) is applied throughout V_2 and thus also to the boundaries of the composite cylinders. If now the boundary value problem for the composite cylinder with (2.1) prescribed on its surface is solved, the ensuing displacement fields in all composite cylinders which form V_1 and the field (2.1) in V_2 are an admissible displacement field for the principle of minimum potential energy for the whole composite(+). Let the "strain energy" for this field be denoted by $\tilde{U}^{\epsilon}$ and the actual strain energy whose density is given by (2.4), by U^{ϵ}. It follows from minimum potential energy that

$$U^{\epsilon} \leq \tilde{U}^{\epsilon} \tag{2.19}$$

and an upper bound for the effective elastic modulus under consideration is thus obtained. To obtain a lower bound an appropriate homogeneous stress field, which gives stress vectors of form (2.2) is applied throughout V_2. Then (2.2) acts on the boundaries of the composite cylinders. If the stress boundary value problem is solved, the ensuing stresses in

(+) The specimen boundary displacement (2.1) is transformed to the local coordinate systems of the composite cylinders by addition of rigid body translations which do not contribute to the strain energy.

V_1 and the homogeneous stresses in V_2 now form an admissible stress field for the principle of minimum complementary energy. The "stress energy" $\tilde{U}^{\sigma}$ is now calculated while the actual stress energy U^{σ} is given by (2.5) multiplied by the composite volume. It follows from minimum complementary energy that

$$U^{\sigma} \leq \tilde{U}^{\sigma} \tag{2.20}$$

which provides an upper bound on an effective compliance and thus a lower bound on an effective elastic modulus.

For random arrangement of fibers the bounding method has to be modified. The fiber diameters may be different but their r_o/r_f ratio is the same. The reinforced specimen is here subdivided into composite cylinders extending from lower to upper specimen base, filling its space completely (Fig. 1_b). Each composite cylinder contains one and only one fiber and the volume ratio of fiber to binder is the same in all composite cylinders. In this case either (2.1) or (2.2) is applied to all the surfaces of the composite cylinders, and the displacement or stress fields in their interiors form the admissible fields. Since the cross sections of the composite cylinders are of irregular shape the interior fields can not be found in general. In the present work the outer cylindrical surfaces are approximated by circular cylinders, concentric with the fibers, so that binder volume is preserved. Thus, the composite cylinder solution needed for the hexagonal array becomes immediately applicable in the random case. In fact the results for the latter case are immediately obtained from the former for vanishing V_2.

3. The Plane Strain Bulk Modulus K_{23}^*

The strain system associated with (2.1) is chosen here as the plane strain system

$$\epsilon^o_{22} = \epsilon^o_{33} = \epsilon^o \tag{3.1}$$

while all other strain components vanish, whence (2.1) assumes the form

$$u^o_1 = 0 \; ; \quad u^o_2 = \epsilon^o x_2 \; ; \quad u^o_3 = \epsilon^o x_3 \tag{3.2}$$

From (3.1), (2.6-11) and (2.12), the strain energy density (2.4) simplifies to

$$W = 2K^*_{23} \epsilon^{o\,2} \tag{3.3}$$

Consider first the hexagonal array. The displacement field (3.2) is applied throughout V_2 and thus also to the boundary of the composite cylinders. For any such cylinder, in cylindrical coordinates (Fig. 2)

$$u^o_1 = u^o_z = 0 \; ; \quad u^o_r = \epsilon^o r \; ; \quad u^o_\theta = 0 \qquad (r=r_b) \tag{3.4}$$

The displacement boundary value problem for the composite cylinder thus reduces to an elementary axially symmetric plane strain problem. The general solution for adial displacement u_r and radial stress σ_{rr} for such a problem may be written in the form

$$u_r = Ar + \frac{B}{r} \tag{3.5}$$

$$\sigma_{rr} = 2\bar{K}A - 2G\frac{B}{r^2} \tag{3.6}$$

(compare e.g. Love [11]). Here $\overline{K}$ is the plane strain bulk modulus given by

$$\overline{K} = \lambda + G$$

where λ is a Lamé modulus and G the shear modulus. A and B are arbitrary constants. Two different solutions of type (3.5), (3.6) hold for fiber region $r_o \leq r \leq r_f$ and binder region $r_f \leq r \leq r_b$, respectively, with the appropriate elastic moduli. In the following quantities defined for fiber region will be given subscripts or superscripts f and for binder region, subscripts or superscripts b. There are altogether four arbitrary constants for which four boundary conditions are available. One of these is the second of (3.4), and three additional ones are provided by u_r and σ_{rr} continuity at the interface $r = r_f$ and the vanishing of σ_{rr} at the void surface $r = r_o$. For the present purpose only the radial stress at $r = r_b$ is needed which is easily found to be

$$\sigma_{rr}^{b}(r_b) = 2\epsilon^{o}\ \overline{K}_b n_k \tag{3.7}$$

where

$$m_k = \frac{\phi(1-\alpha^2)(1+2\nu_b\beta^2) + (1+\frac{\alpha^2}{2\nu_f})(1-\beta^2)2\nu_b}{\phi(1-\alpha^2)(1-\beta^2) + (1+\frac{\alpha^2}{2\nu_f})(\beta^2+2\nu_b)} \tag{3.8}$$

Here

$$\alpha = \frac{r_o}{r_f}\ ; \qquad \beta = \frac{r_f}{r_b} \tag{3.9}$$

$$\phi = \frac{\bar{K}_f}{\bar{K}_b} \tag{3.10}$$

and ν_f and ν_b are the Poisson's ratios of fiber and binder materials, respectively.

The strain energy stored in a composite cylinder is given in the present case by

$$U_c^{\epsilon} = \frac{1}{2} \sigma_{rr}^b(r_b) \; u_r^b(r_b) \; 2\pi r_b l \tag{3.11}$$

where l is the length of the cylinder. Introducing u_r from (3.4) and σ_{rr}^b given by (3.7) into (3.11) one obtains

$$U_c^{\epsilon} = 2\bar{K}_b m_k \epsilon^{o^2} V_c \tag{3.12}$$

where

$$V_c = \pi r_b^2 l \tag{3.13}$$

is the gross volume of the composite cylinder. The "strain energy" $\tilde{U}^{\epsilon}$ stored in the entire composite is now given by

$$\tilde{U}^{\epsilon} = 2\bar{K}_b m_k \epsilon^{o^2} V_1 + 2\bar{K}_b \epsilon^{o^2} V_2 \tag{3.14}$$

where V_1 is the sum of the gross volumes of all composite cylinders and V_2 the remaining volume. From (3.3) the actual strain energy is

$$U^{\epsilon} = 2K^*_{23} \epsilon^{o^2} V \tag{3.15}$$

where $V = V_1 + V_2$ is the total volume. Substituting (3.14) and (3.15) into inequality (2.19) the following upper bound $K^{*(+)}_{23}$ is obtained for K^*_{23}

$$K^{*(+)}_{23(h)} = \bar{K}_b(m_k v_1 + v_2) \tag{3.16}$$

where $_1$ and $_2$ are the fractional volumes of V_1 and V_2 relative to V and the subscript (h) denotes hexagonal array. From the geometry of the hexagonal array

$$v_1 = \frac{\pi}{2\sqrt{3}} \cong 0.907 \tag{3.17}$$

$$v_2 = 1 - v_1 \tag{3.18}$$

For lower bound construction the stress system associated with (2.2) is chosen as

$$\sigma^o_{22} = \sigma^o_{33} = \sigma^o \tag{3.19}$$

A stress σ^o_{11} is needed to prevent ϵ_{11}. Its actual magnitude is immaterial for the present analysis since it does no work. The remaining stress components vanish. The stress system (3.27) is applied throughout V_2, whence on the composite cylinders a constant radial stress σ^o is produced. Composite cylinder analysis can now be carried out by the same method as before. Bound construction follows by calculation of the "stress energy" $\tilde{U}^\sigma$ associated with the present admissible stress system and use of inequality (2.20). From (3.19), (2.6-11) and (2.12), the true energy density now has the form

$$W^\sigma = \frac{\sigma^{o^2}}{2K^*_{23}} \tag{3.20}$$

The lower bound is found to be

$$K^{*(-)}_{23(h)} = \frac{\overline{K}_b}{\frac{v_1}{m_k} + v_2} \tag{3.21}$$

where m_k, v_1 and v_2 are given by (3.8), (3.17) and (3.18) respectively. If the fractional volume of the composite taken up by gross fiber volume (including voids) is denoted by v_t then by an elementary calculation β^2 in (3.8) is given by

$$\beta^2 = \frac{v_t}{v_1} \tag{3.22}$$

and thus from (3.17) β^2 is here given by $1.103\, v_t$.

For the case of random fiber arrangement the general procedure has been described above. It is not difficult to realize that the procedure of bound construction is entirely the same as for the hexagonal array except that V_2 now disappears. Consequently the bounds are obtained by setting v_2 equal to zero and v_1 equal to unity in (3.16) and (3.21), whence these bounds coincide.

Accordingly

$$K^{*}_{23(r)} = \overline{K}_b m_k \tag{3.23}$$

where the subscript (r) denotes random array. In the present case, however

$$\beta^2 = v_t \tag{3.24}$$

so (3.23) can be rewritten in the form

$$K^*_{23(r)} = \overline{K}_b \frac{\phi(1-\alpha^2)(1+2\nu_b v_t) + (1+\frac{\alpha^2}{2\nu_f})\,2\nu_b v_b}{\phi(1-\alpha^2)v_b + (1+\frac{\alpha^2}{2\nu_f})(v_t + 2\nu_b)} \tag{3.25}$$

where

$$v_b = 1 - v_t \tag{3.26}$$

is the fractional volume of binder material.

While the bounds (3.16) and (3.21) are exact results, the expression (3.25) is in general approximate. There exists, however, a very special case when (3.25) becomes exact in the limit. Consider a cylindrical specimen of reinforced material which consists of circular composite cylinders of varying sizes, of total volume V_1, and remaining binder volume V_2. In all composite cylinders the ratios $r_o : r_f : r_b$ are the same. The volume V_2 can be filled out progressively by such composite cylinders of smaller and smaller cross sections. Bound expressions for this case are exactly the same as for the hexagonal array. Since v_2 in (3.16) and (3.21) can thus be made as small as desired by the filling process, the bounds will in the limit converge to (3.25). On the basis of this rather artificial case it is to be expected that (3.25) will be a better approximation for fibers of varying cross sections, than for equal fibers. The present discussion also applies to subsequent results for elastic moduli of the random array.

Results for solid fibers are easily obtained by setting $\alpha = 0$ in all of the preceding results.

4. The Shear Modulus G^*_{23}

For upper bound construction the displacements (2.1) are chosen as

$$u_1^o = 0 \; ; \; u_2^o = \frac{1}{2} \gamma^o x_3 \; ; \; u_3^o = \frac{1}{2} \gamma^o x_2 \tag{4.1}$$

and are thus associated with a pure shear strain

$$\epsilon^o_{23} = \epsilon^o_{32} = \frac{1}{2} \gamma^o \tag{4.2}$$

and all other strain components vanish.

For lower bound construction the stress vectors (2.2) are chosen as

$$T^o_1 = 0 \; ; \; T^o_2 = \tau^o n_3 \; ; \; T^o_3 = \tau^o n_2 \tag{4.3}$$

The stress vectors (4.2) are equivalent to a pure shear of magnitude τ^o in the transverse plane. The bounding method is the same as for K^*_{23}. For (4.1) prescribed the macroscopic strain energy density (2.4) is easily found to be

$$W^\epsilon = \frac{1}{2} G^*_{23} \gamma^{o\,2} \tag{4.4}$$

while for (4.3) prescribed (2.5) reduces to

$$W^\sigma = \frac{\tau^{o\,2}}{2G^*_{23}} \tag{4.5}$$

For upper bound derivation (4.1) is applied throughout V_2 and for lower bound derivation (4.3) is used. Composite cylinder analysis in the present case is however much more complicated. Solutions for

the boundary conditions here applied have been carried out by the method of plane harmonics. The method is outlined in section 8 and the results are given by the following expressions. For random fiber arrangement, on the basis of the previously used approximation

$$G_{23\,(r)}^{(+)} = G_b \left[1 - \frac{2(1-\nu_b)}{1-2\nu_b} v_t \bar{A}_4^{\epsilon}\right] \tag{4.6}$$

$$G_{23(r)}^{(-)} = G_b \Big/ \left[1 + \frac{2(1-\nu_b)}{1-2\nu_b} v_t \bar{A}_4^{\sigma}\right] \tag{4.7}$$

where $\bar{A}_4^{\epsilon}$ and $\bar{A}_4^{\sigma}$ have to be found from the systems of linear equations (10-17) and (19-20), (12-17) respectively, given in section 8. The bounds (4.6-7) do not in general coincide.

For the hexagonal array the bounds are given by

$$G_{23(h)}^{(+)} = G_b \left[1 - \frac{2(1-\nu_b)}{1-2\nu_b} v_t \bar{A}_4^{'\epsilon}\right] \tag{4.8}$$

$$G_{23(h)}^{(-)} = G_b \Big/ \left[1 + \frac{2(1-\nu_b)}{1-2\nu_b} v_t \bar{A}_4^{'\sigma}\right] \tag{4.9}$$

where $\bar{A}_4^{'\epsilon}$ and $\bar{A}_4^{'\sigma}$ are given by the same systems of equations with v_t replaced by $\frac{v_t}{v_1}$ (compare (3.22)).

The necessary modifications for the case of solid fibers are stated in section 8.

5. The Shear Modulus G^*_1

The strain system associated with (2.1) is chosen as a pure shear in x_1x_2 directions

$$\epsilon^o_{12} = \epsilon^o_{21} = \frac{1}{2}\gamma^o \tag{5.1}$$

with all other strains vanish. With addition of a rigid body rotation displacements (2.1) can then be written in the form

$$u_1^o = 0 \; ; \quad u_2^o = \gamma^o x_1 \; ; \quad u_3^o = 0 \tag{5.2}$$

Using (5.1), (2.6-11) and (2.14), the strain energy density (2.4) assumes the form

$$W^{\epsilon} = \frac{1}{2} G^*_1 \gamma^{o^2} \tag{5.3}$$

The stresses associated with (2.2) are chosen analogously as a pure shear in x_1x_2 directions:

$$\sigma^c_{12} = \sigma^o_{21} = \tau^o \tag{5.4}$$

and the remaining stress components vanish. The stress energy density (2.5) then assumes the form

$$W^{\sigma} = \frac{\tau^{o^2}}{2G^*_1} \tag{5.5}$$

For upper bound construction, for the hexagonal array, (5.2) is applied throughout V_2 and thus to the composite cylinder surfaces. In cylindrical coordinates referred to composite cylinder axis, (5.2) transform to the following displacement boundary conditions

$$u_r^b = \gamma^o z \cos\theta \; ; \quad u_\theta^b = -\gamma^o z \sin\theta \; ; \quad u_z^b = 0 \qquad (r=r_b) \qquad (5.6)$$

For lower bound construction (5.6) is applied throughout V_2, whence on the surfaces of the composite cylinders the following stress boundary conditions are obtained in cylindrical coordinates

$$\sigma_{rr}^b = 0 \; ; \quad \sigma_{r\theta}^b = 0 \; ; \quad \sigma_{rz}^b = \tau^o \cos\theta \qquad (r=r_b) \qquad (5.7)$$

The other boundary conditions to be satisfied in both cases are displacement and stress continuity at fiber-binder interface $r=r_f$ and vanishing of stresses at void surface $r=r_o$. To the authors' knowledge a solution to the boundary value problems described above is not to be found in the literature. A closed form solution has been here derived. The method is outlined in section 9. Here only those quantities required for strain energy calculation will be given. For displacement boundary conditions (5.6) the boundary stresses at $r=r_b$ are:

$$\sigma_{rr}^b = 0 \; ; \quad \sigma_{r\theta}^b = 0 \; ; \quad \sigma_{rz}^b = G_b m_G \gamma^o \cos\theta \qquad (5.8)$$

where

$$m_G = \frac{\eta(1-\alpha^2)(1+\beta^2) + (1+\alpha^2)(1-\beta^2)}{\eta(1-\alpha^2)(1-\beta^2) + (1+\alpha^2)(1+\beta^2)} \qquad (5.9)$$

Here

$$\eta = \frac{G_f}{G_b} \qquad (5.10)$$

and α and β are given by (3.9). The strain energy stored in a composite cylinder is calculable in terms of (5.6) and (5.8) and is given by

$$U_{c.} = \frac{1}{2} G_b m_G \gamma^{o^2} V_c \tag{5.11}$$

where V_c is given by (3.13). For stress boundary conditions (5.7) the surface displacements at $r = r_b$ are found to be:

$$u_r^b = \frac{\tau^o}{G_b m_G} z \cos\theta; \quad u^b = -\frac{\tau^o}{G_b m_G} z \sin\theta; \quad u_z^b = 0 \tag{5.12}$$

The strain energy stored in a composite cylinder is then given by

$$U_c = \frac{\tau_o^2}{2G_b m_G} V_c \tag{5.13}$$

All the information necessary for bound construction is now available and the method is exactly the one employed above. For the hexagonal array the results are

$$G^{*(+)}_{1(h)} = G_b(m_G v_1 + v_2) \tag{5.14}$$

$$G^{*(-)}_{1(h)} = \frac{G_b}{\frac{v_1}{m_G} + v_2} \tag{5.15}$$

where v_1 and v_2 are given by (3.17) and (3.18), respectively and β^2 in (5.9) is given by (3.22). For the random array, on the basis of the previously used approximation, the bounds coincide and are both given by

$$G^*_{1(r)} = G_b \frac{\eta(1-\alpha^2)(1+v_t) + (1+\alpha^2)\, v_b}{\eta(1-\alpha^2)\, v_b + (1+\alpha^2)(1+v_t)} \tag{5.16}$$

where again v_t is the fractional volume of gross fiber volume and v_b the fractional volume of binder material given by (3.26). For solid fibers, $\alpha = 0$ in (5.9) and (5.14-16).

6. Longitudinal Young's Modulus E_1^* and Poisson's Ratio ν_1^*

The cylindrical specimen is subjected to uniaxial strain in fiber direction. Accordingly the strain system associated with (2.1) is chosen as:

$$\epsilon^o_{11} = \epsilon^o \; ; \; \epsilon_{22}{}^o = \epsilon_{33}{}^o = -\mu\epsilon^o \tag{6.1}$$

$$\epsilon_{12}{}^o = \epsilon_{23}{}^o = \epsilon_{31}{}^o = 0$$

The displacements (2.1) are then given by

$$u^o_1 = \epsilon^o x_1 \; ; \; u^o_2 = -\mu\epsilon^o x_2 \; ; \; u^o_3 = -\mu\epsilon^o x_3 \tag{6.2}$$

The lateral surface of the specimen is not loaded, thus on this boundary

$$T_2{}^o = T_3{}^o = 0 \tag{6.3}$$

The constant μ in (6.1) and (6.2) is dependent on (6.3) and will be evaluated below. The macroscopic strain energy density (2.4) reduces here to

$$W = \frac{1}{2} E_1^* \epsilon^{o2} \tag{6.4}$$

where E_1^* is given by (2.15).

Consider first the case of the random array. The displacements (6.2) are applied to the boundaries of the composite cylinders. The boundary conditions of the axially symmetric composite cylinder problem are then given in cylindrical coordinates by

$$u_r^b = -\mu\epsilon^o r \quad (r=r_b) \quad ; \quad u_z^b = \epsilon^o z \quad (z=0,1) \tag{6.5}$$

A suitable general displacement solution is

$$u_r = A_r + \frac{B}{r} \tag{6.6}$$

$$u_z = \epsilon^o z \tag{6.7}$$

Here (6.6) has different constants in fiber and binder regions and (6.7) is the same throughout both regions. There are thus four constants A_f, B_f, A_b and B_b to be determined. The four necessary boundary conditions are the first of (6.5), u_r and σ_{rr} continuity at $r=r_f$ and vanishing of σ_{rr} at $r=r_o$. Furthermore μ is evaluated by making σ_{rr}^b vanish at $r=r_b$. For the present purpose only the average axial stress $\bar{\sigma}_{zz}$ is needed, which is found to be:

$$\bar{\sigma}_{zz} = m_E E_b \epsilon^o \tag{6.8}$$

where

$$m_E = (V_f \frac{E_f}{E_b} + v_b) \frac{E_b(D_1 - D_3F_1) + E_f(D_2 - D_4F_2)}{E_b(D_1 - D_3) + E_f(D_2 - D_4)} \tag{6.9}$$

Here

$$D_1 = \frac{1+\alpha^2}{1-\alpha^2} - \nu_f \qquad D_2 = \frac{1+v_t}{v_b} + \nu_b$$

$$D_3 = \frac{2\nu_f^2}{1-\alpha^2} \qquad \dot{D}_4 = 2\nu_b^2 \frac{v_t}{v_b}$$

$$F_1 = \frac{\nu_b v_f E_f + \nu_f v_b E_b}{\nu_f v_f E_f + v_b E_b} \tag{6.10}$$

$$F_2 = \frac{\nu_f}{\nu_b} F_1$$

and v_t is the fractional volume of gross fibers, v_b is given by (3.26) and $v_f = (1-\alpha^2) v_t$ is the fractional volume of net fiber material (α is defined by (3.9)).

Since σ_{rr} was made to vanish at $r = r_b$ the strain energy stored in the composite cylinder is simply

$$U_c^{\epsilon} = \frac{1}{2} m_E E_b \epsilon^{o2} V_c \tag{6.11}$$

where (6.8) has been used. The displacement fields in all composite cylinders are now an admissible field. Using (2.19) as previously with (6.11) and (6.4) adjusted to the whole specimen volume, $m_E E_b$ is obtained as an upper bound for E^*_1.

For lower bound construction the specimen is subjected to

$$\sigma^o_{11} = \sigma^o \tag{6.12}$$

on it's faces and (6.3) on the lateral surface. The macroscopic stress energy density (2.5) is now

$$W^{\sigma} = \frac{\sigma^{o2}}{2E^*_1} \tag{6.13}$$

The composite cylinder boundary conditions are now

$$\sigma_{zz} = \underset{(z=0,1)}{\sigma^{o}} \quad ; \quad \underset{(r=r_b)}{\sigma^{b}_{rr}} = 0 \tag{6.14}$$

Because of St. Venant's principle, at sufficient distance from the fiber ends the solution is the same as the previous one with

$$\epsilon^{o} = \frac{\sigma^{o}}{m_E E_b} \tag{6.15}$$

Using (6.15) in (6.11) the stress energy stored in the composite cylinder becomes

$$U_c^{\sigma} = \frac{\sigma^{o2}}{2m_E E_b} V_c$$

The energy discrepancy due to the St. Venant approximation is insignificant because of the very large length to diameter ratio of the composite cylinder. The stresses in all composite cylinders are now admissible. Using (6.13) and (6.16) adjusted to specimen volume in (2.20), $m_E E_b$ also becomes a lower bound for E^*_1. Thus to the order of approximation of the random fiber array model

$$E^*_{1(r)} = m_E E_b \tag{6.17}$$

Unfortunately (6.17) is a very unwieldy expression. However, inspection of (6.9) shows that the fraction on the right side is different from unity only because $F_1 \neq F_2$ (see last eq. (6.10). For most practical purposes the fraction seems to be close to unity and it can thust be concluded that the "law of mixtures"

$$E^*_1 = v_f E_f + v_b B_b \tag{6.17a}$$

is a good approximation to (6.17). For $\nu_f = \nu_b$ (6.17a) is exactly equal to (6.17). In fact for equal Poisson's ratios (6.17a) is an exact result for any macroscopically homogeneous fiber array regardless of transverse section geometry.

It is evident from the first three strains in (6.1) that μ is the Poisson's ratio ν^*_1. Since for the random array the bounds coincided the value of μ determined to make σ_{rr} vanish on the composite cylinder boundary gives ν^*_1 to the order of approximation of (6.17). The result is

$$\nu^*_1(r) = \frac{v_f E_f L_1 + v_b E_b L_2 \nu_b}{v_f E_f L_3 + v_b E_b L_2} \tag{6.18}$$

where

$$\begin{aligned} L_1 &= 2\nu_f (1 - \nu^2_b)\, v_t + \nu_b (1 + \nu_b) v_b \\ L_2 &= v_t [(1 + \nu_f)\alpha^2 + 1 - \nu_f - 2\nu^2_f] \\ L_3 &= 2(1 - \nu^2_b) v_t + (1 + \nu_b) v_b \end{aligned} \tag{6.19}$$

and the rest of the notation is identical to the one used in (6.9-10). Note that for $\nu_b = \nu_f$, (6.18) is also equal to $\nu_b = \nu_f$, regardless of the values of the phase Young's moduli.

For hexagonal arrays it can be shown by the same method as previously used that the upper and lower bounds for E^*_1 are given by

$$E^{*(+)}_{1(h)} = E_b(m'_E v_1 + p v_2) \tag{6.20}$$

$$E^{*(-)}_{1(h)} = \frac{E_b}{\frac{v_1}{m'_E} + v_2} \tag{6.21}$$

Here

$$p = \frac{1 - \nu_b - 2\nu'^{*2}_{1(r)}}{1 - \nu_b - 2\nu_b^2} \tag{6.22}$$

and v_1, v_2 are given by (3.17-18). The prime on m_E and $\nu^*_{1(r)}$ in (6.20-22) indicates that these quantities have to be computed by replacement of v_t and v_f by $\frac{v_t}{v_1}$ and $\frac{v_f}{v_1}$, respectively, and of v_b by $1 - \frac{v_t}{v_1}$. For $\nu_f = \nu_b$ the upper bound (6.20) reduces to (6.17a) and is an exact result for E_1^* of the hexagonal array. It is believed that for any Poisson's ratios E_1^* is considerably closer to the upper bound than to the lower one.

For the Poisson's ratio ν_1^* of the hexagonal array the situation is more complicated and bounds cannot be directly obtained. For this case ν_1^* can be bounded by use of bounds on K^*_{23}, E^*_1 and C^*_{11}, using (2.16). Bounds for C^*_{11} will be given below. Because of this indirect bounding procedure the bounds on ν^*_1 are further apart then the bounds obtained by direct methods and they may be of little practical value.

7. The Modulus C^*_{11}

The modulus C^*_{11} can be treated by assigning to the specimen a uniform macroscopic stress or strain in x_1 direction and preventing lateral deformation in the x_2x_3 plane by a rigid enclosure. For $\bar{\epsilon}_{11} = \epsilon^o$ the energy density (2.4) reduces in this case to

$$W^{\epsilon} = \frac{1}{2} C^*_{11} \epsilon^{o2} \tag{7.1}$$

while for $\bar{\sigma}_{11} = \sigma_o$ the energy density (2.5) reduces to

$$W^{\sigma} = \frac{\sigma^{o2}}{2C^*_{11}} \tag{7.2}$$

The bounding procedure is completely analogous to the one used for E^*_1. For the random array C^*_{11} can be immediately written down in the form

$$C^*_{11(r)} = E^*_{1(r)} + 4\nu^{*2}_{1(r)} K^*_{23(r)} \tag{7.3}$$

which follows directly from (2.16). Here $E^*_{1(r)}$ is given by (6.9) and (6.17), $\nu^*_{1(r)}$ by (6.20) and $K^*_{23(r)}$ by (3.25).

For the hexagonal array the bounds are given by

$$C^{*(+)}_{11(h)} = C'^*_{11(r)} v_1 + \frac{E_b(1-\nu_b)}{(1+\nu_b)(1-2\nu_b)} v_2 \tag{7.4}$$

$$C^{*(-)}_{11(h)} = \frac{1}{\frac{v_1}{C'^*_{11(r)}} + \frac{qv_2}{E_b}} \tag{7.5}$$

Here v_1 and v_2 are given by (3.17-18), q is given by the expression

$$q = 1 - 4\nu_b n + 2(1 - \nu_b)n^2$$

where

$$n = \frac{2\nu'^*_{1(r)} K'^*_{23(r)}}{C'^*_{11(r)}} \tag{7.6}$$

The primes on the elastic constants in (7.4-6) mean that they are computed from (3.25), (6.9) and (6.18) with modified v_t, v_f, α^2 and v_b as listed after (6.22).

8. Shear of Composite Cylinder in x_2x_3 Plane

A convenient form of solution is in terms of plane harmonics (compare Love [11], p. 270. Goodier [12]). Plane harmonics are homogeneous polynomials which satisfy the two dimensional Laplace equation. For the present purpose only the following plane harmonics are needed:

$$\phi_2 = x_2x_3 \tag{8.1}$$

$$\phi_{-2} = \frac{x_2x_3}{r^4} \tag{8.2}$$

The displacement vector is given in terms of these by

$$u = A_1u^1 + \frac{A_2}{r_f^2}u^2 + A_3r_f^4u^3 + A_4r^2u^4 \tag{8.3}$$

where

$$u^1 = \nabla\phi_2 \tag{8.4}$$

$$u^2 = r^2 \nabla\phi_2 + \alpha_2 \phi_2 r \tag{8.5}$$

$$u^3 = \nabla\phi_{-2} \tag{8.6}$$

$$u^4 = r^2 \nabla\phi_{-2} + \alpha_{-2} \phi_{-2} r \tag{8.7}$$

where ∇ is the gradient operator and A_1, A_2, A_3, A_4 are arbitrary nondimensional constants. The parameters α_2 and α_{-2} are defined by

$$\alpha_2 = -\frac{2(3-4\nu)}{3-2\nu} \tag{8.8}$$

$$\alpha_{-2} = \frac{2(3-4\nu)}{1-2\nu} \tag{8.9}$$

where ν is the Poisson's ratio. From the displacements, strains can be calculated by differentiation. The stresses are then found by Hooke's law and stress vectors from $T_i = \sigma_{ij} n_j$. The n_i are here the components of a unit normal to a circular cylindrical surface and are given by $n_i = \frac{x_i}{r}$, $i = 2, 3$. There are two such displacement solutions, one for binder region $r_o \leq r \leq r_f$ and the other for fiber region $r_f \leq r \leq r_b$. In each of these the appropriate elastic constants of the material have to be used. There are thus eight arbitrary constants to be determined, four of these for binder region are denoted by A_k and the remaining four for fiber region by B_k; $k=1, 2, 3, 4$. In addition to the boundary conditions on $r=r_b$, given by (4.1) or (4.3) stress vector and displace-

ment continuity at fiber-binder interface $r = r_f$ and vanishing of stress-vectors at void surface $r = r_o$, must be satisfied. These boundary conditions provide exactly eight linear equations for the eight unknowns.

For boundary conditions (4.1) these equations are:

$$\bar{A}_1^{\epsilon} + v_t^{-1}\bar{A}_2^{\epsilon} + v_t^2\bar{A}_3^{\epsilon} + v_t\bar{A}_4^{\epsilon} = 1 \tag{8.10}$$

$$-\frac{3-4\nu_b}{3-2\nu_b}v_t^{-1}\bar{A}_2^{\epsilon} - 2v_t^2\bar{A}_3^{\epsilon} + \frac{v_t}{1-2\nu_b}\bar{A}_4^{\epsilon} = 0 \tag{8.11}$$

$$\bar{A}_1^{\epsilon} + \bar{A}_2^{\epsilon} + \bar{A}_3^{\epsilon} + \bar{A}_4^{\epsilon} - \bar{B}_1^{\epsilon} - \bar{B}_2^{\epsilon} - \bar{B}_3^{\epsilon} - \bar{B}_4^{\epsilon} = 0 \tag{8.12}$$

$$-\frac{3-4\nu_b}{3-2\nu_b}\bar{A}_2^{\epsilon} - 2\bar{A}_3^{\epsilon} + \frac{1}{1-2\nu_b}\bar{A}_4^{\epsilon} + \frac{3-4\nu_f}{3-2\nu_f}\bar{B}_3^{\epsilon} + 2\bar{B}_3^{\epsilon} - \frac{1}{1-2\nu_f}\bar{B}_4^{\epsilon} = 0 \tag{8.13}$$

$$\bar{A}_1^{\epsilon} + \frac{3}{3-2\nu_b}\bar{A}_2^{\epsilon} - 3\bar{A}_3^{\epsilon} + \frac{1}{1-2\nu_b}\bar{A}_4^{\epsilon} - \eta\bar{B}_1^{\epsilon} - \frac{3\eta}{3-2\nu_f}\bar{B}_2^{\epsilon} + 3\eta\bar{B}_3^{\epsilon} - \frac{\eta}{1-2\nu_f}\bar{B}_4^{\epsilon} = 0 \tag{8.14}$$

$$-\frac{1}{3-2\nu_b}\bar{A}_2^{\epsilon} + 2\bar{A}_3^{\epsilon} - \frac{1}{1-2\nu_b}\bar{A}_4^{\epsilon} + \frac{\eta}{3-2\nu_f}\bar{B}_2^{\epsilon} - 2\eta\bar{B}_3^{\epsilon} + \frac{\eta}{1-2\nu_f}\bar{B}_4^{\epsilon} = 0 \tag{8.15}$$

$$\bar{B}_1^{\epsilon} + \frac{3\alpha^2}{3-2\nu_f}\bar{B}_2^{\epsilon} - 3\alpha^{-4}\bar{B}_3^{\epsilon} + \frac{\alpha^{-2}}{1-2\nu_f}\bar{B}_4^{\epsilon} = 0 \tag{8.16}$$

$$-\frac{\alpha^2}{3-2\nu_f}\bar{B}_2^{\epsilon} + 2\alpha^{-4}\bar{B}_3^{\epsilon} - \frac{\alpha^{-2}}{1-2\nu_f}\bar{B}_4^{\epsilon} = 0 \tag{8.17}$$

where $\bar{A}_k^{\epsilon}, \bar{B}_k^{\epsilon} = \frac{2}{\gamma_o}A_k^{\epsilon}, \frac{2}{\gamma_o}B_k^{\epsilon}$

and $$n = \frac{G_f}{G_b} \tag{8.18}$$

α is given by the first (3.9) and the superscript ϵ denotes displacement boundary value problem.

For boundary conditions (4.3) the solution is analogous. Equs. (8.10) and (8.11) have to be replaced by

$$\bar{A}^{\sigma}_1 + \frac{3}{3-2\nu_b} v_t^{-1} \bar{A}^{\sigma}_2 - 3v_t^2 \bar{A}^{\sigma}_3 + \frac{v_t}{1-2\nu_b} \bar{A}^{\sigma}_4 = 1 \qquad (8.19)$$

$$-\frac{1}{3-2\nu_b} v_t^{-1} \bar{A}^{\sigma}_2 + 2v_t^2 \bar{A}^{\sigma}_3 - \frac{v_t}{1-2\nu_b} \bar{A}^{\sigma}_4 = 0 \qquad (8.20)$$

Here $\bar{A}^{\sigma}_k$, $\bar{B}^{\sigma}_k = \frac{2G_b}{\tau^o} A^{\sigma}_k$, $\frac{2G_b}{\tau^o} B^{\sigma}_k$ and equs. (8.12-17) remain the same. The constants now have thesu perscripts σ to denote stress boundary value problem.

The composite cylinder strain energy can in each case be calculated from the boundary displacements and stress vectors. In each case the strain energy is expressible in terms of the constant $\bar{A}_4$ only. The bounds (4.6-9) then follow immediately.

For solid fibers the solutions have to be modified. In this case the solution for the fiber region has no singular part at r = 0. Accordingly the constants $\bar{B}_3$ and $\bar{B}_4$ vanish and eqs. (8.16) and (8.17) have to be deleted. The expressions for the bounds remain unchanged.

9. Shear of Composite Cylinder in x_1x_2 Plane

The boundary value problems formulated in section 5 can be solved in terms of displacement fields for which the volume dilation vanishes. In this case the cartesian equations of elasticity reduce to

$$\nabla^2 u_i = 0 \tag{9.1}$$

where i = 1, 2, 3 and ∇^2 is the three dimensional Laplacian. For the present purpose the following simple displacement solution in cylindrical coordinates is sufficient

$$u_1 = u_z = (Ar + \frac{B}{r}) \cos \theta \tag{9.2}$$

$$u_r = C\, z \cos \theta \tag{9.3}$$

$$u_\theta = -C\, z \sin \theta \tag{9.4}$$

where A, B and C are arbitrary constants. The stresses associated with these solutions are

$$\sigma_{rz} = G(A + C - \frac{B}{r^2}) \cos \theta \tag{9.5}$$

$$\sigma_{\theta z} = -G(A + C + \frac{B}{r^2}) \sin \theta \tag{9.6}$$

$$\sigma_{rr} = \sigma_{\theta\theta} = \sigma_{zz} = \sigma_{r\theta} = \theta \tag{9.7}$$

There are two such solutions, one for binder and one for fiber region. The boundary conditions to be satisfied are either (5.6) or (5.8) on $r = r_b$, displacement and stress continuity at $r = r_f$ and zero stresses on $r = r_o$. All boundary conditions can be satisfied and the unknown constants are uniquely determined. On the terminal sections of the cylinder, conditions are only satisfied in the St. Venant sense. Since the cylinder is very long this is of consequence. For (5.6) prescribed the surface stresses are given by (5.8) where the first two of (5.8) follow from (9.7). For (5.7) prescribed the surface displacements are given by (5.12). Note that the last of (5.12) is a consequence of the elimination of a rigid body rotation of the composite cylinder.

10. Numerical Results

The nature of the results is indicated by the curves of figs. 3-7 in which the effective elastic constants of glass fiber reinforced plastics are plotted as a function of v_t, the gross directional volume of fibers. Results are presented for $\alpha = 0$, solid fibers, and for $\alpha = 0.8$, hollow fibers for which the inner radius is 80% of the outer radius. The computations are all for random arrays, except for the case of the shear modulus G^*_1, where the hexagonal bounds are also presented. It can be seen from fig. 3, that although the fibers are relatively ineffective in the transverse direction as compared to the longitudinal direction, the modulus, E^*_2, is still significantly higher than the modulus of the binder material for practical fiber volume fractions. The variation of ν^*_{23} shown in fig. 4 indicates that for solid fibers the effective Poisson ratio is larger than that of either constituent. For hollow fibers, values significantly lower than that of either constituent are indicated. As shown in fig. 5 the hexagonal array bounds contain the random array bounds which here coincide. The variations of E^*_1 with v_t, shown in fig. 6, are practically linear and are given with good accuracy by the "law of mixtures" (6.17a). Also the longitudinal Poissons ratio, ν^*_1, appears to be well approximated by the "law of mixture" result.

A second parametric study indicates the interaction of fiber geometry and properties upon composite properties. Fig. 8 shows the transverse elastic modulus for hollow fiber composites, of fixed binder volume fraction, as a fraction of the fiber radius ratio, α. The bounds

are shown for two values of Poisson's ratio of the fiber material. It is seen that this parameter is of importance for large fiber radius ratio values. A similar comparison is made in fig. 9 for the transverse effective Poisson's ratio, ν_{23}^{*}. This quantity is extremely sensitive to both geometry and individual Poisson ratio values.

An interesting sidelight is the result for equal fiber and binder properties; that is a material with holes. Transverse properties for such a material are shown in figs. 10 and 11.

For a given geometry the effect of mechanical properties is studied by fixing the matrix properties and varying the Young's modulus of the fiber. The results for three principal moduli are shown in figs. 12-14. As expected, the longitudinal modulus, E_1, increases linearly with the fiber modulus. The longitudinal shear modulus and the transverse Young's modulus increase rapidly for low values of fiber modulus and then level off and approach the value for rigid inclusions. At high values of fiber modulus a change in the binder modulus has a far more significant effect upon G_1^{*} and E_2^{*} than a change in fiber modulus. This is shown more clearly in fig. 15 where the reference properties for glass reinforced plastic are perturbed and the effect on E_2^{*} is indicated.

It would be of great importance to compare the present theoretical results with experimental findings. To the author's knowledge published experimental results are available only for E_1^{*}. These agree generally very well with the law of mixtures.

11. Conclusions

Results for the elastic moduli of fiber reinforced material have been here derived for hexagonal fiber arrays of equal cross sections and for random arrays of fibers whose diameters may be unequal. It is not obvious which of the results apply best to a real fiber reinforced material. While for hexagonal arrays the results are rigorous (except for the insignificant effect of non exact fulfillment of fiber end conditions), no real material satisfies such stringent symmetry conditions. On the other hand the random array analysis, which is based on a model which is much closer to reality, is not rigorous because of the geometric approximation of irregular shapes by circles. The special case when these results become exact in the limit (see discussion at end of section 3) seems to be of theoretical interest only.

However, the random array results are much to be preferred because of their much simpler form and the coincidence of the bounds, except for $G^*_{23(r)}$. It should be noted that the distance between the hexagonal array bounds can become quite appreciable for elevated ratios of fiber to binder elastic moduli. The advantage of the random array results is even more predominant when it becomes necessary to derive results for the other effective elastic moduli (such as (2.16-18) in terms of the expressions here given. For such cases the hexagonal array bounds may become very far apart and thus of little value. The case of ν^*_1 discussed in section 6 is a good example.

Finally, it should be inquired whether the present models of a fiber reinforced material include sufficient information for unique determination of it's effective elastic moduli. The hexagonal array is certainly uniquely determinate in this respect because of its periodic geometry. However, for a random array it is to be expected that the statistical details (correlation functions) of fiber arrangement will enter into the results. The present method avoids this problem by use of the geometrical approximation involved in the random array model, and thus gives one approximate answer for different statistical arrangements of fibers.

B. ORIENTED VOID MATERIALS

1. Introduction

The study of oriented voids serves a double purpose. The first is to determine whether by the judicious removal of material the effective density may be reduced with little or no reduction in mechanical properties. The second is to provide a more general insight into the importance of angular orientation on load-carrying ability.

The study made here was a fairly exhaustive one; as will become apparent, to absorb all the implications of the results requires tedious study. In the following discussion every effort will accordingly be made to extract only the significant implications, but the curves calculated to yield the results will be presented in toto.

2. Analytical Model and Method of Analysis

The model used for analysis is sketched in figure 16. Starting with a regular array of round holes (fig. 16a), we extracted the repeating cross-section (fig. 16b) and then allowed the semi-circular grooves on opposite sides to be skewed at equal angles as shown in figure 16c. Thus the model becomes similar to a plate having integral, waffle-like stiffening such that the rib height is equal to the fillet radius between ribs and plates. Accordingly, the analysis of reference 13 was employed to find the plate stiffnesses.

In the analysis of stretching stiffnesses in reference 13, two undefined constants are employed which are associated with the transverse effectiveness of the integral ribbing. These constants, labelled β and β',

denote the fraction of the rib material active in resisting stretching and shearing deformations respectively. For true waffle plates, β' has been evaluated (ref. 14). For the oriented voids considered here, the fact that the tops of all "ribs" are joined integrally with those of the next repeating element requires that a somewhat high value of β' be used then that of reference 14 to take into account the mutual restraints provided by these interconnected ribs. No attempt has been made here to evaluate this higher value of β', and no better evaluation of β has been attempted than that suggested in reference 13. Really the exact evaluation of β and β' in unimportant to the general trends desired by the present study. Rather, it is of greater interest to allow β and β' to vary over their extreme limits and determine the resulting effects on the material stiffnesses. This variation has therefore been made, and also some calculations for β and β' equal to the values derived from reference 14 as approximately representative of realistic stiffnesses have been included for comparison.

3. Ranges of Proportions Considered

Calculations were made of stiffnesses for five series of configurations of oriented voids in order to survey systematically the effects produced by various characteristic changes. These five series of calculations comprised the following:

(1) Determination of the principal stretching stiffness, E_1, for various angles of orientation, θ, of the holes. Values of β and β' between zero and full effectiveness were considered.

(2) Evaluation of the importance of transverse shearing effectiveness (as measured by β') for all angles θ of the holes, and for all directions of stretching relative to the principal stiffness direction.

(3) Evaluation of importance of both transverse stretching and shearing effectiveness for all angles θ and all stiffness directions.

(4) Study of the effects of varying Poisson's ratio for all angles of orientation of the voids and "representative" values of transverse effectiveness.

(5) Study of combined effects of variation in angles, transverse effectiveness, and Poisson's ratio.

Throughout all calculations a hole size and spacing was used such that 40% of the "original" material was "removed" by the holes. The holes were located in square arrays as suggested in figure 1. Sample calculations for greater or lesser void percentage revealed that the magnitude of the variations under investigation were simply proportional to the percentage of voids, so that the 40% values may be considered as representative. The use of rectangular arrays instead of square can be used to increase the stiffness in one direction at the expense of that at right angles thereto. The effect is again simply proportional to the relative amounts of material in the two directions, and it will not be considered further here.

4. Results

The results of the computations are plotted as figures 17 to 21 inclusive. The results are all presented as the ratio of stretching stiffness

to the stretching stiffness in the principal direction of an element having one-way holes aligned in the direction ($\theta = 0^{o}$), and a Poisson's ratio, μ, of 0.3. Each Figure contains the results of one of the five sub-investigations described in the preceding section, and the following summarizations will categorize the results in corresponding sequency.

(1) Angular orientation - Unless the transverse shearing effectiveness (measured by β') is high, the principal stretching stiffness, E_1, falls off rapidly as the angle of the holes (e) is increased from zero degrees. If the material is 100% effective against shearing, however ($\beta' = 1 + \mu$), E_1 increases to a maximum at $\theta = 22.5^{o}$.

(2) Even with 100% transverse shearing effectiveness, a material with oriented voids is still highly anisotropic if the transverse stretching stiffness is low, especially for low angles of θ (i.e. holes mostly in the same direction). Isotropy is improved at $\theta = 30^{o}$ or 45^{o}.

(3) As both β and β' increase, as would be expected, the material as a whole becomes more effective and more nearly isotropic. The The most nearly isotropic material is achieved, at angles θ somewhat less than 45^{o}, but for no angle of the voids or of loading does the material exceed 100% effectiveness (i.e. $\frac{E_\lambda}{E_{1_{max}}} \leq 1.0$).

(4) For a material with oriented voids, Poisson's ratio is a multiplier of anistropy. Abnormally high values of μ produce greater than normal variations of stiffness with changing hole or load angle.

(5) As β, β', and μ are varied from one extreme to another, the resulting stretching stiffness and anisotropies vary over a wide range. The upper limits reached are in all cases determined by the values of Poisson's ratio while the lower limits appear to be primarily a function of the transverse stretching stiffness as measured by β. Whether or not the removal of 40% of the material as holes reduces the stiffness to density ratio by more or less than 40% depends upon all of the variables. If both β and β' are zero, the reduction can not be kept below 40% for all load incidence angles, but it can for angles up to as much as 60° to the principal stiffness direction. For values of β and β' which can perhaps be considered realistic (refer back to fig. 20), 40% of the material can be removed with less than 25% reduction in stiffness/density ratio for all angles of load incidence.

5. Conclusions and Discussion

The first and perhaps most important conclusion that may be drawn from the many parametric variations considered is that the stiffness-to-density ratio of a material can not be increased by drilling holes in it, unless by so doing the Poisson's ratio for the material is increased. Even such a hypothetical increase would be small, and would require a prior knowledge of load application direction and/or high transverse material effectiveness.

On the other hand properly oriented holes can be used to reduce density with little or no loss in stiffness-to-density ratio, particularly if

a limited range of angles of load application is to be accommodated. The fact that a possible increased stiffness-to-density ratio for oriented rods was suggested in ref. 15 must be simply a result of the assumptions employed as a basis for the calculations made therein.

C. EXPERIMENTAL STUDIES

Studies of elliptical fibers and particle-matrix composites are described below.

1. Elliptical Fibers

The evaluation of the transverse modulus, E^*_2, for fibrous composites indicated that, for geometry typical of filament wound structures, the transverse modulus is not negligible relative to the longitudinal modulus. Thus, any improvement in this transverse modulus could reflect itself as a significant improvement in the performance of biaxially stiffened composites. Possible techniques for doing this include improving the matrix modulus as shown in fig. 15 or changing the fiber cross-section to improve one transverse direction.

The possibility of using elliptical filaments instead of round ones is not new, but it has never been adquately investigated. Such questions as: What is the transverse effectiveness of elliptical inclusions of various aspeft ratios? and How long need the ellipse be to permit substantial load transmission into it by shear from the binder? have note been answered. In order to evaluate the first, an experimental approach has been started using large, aluminum inclusions in an epoxy matrix. Photographs of the test specimens are shown in fig. 22. Strain measurements were made with Tuckerman optical gages between interior inclusions as identified in the figure. The effective modulus was defined as the average stress over the cross-section divided by the strain in the indicated gage length. The resulting values are shown in fig. 22. It is seen that ellipses

with an aspect ratio of four provide an 80% increase in transverse stiffness at a fiber volume fraction of less than 50%. The potential for improved performance of fibrous composites utilizing shaped fibers appears to warrant further consideration.

2. Particle Composites

The potential for improving composite performance by adding stiff particles to the matrix material has been studied experimentally for several applications. As discussed previously, an improvement in matrix modulus can provide a substantial improvement in the transverse Young's modulus of a fibrous composite. Also an increase in matrix modulus can result in an improvement in compressive strength due to the improved support stiffness provided for the fibers. Further, the combined variation of stiffness and density may lead to a low density material suitable for large dimension, low load, compression applications. The experimental results for various additives to an epoxy plastic matrix are described below.

Glass particles

Glass particles ranging in characteristic dimension from 10 to 200 microns were used in an epoxy matrix. The compression modulus was measured on a specimen with volume fractions of 0.284 of glass, 0.660 of epoxy and 0.056 of void spaces. The results are given in the following table:

Glass Particle-Epoxy Composite

	Epoxy	Glass-Epoxy
Density (lb/in^3)	0.0462	0.0565
Young's Modulus (10^6 psi) (compression)	0.46	1.04
Modulus/Density Ratio (arbitrary units)	1.0	1.8
$(Modulus)^{1/2}$/Density Ratio (arbitrary units)	1.0	1.0

Alumina particles

The effect of the addition of small solid alumina particles (900 mesh and smaller) upon the modulus of an epoxy was measured. The test specimens are shown in fig. 23. The loaded epoxy contained 40.9% alumina by volume and the results are shown in the following table.

Powdered Alumina-Epoxy Composites

	Epoxy	Alumina-Epoxy
Density (lb/in^3)	0.0464	0.0746
Young's Modulus (10^6 psi) (compression)	0.52	1.32
Modulus/Density Ratio (arbitrary units)	1.0	1.6
$(Modulus)^{1/2}$/Density Ratio (arbitrary units)	1.0	1.6

Hollow alumina particles

The attainment of a relatively stiff but low density material through the introduction of voids was studied by using hollow alumina spheres as a stiffening material in an epoxy matrix. The average specific gravity of the spheres was 0.73 and the samples contained 57% spheres by volume. The sphere diameters were between 0.065 and o.131 in. The specimens are shown in fig. 24 and the test results in the following table:

Hollow Alumina-Epoxy Composites

	Epoxy	Alumina-Epoxy
Density (lb/in^3)	0.0464	0.0341
Young's Modulus (10^6 psi) (compression)	0.55	0.84
Modulus/Density Ratio (arbitrary units)	1.0	2.1
$(Modulus)^{1/2}$/Density Ratio	1.0	1.7

Further studies of these materials under tensile loads are described in section IIIC. From the above results, it can be seen that the addition of alumina and glass particles produced a significant and expected increase in the matrix modulus. It appears that a loaded plastic may be a useful constituent in a fiber glass composite. The question of proper geometry to achieve both suitable mechanical properties and also proper viscosity to permit fabrication remains unanswered.

The low density alumina material offers improved stiffness at reduced density, but has low strength. Failure for the test specimen occurred at 7200 psi.

III. TENSILE STRENGTH

A frequent criterion to be used in the selection of composite materials is the ultimate tensile strength of the material. Section A contains an analysis of the tensile strength of uniaxially reinforced fibrous composites. The validity of the analysis is tested by the experimental program described in section B. The modification of matrix properties to improve composite strength is treated in section C.

A. FIBER REINFORCED MATERIALS

1. Introduction

Composite materials consisting of a ductile matrix reinforced by high-strength, high-stiffness fibers are materials of considerable engineering practicality. The strength of such materials under tensile loads has been studied theoretically with only limited success. An analytical understanding of the failure of such materials is desirable, not only to provide adequate design methods for existing materials, but also to enable the definition of desirable characteristics of constituents of composites for future applications. The problem treated here is the failure of a composite, consisting of a matrix stiffened by uniaxially oriented fibers when subjected to a uniaxial tensile load parallel to the fiber direction.

The failure of a uniaxially stiffened matrix has been studied previously by several investigators. Their findings are summarized in [16]. The simplest failure model treated assumes that a uniform strain exists throughout the composite and that fracture occurs at the failure strain of the fibers alone (e.g. [17]). The effect of a non-uniform strain distribution was studied in [18] which suggests the influence of fiber flaws on composite failure. In [18], failure occurs when the accumulation of fiber fractures resulting from increasing load shortens the fiber lengths to the point that further increases in load could not be transmitted to the fibers because the maximum matrix shear stress was exceeded. Thus, composite failure resulted from a shear failure of the matrix.

In the present paper fibers are treated as having a statistical distribution of flaws or imperfections which result in fiber failure at various stress levels. Composite failure occurs when the remaining unbroken fibers, at the weakest cross-section, are unable to resist the applied load. Thus, composite failure results from tensile fracture of the fibers. The composite strength is evaluated herein as a function of the statistical strength characteristics of the fiber population and of the significant parameters defining composite geometry. A numerical example is presented for fiber-glass reinforced plastic composites utilizing the existing data for tensile strength of glass fibers.

2. Description of The Model

The composite treated is shown in Fig. 25 and consists of parallel fibers in an otherwise homogeneous matrix. The fibers are treated as having a statistical distribution of flaws or imperfections which result in fiber failure under applied stress. The statistical accumulation of such flaws within a composite material results in composite failure. The computation of stress is quite complex when there are discontinuous fibers present. These internal discontinuities result in shear stresses which may locally attain very high values. An exact evaluation of this stress distribution for the complex geometry of circular cross section fibers arrayed within a matrix and for inelastic matrix stress-strain characteristics appears to be unattainable from a practical viewpoint. Such stresses were evaluated in [19] for idealized fiber shape and without the effect of surrounding fibers. An approximate solution, similar to that of [20], but including the effect of surrounding fibers is obtained herein.

In the present model, the extensional stresses in the matrix are neglected relative to those in the fiber and the shear strains in the fiber are neglected relative to those in the matrix. This approximation of the model is considered appropriate for fibers which are very strong and stiff relative to the matrix. In the vicinity of an internal fiber end, in such a composite, (fig. 25) the axial load carried by the fiber is transmitted by shear through the matrix to adjacent fibers. A portion of the fiber at each end is therefore not fully effective in resisting the applied stress. As the fibers are loaded, failure occurs at points of imperfection along the fibers. Increasing load produces an increasing accumulation of fiber fractures until a sufficient number of ineffective fiber lengths combine to produce a weak surface and composite fracture. Basically, then, the model considers fibers which fail as a result of statistically distributed flaws or imperfections, and composites which fail as a result of a statistical accumulation of such flaws over a given region.

At some distance from an internal fiber break the fiber stress will be a given fraction, φ, of the undisturbed fiber stress σ_a. One may define this fraction of the average stress such that the fiber length, δ, over which the stress, σ, is less than σ_a may be considered ineffective. Thus, this ineffective length, δ, is defined:

$$\sigma(\delta) = \varphi\sigma_a$$

Then, the composite may be considered to be composed of a series of layers of dimension, δ. Any fiber which fractures within this layer, in addition to being unable to transmit a load across the layer, will also

not be stressed within that layer to more than the stress, σ_a. The applied load is treated as uniformly distributed among the unbroken fibers in each layer. The segment of a fiber within a layer may be considered as a link in the chain which constitutes the fiber. Each layer is then a bundle of such links; and the composite is a series of such bundles.

The treatment of a fiber as a chain of links is appropriate to the hypothesis that fracture is a result of local imperfections. The links may be considered to have a statistical strength distribution which is equivalent to the statistical flaw distribution along the fibers. The realism of such a model is demonstrated by the length dependence of fiber strength. That is, longer chains have a high probability of having aweaker link than shorter chains and this agrees with experimental data (e.g. [21]) which demonstrate that fiber strength is a monotonically decreasing function of fiber length.

For this model, the link dimension is defined by a shear lag type approximate analysis of the stress distribution in the vicinity of a broken end. The statistical strength distribution of the links is then expressed as a function of the fiber strength-length relationship, which can be experimentally determined. Then these results are used in a statistical study of a series of bundles of links to define the distribution of bundle strengths. (Statistical techniques for a series of bundles have been studied in [22] for application to particle reinforced composites.) The composite fails when any bundle fails and the composite strength is thus determined as a function of fiber and matrix characteristics. These aspects of the problem are discussed in further detail below.

$$f(\sigma) = \frac{g(\sigma)}{n} \left[1 - G(\sigma) \right]^{(1/n)-1} \qquad (6)$$

Consider fibers characterized by a strength distribution of the Weibull type [23]:

$$g(\sigma) = L\, \alpha\, \beta \sigma^{\beta-1} \exp\left(-L\, \alpha \sigma^{\beta}\right) \qquad (7)$$

This form has been shown to characterize the experimental length-strength relationship of fibers. Using equation (7) in (3) and (6) yields:

$$f(\sigma) = \alpha^{\delta}\, \beta \sigma^{\beta-1} \exp\left(-\alpha^{\delta} \sigma^{\beta}\right) \qquad (8)$$

where: $L = n\delta$

The constants α and β can be evaluated by using experimental strength-length data. To do this, consider the mean fiber strength, $\bar{\sigma}_f$ for a given length which, is defined by:

$$\bar{\sigma}_f = \int_c^{\infty} \sigma\, g(\sigma)\, d\sigma \qquad (9)$$

Substituting eq. (7) into (9) and integrating yields:

$$\bar{\sigma}_f = (L\alpha)^{-1/\beta}\, \Gamma\left(1 + \frac{1}{\beta}\right) \qquad (10)$$

A logarithmic plot of the available data for $\bar{\sigma}_f$ as a function of L will define the constants. Such a plot is presented in fig. 26 for the data of [21]. The linearity of the data support the choice of the distribution function given by eq. (7). The constants are found to be:

$$\alpha = 7.74 \times 10^{-2}$$

$$\beta = 7.70$$

The constant β is an inverse measure of the dispersion of material strength. Values of β between two and four correspond to brittle ceramics,

3. Fiber Strength

The statistical distribution of link strength is obtained from the fiber strength distributions. Consider links characterized by the distribution function $f(\sigma)$ and the associated cumulative distribution function $F(\sigma)$ where:

$$F(\sigma) = \int_0^{\sigma} f(\sigma)\, d\sigma \tag{1}$$

For n such links forming a chain which fails when the weakest link fails the distribution function $g(\sigma)$ for the chain is defined by:

$$g(\sigma) = nf(\sigma) \left[1 - F(\sigma) \right]^{n-1} \tag{2}$$

That is, $g(\sigma)\, d\sigma$ is the probability that one link fails between σ and $\sigma + d\sigma$ (which is equal to $f(\sigma)\, d\sigma$), multiplied by the probability that all remaining $(n - 1)$ links exceed $\sigma + d\sigma$ (which is $\left[1 - F(\sigma) \right]^{n-1}$) and failure can occur at any of the n links. From this, the cumulative distribution function, $G(\sigma)$, for the fibers is obtained:

$$G(\sigma) = \int_0^{\sigma} g(\sigma)\, d\sigma \tag{3}$$

$$\therefore\ G(\sigma) = 1 - \left[1 - F(\sigma) \right]^{n} \tag{4}$$

The solution of the inverse problem is desired. That is, given the fiber data, $g(\sigma)$ and $G(\sigma)$, define the link data for a link length, δ. From eq. (4):

$$F(\sigma) = 1 - \left[1 - G(\sigma) \right]^{1/n} \tag{5}$$

and thus from (1) and (5):

while a value of twenty is appropriate for a ductile metal [22]. The constant α, as seen from eq. (10), defines a characteristic stress level, $\alpha^{-1/\beta}$. For this distribution, $\alpha^{-1/\beta}$ is 305 ksi. A more useful reference stress level is mentioned in the discussion section.

4. Effective Fiber Length

The definition of ineffective length, δ, involves the determination of the shear stress distribution along the fiber-matrix interface. The model used is shown in fig. 27 and consists of a fiber surrounded by a matrix which in turn is imbedded within a composite material. The latter has the average or effective properties of the composite under consideration. This configuration is subject to axial stress and a shear lag type analysis is utilized to estimate the stresses.

Load is applied parallel to the fiber direction. The fiber is assumed to carry only extension and the matrix to transmit only shear stresses. No stress is transmitted axially from the fiber end to the average material. Shear stresses in the average material are considered to decay in a negligible distance from the inclusion interface.

For equilibrium of a fiber element in the axial direction:

$$\tau + \frac{r_f}{2} \frac{d\sigma_f}{dz} = 0 \tag{12}$$

where τ = shear stress in matrix material

σ_f = axial stress in fiber

For equilibrium of the composite in the axial direction:

$$\left(\frac{r_f}{r_a}\right)^2 \sigma_f + \left(\frac{r_a^2 - r_b^2}{r_a^2}\right) \sigma_a = \bar{\sigma} \tag{13}$$

where σ_a = axial stress in average material

$\bar{\sigma}$ = applied axial stress

The displacements in the fiber, u_f, and in the average material, u_a, define the binder shear strain, γ, as follows:

$$u_a - u_f = (r_b - r_f)\,\gamma \tag{14}$$

Differentiating eq. (14) twice and using the stress-strain relations yields:

$$\frac{1}{E_a}\frac{d\sigma_a}{dz} - \frac{1}{E_f}\frac{d\sigma_f}{dz} = \frac{r_b - r_f}{G_b}\,\frac{d^2\tau}{dz^2} \tag{15}$$

where E_a = effective Young's modulus of the composite

E_f = Young's modulus of the fiber

G_b = shear modulus of the binder

Differentiating eq. (13) and substituting the result and eq. (12) into eq. (15) yields:

$$\frac{d^2\tau}{dz^2} - \eta^2\tau = 0 \tag{16}$$

where

$$\eta^2 = \frac{2G_b}{E_f\,(r_b - r_f)\,(r_f)}\left[1 + \frac{E_f}{E_a}\left(\frac{r_f^2}{r_a^2 - r_b^2}\right)\right] \tag{17}$$

The solution to eq. (16) is of the form

$$\tau = A \sinh \eta z + B \cosh \eta z \tag{18}$$

The boundary conditions are:

$$\tau(o) = 0$$

$$\sigma_f(\ell) = 0 \tag{19}$$

$$\therefore \quad B = 0$$

$$A = \frac{G_b \bar{\sigma} r_a^2}{\eta E_a (r_b - r_f)(r_a^2 - r_b^2) \cosh \eta \ell}$$

and

$$\tau = \frac{G_b \bar{\sigma} r_a^2 \sinh \eta z}{\eta E_a (r_b - r_f)(r_a^2 - r_b^2) \cosh \eta \ell} \tag{20}$$

From eqs. (12) and (20):

$$\sigma_f = - \frac{\bar{\sigma} r_a^2 E_f}{[E_a (r_a^2 - r_b^2) + E_f r_f^2]} \left(\frac{\cosh \eta z}{\cosh \eta \ell} - 1 \right) \tag{21}$$

Consider $r_a >> r_b$

$$\therefore \quad \eta^2 \approx \frac{2G_2}{a r E_1} \tag{22}$$

and from eq. (21):

$$\sigma_f = - \frac{\bar{\sigma} E_t}{E_a} \left[\frac{\cosh \eta z}{\cosh \eta \ell} - 1 \right] \tag{23}$$

The maximum axial stress is

$$\sigma_f (o) \Big|_{\ell \to \infty} = \frac{\bar{\sigma} E_f}{E_a} \tag{24}$$

Using the results of this elastic analysis, the stress ratio φ is evaluated from the ratio of the stress at a distance δ from the end of a given fiber to the stress at the midpoint of a very long fiber. The stress at a point at distance δ from a fiber end is:

$$\sigma_f (\ell - \delta) = - \frac{\sigma E_f}{E_a} \left[\frac{\cosh \eta (\ell - \delta)}{\cosh \eta \ell} - 1 \right] \qquad (25)$$

The fiber efficiency, φ , at this point is therefore defined by:

$$\varphi = \frac{\sigma_f (\ell - \delta)}{\sigma_f (o)\Big|_{\ell \to \infty}} = 1 - \cosh \eta \delta + \tanh \eta \ell \sinh \eta \delta \qquad (26)$$

for large ℓ :

$$\tanh \eta \ell = 1$$

$$\therefore \varphi = 1 - \cosh \eta \delta + (\cosh^2 \eta \delta - 1)^{1/2} \qquad (27)$$

From which

$$\cosh \eta \delta = \frac{1 + (1 - \varphi)^2}{2 (1 - \varphi)} \qquad (28)$$

and

$$\frac{\delta}{d_f} = \frac{1}{2\sqrt{3}} \left[(V_f^{-1/2} - 1) \frac{E_f}{G_b} \right]^{1/2} \cosh^{-1} \left[\frac{1 + (1 - \varphi)^2}{2 (1 - \varphi)} \right] \qquad (29)$$

For the purposes of this analysis a value of $\varphi = 0.9$ is considered, and δ is evaluated for this stress ratio value. Thus, effective length is that portion of the fiber in which the average axial stress is greater than 90% of the stress which would exist for infinite fibers. Fig. 28 shows the variation of ineffective length with constituent moduli for various fiber concentrations.

The stresses upon which these results are based are shown in fig. 29. It is clear that for many composites the matrix shear stresses will exceed the elastic limit of the material. The point at which the elastic

limit is reached is indicated on each curve of fig. 29 for a matrix shear yield stress of one tenth the fiber strength. Since for high concentrations most of the curves are above the elastic limit, further inelastic analysis is required. Note also that the results of this shear lag model differ in character from those of ref. 20. The difference is attributable to the addition of the third or average material to the model.

The elastic analysis of this section has been extended to include the effects of an elastic plastic binder. To do this, consider a region at the fiber end in which the shear stress is equal to the shear yield stress, τ_y, thus:

$$\sigma_z = \frac{2\tau_y}{r_f}(\ell - z) \qquad \ell - b \le z \le \ell \tag{30}$$

Equation (12) applies for: $0 \le z \le \ell - b$. The analysis for the elastic region is unchanged except that the boundary conditions (19) are replaced by:

$$\begin{aligned} \tau(o) &= 0 \\ \tau(\ell - b) &= \tau_y \end{aligned} \tag{31}$$

Substitution of (31) into (18) yields

$$\tau = \tau_y \frac{\sin \eta z}{\sin \eta(\ell - b)} \tag{32}$$

From eqs. (12), (13) and (32) it can be shown that:

$$\sigma_f = \frac{\bar{\sigma}}{\left(\frac{r_f}{r_a}\right)^2 + \frac{E_a}{E_f}\left[1 - \left(\frac{r_b}{r_a}\right)^2\right]} - \frac{2\tau_y}{\eta r_f} \frac{\cosh \eta \bar{z}}{\sinh \eta(\ell - b)} \tag{33}$$

for $0 \le z \le \ell - b$

The length b is evaluated by assuring continuity of stress at $z = \ell - b$. Thus from eqs. (30) and (33):

$$\frac{2\tau_y b}{r_f} = \frac{\bar{\sigma}}{\left(\frac{r_f}{r_a}\right)^2 + \frac{E_a}{E_f}\left[1 - \left(\frac{r_b}{r_a}\right)^2\right]} - \frac{2\tau_y}{\eta r_f} \coth \eta(\ell - b)$$

For $r_a >> r_b$ this reduces to:

$$b = \frac{\bar{\sigma} E_f r_f}{2\tau_y E_a} - \frac{1}{\eta} \coth \eta(\ell - b)$$

For $b << \ell$:

$$b = \frac{\bar{\sigma} E_f r_f}{2\tau_y E_a} - \frac{1}{\eta} \coth \eta \ell \qquad (34)$$

Now the ineffective length can be evaluated, as defined by eq. (26) by using eq. (33). It will be assumed and subsequently confirmed that: $\delta > b$. Large values of fiber length relative to all other fiber dimensions will be assumed. The result is:

$$\cosh \eta \delta = \frac{1 + \lambda^2}{2\lambda} \qquad (38)$$

where

$$\lambda = \cosh \eta \delta - (\cosh^2 \eta \delta - 1)^{1/2} \qquad (36)$$

Simultaneous solution of eqs. (34) - (36) defines the inneffective length.

A limiting case is obtained for a rigid-plastic material. For a uniform shear stress, the length, δ_p, required to obtain the full strength of the fiber is:

$$\delta_p = \frac{\sigma_f}{4\tau_y} d_f \qquad (37)$$

Thus, for a composite of 400 ksi glass fibers in a 10 ksi plastic binder, the plastic ineffective length is ten fiber diameters. This value is about four times the appropriate elastic value.

5. Composite Strength

With the link length defined, [by eq. (29) for the elastic case; eqs. (34) to (36) for the elastic-plastic case; and eq. (37) for the rigid plastic case] and the link strength characterized by eq. (8), the composite strength can be evaluated. First the strength of the bundle will be determined, then the composite will be treated as a chain of bundles, and weakest link statistical theorems will be applied. This leads to the desired statistical definition of composite strength.

For a bundle of links, Daniels [24] has shown that for a large numer, N, of fibers the distribution of bundle strengths approaches a normal distribution with expectation:

$$\bar{\sigma}_B = \sigma_m [1 - F(\sigma_m)] \tag{38}$$

and standard deviation:

$$\psi_B = \sigma_m \left\{ F(\sigma_m) [1 - F(\sigma_m)] \right\}^{1/2} N^{-1/2} \tag{39}$$

The associated density distribution function is:

$$\omega_B(\sigma_B) = \frac{1}{\psi_B \sqrt{2\pi}} \exp\left[-\frac{1}{2} \left(\frac{\sigma_B - \bar{\sigma}_B}{\psi_B} \right)^2 \right] \tag{40}$$

The maximum stress is obtained by maximizing the total load. Thus:

$$\frac{d}{d\sigma} \left\{ \sigma [1 - F(\sigma)] \right\}_{\sigma = \sigma_m} = 0 \tag{41}$$

For links described by eq. (8):

$$F(\sigma) = 1 - \exp(-\alpha\ \delta\ \sigma^{\beta}) \tag{42}$$

Substitute (42) into (41):

$$\frac{d}{d\sigma}\left[\sigma \exp\left(-\alpha\delta\sigma^{\beta}\right)\right]_{\sigma=\sigma_m} = 0$$

$$\therefore\ \sigma_m = (\alpha\delta\beta)^{-1/\beta} \tag{43}$$

From (38), (42) and (43):

$$\bar{\sigma}_B = (\alpha\ \delta\ \beta)^{-1/\beta}\ \exp\left(-\frac{1}{\beta}\right) \tag{44}$$

From (39), (42) and (43):

$$\psi_B = (\alpha\ \delta\ \beta)^{-1/\beta}\left\{\left[1 - \exp\left(-\frac{1}{\beta}\right)\right]\exp\left(-\frac{1}{\beta}\right)\right\}^{1/2} N^{-1/2} \tag{45}$$

Layers characterized by eqs. (40), (44) and (45) may be considered as links in a chain and the weakest link theorems can be applied again. Thus, applying eq. (2) to this case

$$\lambda(\sigma_c) = n\, w(\sigma_c)\left[1 - \Omega(\sigma_c)\right]^{n-1} \tag{46}$$

where σ_c is the composite failure stress, and λ is the associated distribution function.

The mode of this distribution is found by setting $d\lambda/d\sigma_c = 0$. This yields:

$$\sigma_c^{*} = \bar{\sigma}_B - \psi_B (2\log n)^{1/2} + \psi_B \frac{\log\log n + \log 4\pi}{2(2\log n)^{1/2}} \tag{47}$$

For composite dimensions large compared to fiber cross-section dimensions, $N >> 1$. Therefore:

$$\psi_B \to 0$$

and the statistical mode of the composite strength σ_c^*, is found to be:

$$\sigma_c^* = (\alpha\ \delta\ \beta e)^{-1/\beta} \tag{48}$$

where α and β are the constants defining the link strength and are determined by experimental tests of fiber strength vs. length as described previously. δ is the ineffective length defined by a fiber shear stress analysis and e is the base of natural logarithms.

The results of section 3 are used in eq. (48) to compute composite strength as a function of the effective length. The predicted composite failure stress is plotted in fig. 30 for the range of ineffective lengths of one to one hundred fiber diameters. The range one to ten generally corresponds to the elastic predictions and the range ten to one hundred to the inelastic predictions.

Also shown in fig. 30 are the effects of variations in fiber characteristics. Curves are presented to show the effect of an increase in the dispersion, as measured by a 10% change in β and of a decrease in the reference strength as measured by a 10% change in $\alpha^{-1/\beta}$. For the reference case plotted, the analysis also indicates that at failure the mean number of fractured fibers per layer is less than 10% and that the length at which the mean fiber strength equals the fiber stress in the composite, at the most probable composite failure stress, is on the order of ten ineffective lengths.

For a rigid-plastic representation of the binder material, failure points for two different yield stress values are shown. Thus, for the

fiber data used, and for a yield stress of 10 ksi, the predicted strength of a glass-plastic composite of 70% fibers by volume is 290 ksi. For the same conditions binder yield stress of 20 ksi would indicate a composite failure stress of 310 ksi. The effects of matrix characteristics are more clearly defined by considering the elastic-plastic results obtained in the latter part of section 4.

Mechanically, the elastic-plastic matrix material is characterized by the initial elastic modulus, the yield stress, and the total strain to failure. The influence of these three quantities on the tensile strength of a composite consisting of an elastic-plastic matrix uniaxially reinforced with glass fibers is shown in fig. 31 in the form of shear yield stress vs. elastic shear modulus required to achieve the specified constant values of composite strength.

These results are obtained by selecting a fixed value of composite strength, δ_c^*, and determining the corresponding ineffective length ratio from fig. 30. For the elastic case the modulus ratio E_1/G_2 and the maximum shear stress, τ_{max}, are determined from figs. (28) and (29) respectively. The asymptote for large shear moduli is found from the rigid-plastic solution, eq. (37). For the region between the elastic range, represented by the vertical portion of the curve, and the fully plastic range, represented by the horizontal asymptote, the combinations of values of shear modulus and shear yield stress which result in the desired ineffective length are evaluated from eqs. (34) to (36). The ultimate matrix shear strains required are not shown; however, they

are approximately parallel to the strength curves with decreasing strain required for increasing composite strength.

The stress curves show the nature of property variations required to produce the maximum increase in composite strength. For example, a composite containing an elastic-plastic matrix material with a shear modulus of 150 ksi and a shear yield stress of 15 ksi will be unaffected in strength by a ± 50% change in shear modulus but would improve in strength with increasing shear yield stress and would also require lower shear strain at failure; similarly, a matrix with a modulus of 40 ksi and a strength of 30 ksi would be far more sensitive to modulus changes than to strength changes. This is illustrative of the nature of the results to be obtained from the existing failure model. Other types of fiber and matrix materials need to be considered to complete the picture. Fibers with different strength levels and strength gradients with respect to fiber length, and matrices with monotonically decreasing tangent moduli should be included. In any event, it appears that the qualitative evaluation of the direction of improvement in constituent properties to obtain improved structural composites can be achieved.

One of the reasons for the quantitative uncertainties can be seen by exploring certain assumptions in the shear stress evaluation. First of all, the idealization to a rotationally symmetric problem ignores the variation due to the hexagonal or nearly-hexagonal array of nearest neighbor fibers. Secondly, the selection of an average distance between fiber and surrounding "average" material is not an obvious one. Although

the magnitude of the former problem cannot be assessed without the solution of a complex elasticity problem, the latter can be studied by varying the average distance and determining the resulting effect upon composite strength. The results of such a study are shown in fig. 32, where the ineffective fiber length is plotted as a function of the average matrix thickness expressed as a multiple of the fiber radius. The range of abscissa values cover the range obtained by various reasonable idealizations for a fiber volume fraction of 0.7.

6. Discussion and Conclusions

The analysis attempts to simulate what appears to be the physical failure mode. An effort was made to include what were thought to be the most important parameters influencing failure. Obviously, the model will not provide accurate quantitative answers without further refinements. It is expected, however, that the nature of desirable improvements in constituent characteristics can be ascertained from the present model. Such preliminary conclusions will be described below. The shortcomings of the model include failure to consider fracture involving parts of more than one layer, variation of ineffective length with stress level, stress concentrations in fibers adjacent to failure areas and the initial state of stress. Further, as the analysis indicates that short fiber lengths may exist at failure, the shortcomings at short lengths of the statistical distribution used for the fibers should be corrected. That is, the limit of fiber strength with decreasing length should be a finite value. Fiber experimentation can provide the data for such a

statistical model. On the positive side, however, the model represents the constituents in the major functions of fibers carrying extensional stress and matrix carrying shear stresses; it includes the effect of fiber imperfections on fiber failure; and accounts for the accumulation of internal cracks which combine to produce composite failure. This latter follows the concepts of Parratt [18] who suggests the influence of flaws and ineffective lengths on failure. The failure mode in the present analysis, however, results from an accumulation of cracks rather than from the existence of fully ineffective fibers. In fact the present results, which indicate typical fiber lengths at failure which are an order of magnitude larger than the ineffective length, perhaps explain the quantitative difference between the ineffective lengths of [18] and those of [20] and this paper. The experimental results, described in the following section, appear to be in qualitative agreement with the analytical models.

The conclusions to be drawn from the analysis for the glass fibers considered are as follows: Composite failure stress will be on the order of short fiber failure stress, where short fibers are on the order of ten ineffective lengths. Fiber strength levels appear to have the most direct effect on composite strength. Fiber strength dispersion influences composite strength and ineffective length of fibers has a significant effect on strength. The latter is primarily influenced by the matrix characteristics and an improvement of matrix strength appears desirable. The effect of such changes upon the mode of failure remains to be considered.

The fact that these conclusions are not unexpected for glass reinforced plastics is encouraging, insofar as the possibility of fruitful application of this analysis to consideration of other composites and to the definition of desirable constituent properties. Further, the actual strength levels predicted for glass-plastic composites are higher than those obtained experimentally. This could well be explained by the additional damage incurred in fabrication after the state at which the fiber tests of [21] were performed.

B. FIBER REINFORCED COMPOSITES - EXPERIMENTAL

The experimental study of the mode of failure of fiber reinforced composites under a tensile load utilized specimens consisting of a single layer of parallel glass fibers imbedded in epoxy. The spcimen, as shown in fig. 33, has a test section which is 1/2" x 1" in size and 0.006" thick and contains 90-100 parallel glass fibers of 0.005" diameter. The specimen is loaded in tension and observed microscopically during the test. The design of the specimen was directed towards making this observation possible, so that the nature of failure of fibrous composites could be determined. In particular, the validity of the preceding analysis was to be tested. (Similar test specimens appear to have been used with a somewhat different goal in (25).)

Both visual observation and photographic observation were used on all test specimens. A sequence from a typical set of photographic data is shown in fig. 34. The load was applied parallel to the fibers. Note again, that the fiber diameter is on the order of five times the minimum distance between fibers. The first frame shows the specimen at zero load. Polarized transmitted light has been used and at zero load the fibers are dark and the plastic between fibers appears light. As the load is increased, the fibers appear lighter, although this is not adequately reflected in the photos since the lens aperture was changed during the sequence. The difference between the unloaded specimen photo and the next to the last photo in the sequence is four f stops, or a factor of 16 on the exposure.

At less than 50% of the ultimate load, individual fiber fractures are observed. Since the fractured fiber in the vicinity of the fracture is unstressed, the color returns to the original dark color. Thus, breaks appear as a short dark rectangular area with a thin white line across the center. The length of this dark area is the ineffective length of the fiber. (see section A.) As the load increases, the fibers fracture at random locations. Thus, although there are stress concentrations in the vicinity of the breaks, the variation in fiber strength generally more than offsets the effect of such concentrations. Hence, the breaks occur randomly rather than cumulatively at the site of the initial break. The stress concentrations cause a relative brightening at the highly stressed points of the fibers and this effect appears on the latter photos in the sequence of fig. 34. Also there are examples of breaks which were produced as a result of the stress concentrations.

The specimen is shown in the last frame after fracture. It is not clear that the actual fracture simulates the behavior of a three dimensional composite and it therefore appears that the internal fractures prior to composte failure are the primary data from these tests. The usefulness of the test lies in the potential use of these results in conjunction with the preceding analysis to predict and verify the direction of desired constituent property improvements to achieve higher tensile strength composites. The data for the specimen of fig. 34 are plotted in fig. 35. These results are typical of the scatter of data points around the best fit curve. Such curves for the series of test specimens described in table III-1 are shown

in fig. 36.

TABLE III-1

Tensile Strength Tests - Series A

Spec. Number	Gage length (in.)	Width (in.)	Thickness (in.)	Number of fibers	Ultimate load (lb.)
1	1.10	0.499	0.0066	92	114
2	0.91	0.498	0.0060	93	84*
3	1.10	0.500	0.0067	93	111
4	0.90	0.502	0.0064	94	125
5	1.05	0.494	0.0061	92	116
6	1.02	0.500	0.0062	94	117
7	1.00	0.498	0.0062	93	116
8	1.07	0.503	0.0061		65*
9	1.03	0.490	0.0060	93	107

*Failure in grip section. Test data not used.

C. PARTICLE REINFORCED MATERIALS

The merit of a matrix material having enhanced stiffness and strength properties compared to presently available plastic resins is clearly evident from the analyses of composites. The first, most directly available method of improving matrix properties appears to be to make the matrix itself a composite. To this end a series of specimens were fabricated to investigate the effect of the addition of glass and alumina powder to epoxy resin.

The results bring up more questions than they answer. While the stiffness of the particle-composite specimens were duly increased by the additives to maxima of 1,040,000 psi for the glass particles (10-200 micron characteristic dimensions) and 2,000,000 psi for the alumina (325 mesh or finer), the strength and elongation of the resin were degraded. A curious accompanying phenomenon was a marked increase in viscosity of the glass-filled epoxy resin before curing. This increase prevented the fabrication of specimens of greater than 30% volume percent glass. With the alumina particles 48 volume percent filler was attained without corresponding difficulties, but to reach the maximum value of 62% a larger particle size (325 mesh) was required than for all the other (900 mesh) alumina-filled specimens.

Increase in viscosity with addition of particles is certainly to be expected. What is peculiar is the difference in character of the viscosity change for the two particles used. For successful end use the resin viscosity must be not substantially changed from the unfilled value, a

criterion that could be met by the alumina particles up to a content of approximately 40 volume percent, but the question raised of the relative importance of the many factors affecting viscosity is not answered by the present results.

Of much more interest and eventual importance than viscosity (influence of the fillers in the fluid state) is the decrease in elongation at failure of the filled specimens (influence of the fillers in the plastic state). The influence in the elastic state is as expected. The Young's modulus of the composite is improved substantially, just as desired, and if this were the only effect the implications would be exciting. Accordingly an explanation of the reasons for the poor performance in the plastic range could be useful. Answers are needed to questions like:

1. Is the reduction of elongation dependent upon the material used for the filler, - i.e. would a more compatible or better bonding filler be less harmful?

2. Is the reduction of elongation dependent upon the geometry of the filler, - i.e. would short, very fine fibers be better than essentially spherical particles?

3. Is the entire problem a result of poor fabrication, - i.e. were these first-attempt specimens unsound and can improved fabrication technique restore the strength lost by adding the filler?

4. How would even the low elongation filled resins of these tests behave as the matrix for a filament reinforced composite,

i. e. would the development of "fractures" in the matrix at these elongations lead to premature failure of the composite?

The actual experimental results which generate all these questions are presented in figures 38 and 39 without further discussion. The end objective of an improved matrix material is worthy of continued investigation.

IV. STRUCTURAL APPLICATION STUDIES

Although the bulk of this study has been devoted to determining composite properties as a function of constituent properties, it is important to emphasize that this is not an end in itself. Analysis of basic applications must be performed to indicate the nature of desirable material properties. For example, in the case of elastic constants, the composites are anisotropic and no one simple property of an anisotropic material adequately defines the efficiency of a structure using such a material. Thus, it is necessary to perform a structural efficiency type analysis treating generalized structures and loads. As an example, stability of plates with oriented voids, subjected to in-plane compressive loads are treated in section A. Also, the effective properties cannot be used at the neglect of internal stresses. In the case of a practical fibrous composite structures biaxial stiffening will introduce average stresses in individual layers of a laminate which differ considerably from the average laminate stress. Certain aspects of the internal shear stresses are treated in section B as an example of this problem.

A. STABILITY OF PLATES WITH ORIENTED VOIDS

A quite different measure of material effectiveness than its extensional stiffness is its ability to carry compressive or shear stresses without buckling. This measure must be applied with discretion, because there are many ways of changing the resistance of buckling. For example obviously the least loss in buckling resistance as material is removed to reduce the effective density occurs when the material is taken from the centroidal plane of the plate, as in sandwich construction. The problem we are examining here may be considered applicable to the case in which a uniform material through the entire thickness is desired, for one reason or another. We are then seeking an answer to the question: Is there some angular direction which gives a material uniformly lightened by oriented voids superior resistance to buckling?

Method of analysis

Available equations from the literature of the buckling of flat plates in compression and shear were used to calculate the variation of buckling effectiveness with angle of void. The elastic constants employed in the equations were calculated with the aid of (13) in similar fashion to that employed for the stretching and shearing stiffnesses. Essentially the result is that the bending stiffnesses are proportional to the corresponding stretching stiffnesses, with account taken for the effective Poisson's ratio applicable to the anisotropic plate.

Results

The results are summarized in figure 40, in which are plotted normalized interaction curves for buckling of simply supported, infinitely long plates having voids longitudinally, transversely, and at 45° to the edges. The normalizing factor is the equivalent weight solid plate. The plate with longitudinal holes is shown to have the least buckling resistance, that with transverse holes is better in shear and the same in compression, and the one with 45° holes is better in compression and between the 0° and 90° cases in shear. The differences are not substantial.

Conclusion and Discussion

While material with oriented voids does exhibit increased elastic buckling resistance because of its lower effective density, the orientation of the voids is not important in the elastic range. Probably if any criterion exists it is that the holes should in general be aligned in the direction of principal stress, to delay as long as possible the onset of plasticity.

B. LAMINATE SHEAR STRESSES

A second aspect of the failure problem which has been considered is the study of shear stresses in a biaxially stiffened matrix; that is, a material stiffened by parallel fibers in layers which are oriented alternately in each of two directions. The case analyzed considers the two layer directions to be at equal and opposite angles to the loading direction. The stresses were determined using the methods developed in (26). The results are plotted in fig. 41. The shear stress on planes parallel and normal to the loading direction, τ_{xy} , is shown in fig. 41a, normalized with respect to the applied stress, σ , plotted as a function of the lamina orientation angle, θ . The principal elastic constants of an individual lamina are indicated and are typical of glass reinforced plastic construction. The directions parallel and normal to the fibers are considered to be the weak shear planes and the stress on these planes, τ_{12} , is therefore also shown in fig. 41a. The question of failure due to shear stress involves both the shear stress and the shear strength distributions. The maximum shear stress, τ_{max} , is shown as the upper curve of fig. 41a. The effect of material properties on the shear stresses acting in the principal directions of each lamina, τ_{12} , are shown in fig. 41b. The shear stresses in the fiber direction are seen to constitute a moderately high fraction of the applied axial stress and as such warrant further consideration as a mechanism of failure.

V. CONCLUSIONS

The present study of the relationship of properties of composite materials to properties of their constituents has been primarily concerned with the evaluation of elastic constants and ultimate tensile strength of fibrous composites. The effort has been primarily directed towards the development of the basic theory governing the behavior of such materials. Thus, by the use of variational principles of the theory of elasticity, bounds on the elastic constants of fiber reinforced materials have been obtained. For parallel fibers in an hexagonal array, the bounds are exact. For parallel fibers in a random array, simpler approximate expressions are obtained. These results can be used to study the potential of fibrous composites utilizing any combination of constituents.

The numerical results obtained, indicate that the effect of the matrix upon most of the constants is far from insignificant. The possible means of attaining improved structural composites thus include using an improved fiber or modifying the binder material for a given fiber. Certain aspects of the latter approach have been studied experimentally, with the indication that loaded plastics are advantageous. One type of improved fiber considered has been a non-circular fiber. It was demonstrated that the transverse modulus of composites containing elliptical fibers of aspect ratio four, can be almost doubled for only moderate fiber volume fractions. These studies of elastic constants have demonstrated potential methods of controlling any given elastic constant. It is now necessary to study certain

typical aerospace structural applications to define the desired type of improvement of these constants and the relative merits of various potential improvements. Preliminary structural application studies have been performed. Extension of such structural efficiency studies would permit the present results to be used to define guidelines for the development of improved composite materials.

The second major aspect of the present work is the study of the tensile strength of fibrous composites. The observed influence of fiber imperfections upon fiber strength have been used as the basis of a model which hypothesizes composite failure to be the result of a statistical accumulation of randomly occuring fiber fractures. The study of this problem involved an approximate treatment of the stress distribution in the vicinity of an internal fiber fracture. These results enable the evaluation of alternate possible modes of failure. An experimental study utilizing reinforced plastic film specimens, observed microscopically during loading, was undertaken to qualify the analysis and provide quantitative evaluation of parameters in the analysis. The experimental results correlated closely with the failure model utilized in the analysis and it appears that the joint use of theoretical and experimental results can define the desirable characteristics for improved structural composites. Again, the analysis indicates that significant improvement in composite performance can be obtained by variation of matrix properties as well as by the obvious changes in fiber characteristics.

It appears that the proper understanding of the mechanics of deformation and failure of composites can indeed contribute to the attainment of the many potential improvements composites have long been known to offer

ACKNOWLEDGEMENT

The authors wish to acknowledge the creative contribution of Mr. R. K. Cole to the development of the experimental study of reinforced plastic tensile strength described herein.

REFERENCES

1. Paul, B., "Prediction of Elastic Constants of Multiphase Materials", Trans. AIME Vol. 219, 1960, pp. 36-41.

2. Hashin, Z. and Shtrikman, S., "Note on a Variational Approach to the Theory of Composite Elastic Materials", Journal of the Franklin Institute, Vol. 271, 1961, pp. 336-341.

3. Hashin, Z. and Shtrikman, S., "A Variational Approach to the Theory of the Elastic Behavior of Multiphase Materials", Journal of the Mechanics and Physics of Solids, Vol. 11, 1963, pp. 127-140.

4. Hashin, Z., "The Elastic Moduli of Heterogeneous Materials", Journal of Applied Mechanics, Vol. 29, Trans. ASME, Vol. 84, 1962, pp. 143-150.

5. Dietz, A. G. H., "Design Theory of Reinforced Plastics", in R. H. Sonneborn "Fiberglas Reinforced Plastics", Reinhold Publishing Corp., New York, N. Y., 1956.

6. Outwater, J. O., Jr., "The Mechanics of Plastics Reinforcement in Tension", Modern Plastics, 1956, p. 156.

7. Rosen, B. W., Ketler, A. E., and Hashin, Z., "Hollow Glass Fiber Reinforced Plastics", Contr. NOw 61-0613-d, Final Report Nov. 1962, Space Sciences Lab. GE Co., Philadelphia, Pa.

8. Hill, R., "Report on Theories of the Elastic Properties of Reinforced Solids", British Iron and Steel Research Association, Report D/19/62, 1962 (Unpublished).

9. Hashin, Z., "Theory of Mechanical Behavior of Heterogeneous Media", Applied Mechanics Reviews (to be published).

10. Bishop, J. F. W., and Hill, R., "A Theory of the Plastic Distortion of a Polycrystalline Aggregate under Combined Stresses", Phil. Mag. Vol. 62, 1951, pp. 414-427.

11. Love, A. E. H., "A Treatise on the Mathematical Theory of Elasticity", Dover Publications Inc., New York, N. Y., 1944.

12. Goodier, J. N., "Concentration of Stress around Spherical and Cylindrical Inclusions and Flaws", Journal of Applied Mechanics, Trans. ASME Vol. 55, 1933, pp. A 39-44.

13. Dow, N. F., Libove, C., and Hubka, R. E., "Formulas for the Elastic Constants of Plates with Integral, Waffle-Like Stiffening, NACA TR 1195, 1954.

14. Crawford, R. F. and Libove, C., "Shearing Effectiveness of Integral Stiffening", NACA TN 3443, 1955.

15. Dow, N. F. and Gruntfest, I. J., "Determination of Most Needed, Potentially Possible Improvements in Materials for Ballistic and Space Vehicles, General Electric Company TIS R60SD389, 1960.

16. Machlin, E. S., "Status Report on Non-Metallic Fibrous Reinforced Metal Composites", Status Report, Contract NOw 61-0209-c, Sept. 1961.

17. Jech, R. W., McDanels, D. L. and Weeton, J. W., "Fiber Reinforced Metallic Composites", Proceedings of the 6th Sagamore Ordnance Materials Research Conference, August 1959.

18. Parratt, N. J., "Defects in Glass Fibers and Their Effect on the Strength of Plastic Mouldings", Rubber and Plastics Age, Mar. 1960.

19. Sadowsky, M. A., "Transfer of Force by High-Strength Flakes in a Composite Material", Watervliet Arsenal, TR WVT-RR-6105-R June, 1961.

20. Dow, N. F., "Study of Stresses Near a Discontinuity in a Filament-Reinforced Composite Metal:, Space Mechanics Memo #102, GE Space Sciences Laboratory, Jan. 1961.

21. Schmitz, G. K., "Exploration and Evaluation of New Glasses in Fiber Form", Bi-Monthly Progress Report No. 4, Solar Report RDR 1266-5, August 1962.

22. Gucer, D. E., and Gurland J., "Comparison of the Statistics of Two Fracture Modes", Journal of the Mechanics and Physics of Solids, pp. 365-373, 1962.

23. Weibull, W., "A Statistical Distribution Function of Wide Applicability", Journal of Applied Mechanics, Sept. 1951.

24. Daniels, H. E., "The Statistical Theory of the Strength of Bundles of Threads", Proceedings of the Royal Society, p. 405, 1945.

25. Bouc, C. A., "Microscopic Study of Mode of Fracture in Filament Wound Glass Resin Composites", T&AM Report No. 234, University of Illinois, Nov. 1962.

26. Rosen, B. W., "Elastic Constants of Laminates of Orthotropic Plates", Space Mechanics Memo #112, General Electric Company, June, 1962.

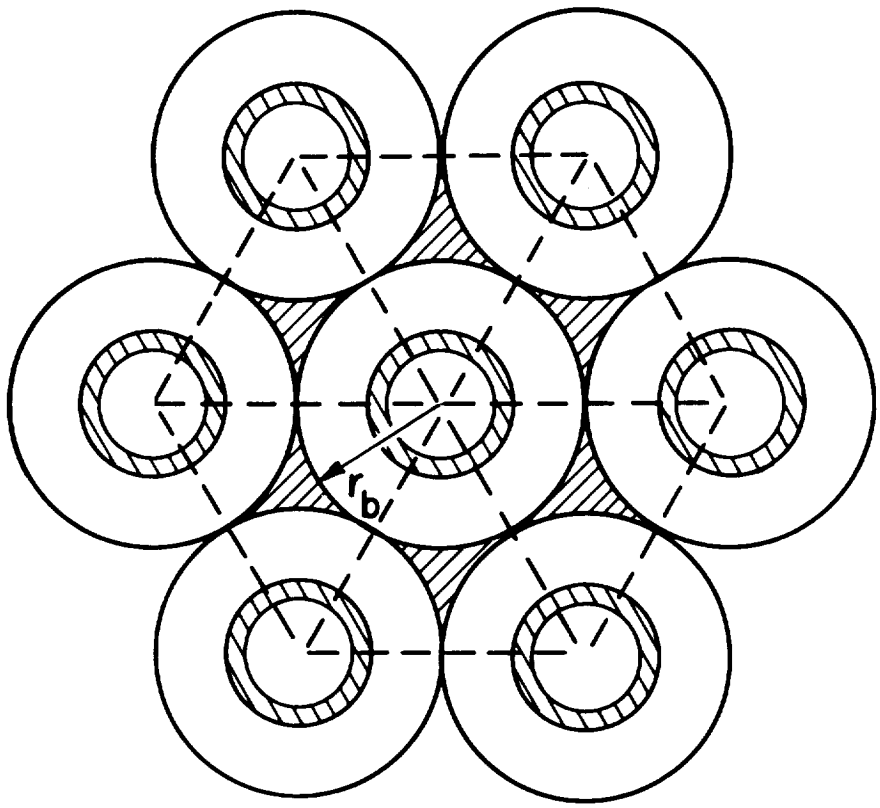

a.) HEXAGONAL ARRAY

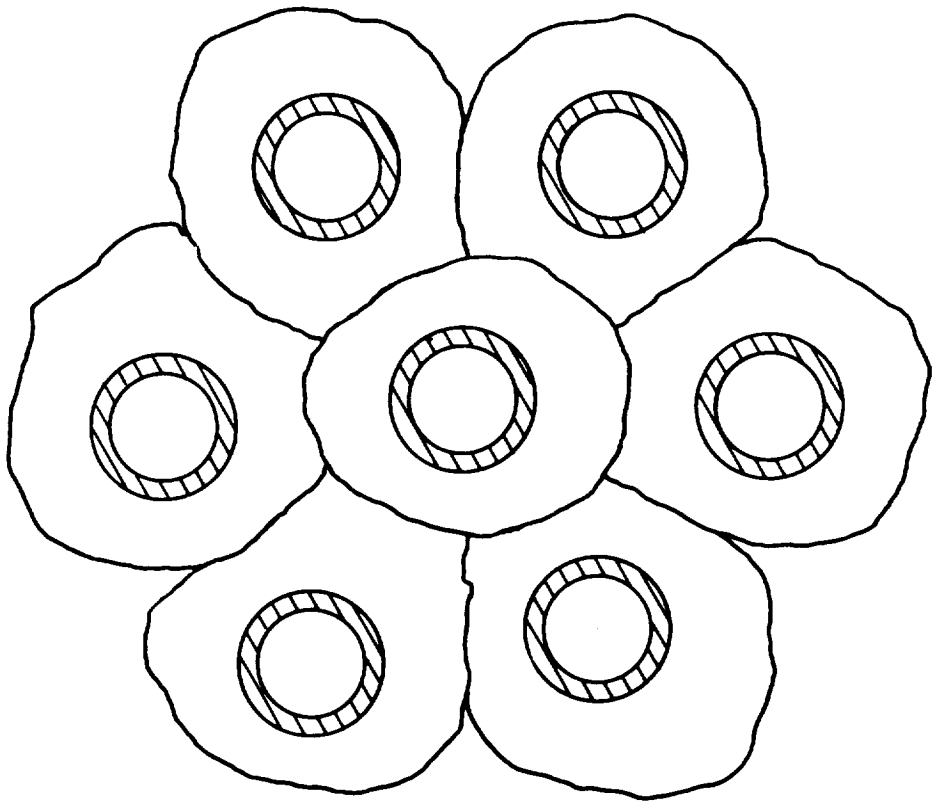

b.) RANDOM ARRAY

Figure 1. Fiber Arrays Considered for Elastic Moduli Analysis

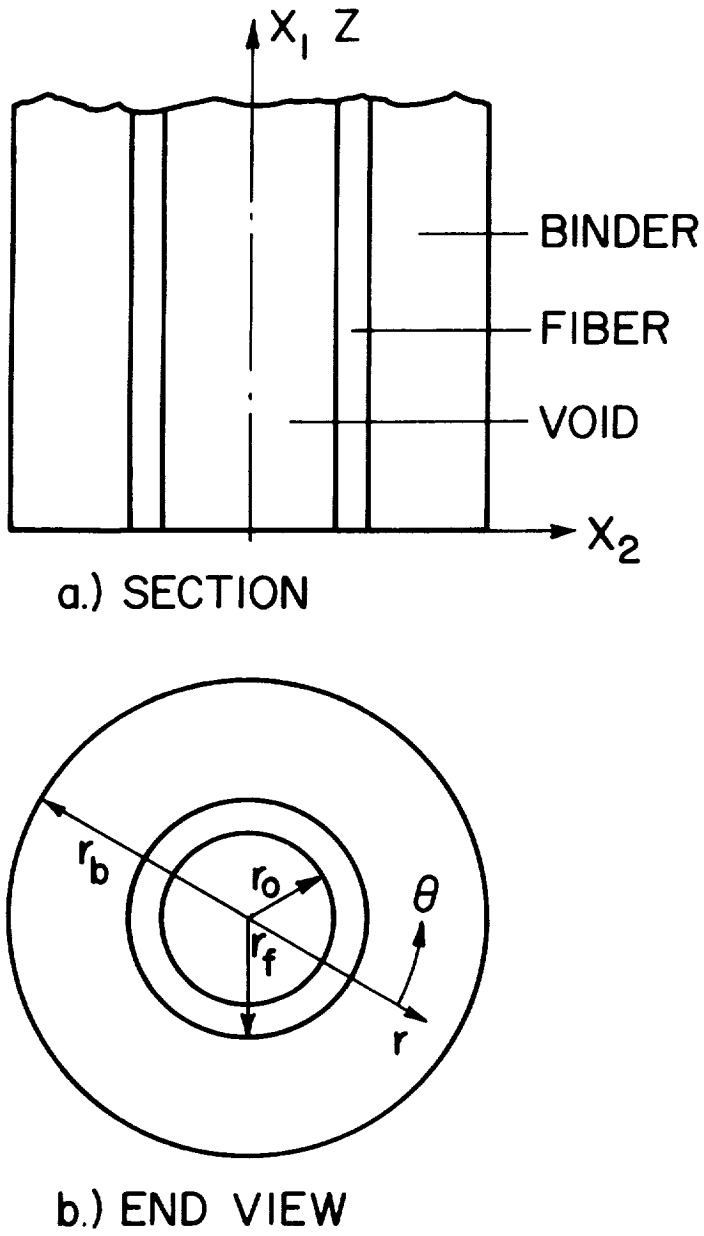

Figure 2. Composite Cylinder Notation for Elastic Moduli Analysis

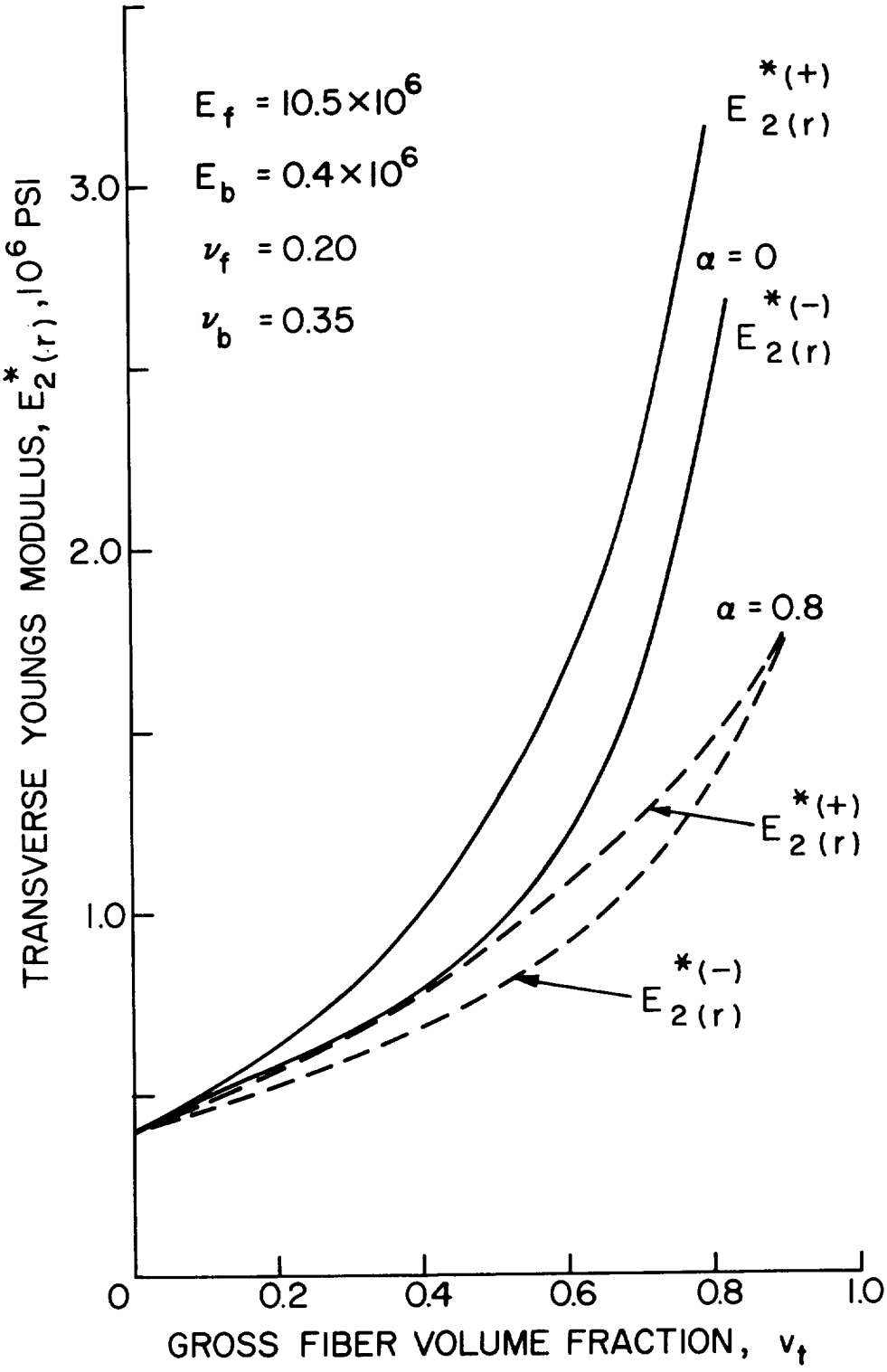

Figure 3. Bounds on the Effective Transverse Young's Modulus for Solid and Hollow Glass Fibers in a Plastic Matrix (Parallel Fibers, Random Array)

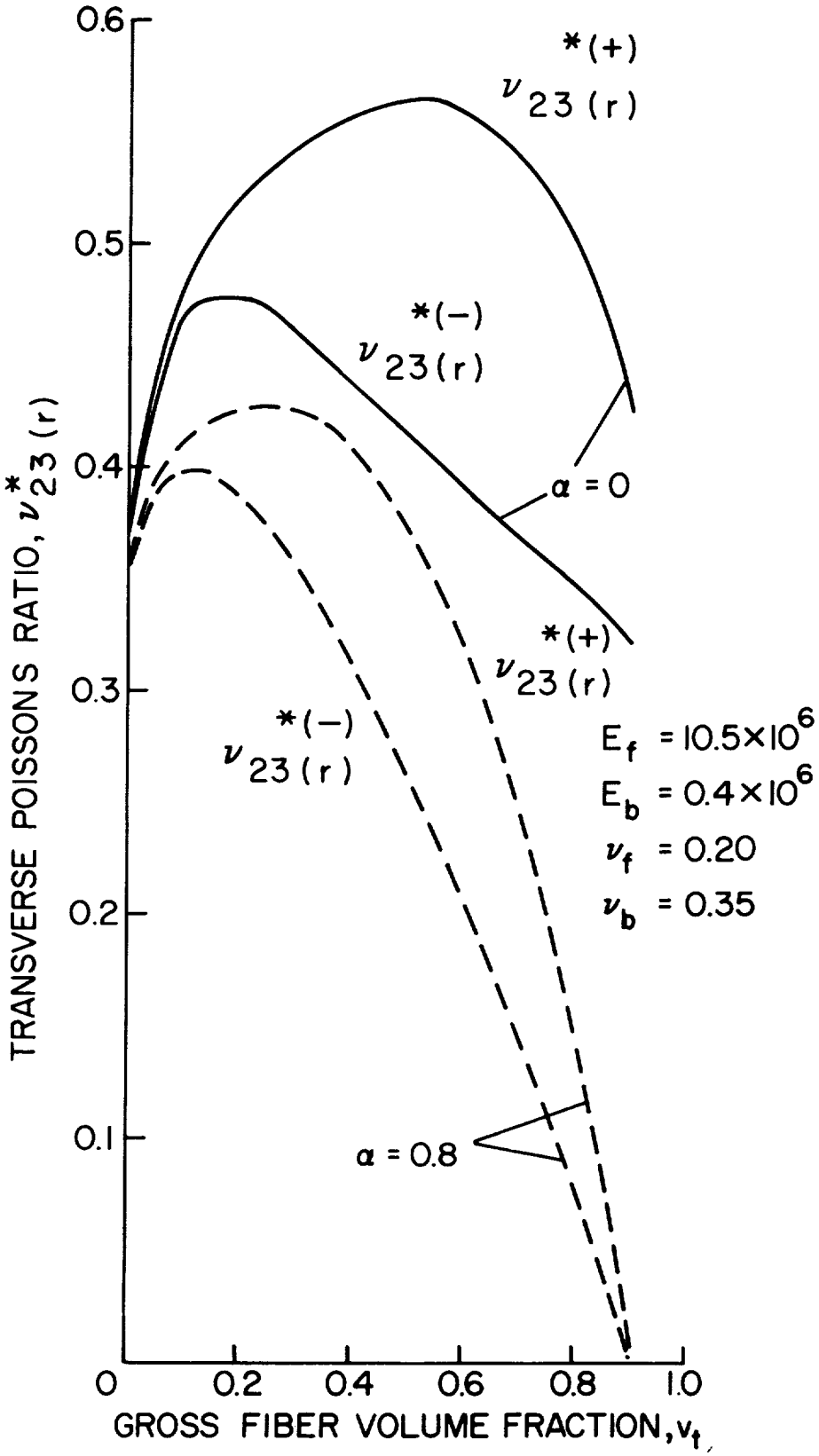

Figure 4. Bounds on the Effective Transverse Poisson's Ratio for Solid and Hollow Glass Fibers in a Plastic Matrix (Parallel Fibers, Random Array)

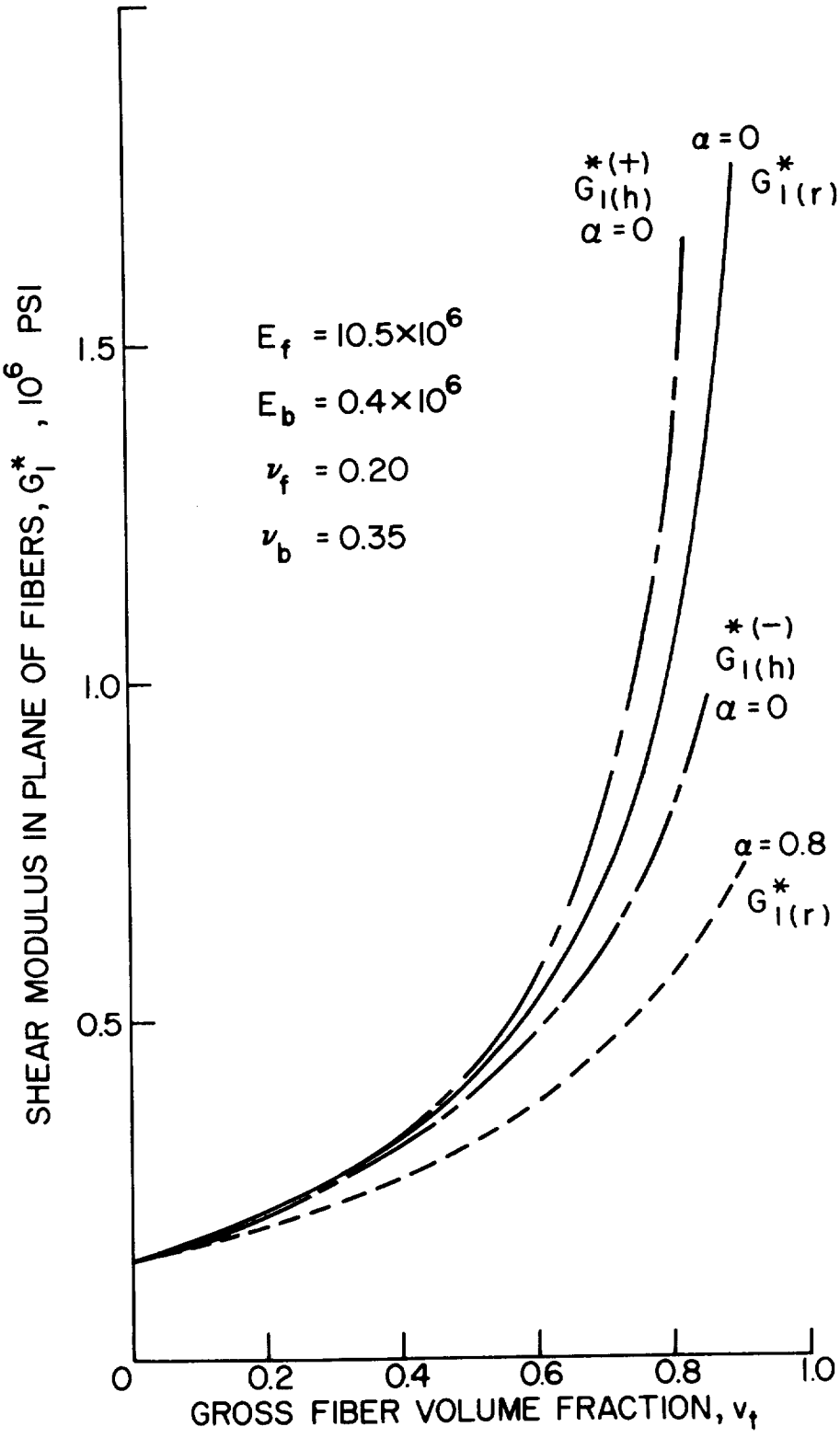

Figure 5. Effective Shear Modulus in the Plane of the Fibers for Solid and Hollow Glass Fibers in a Plastic Matrix (Parallel Fibers, Random and Hexagonal Array)

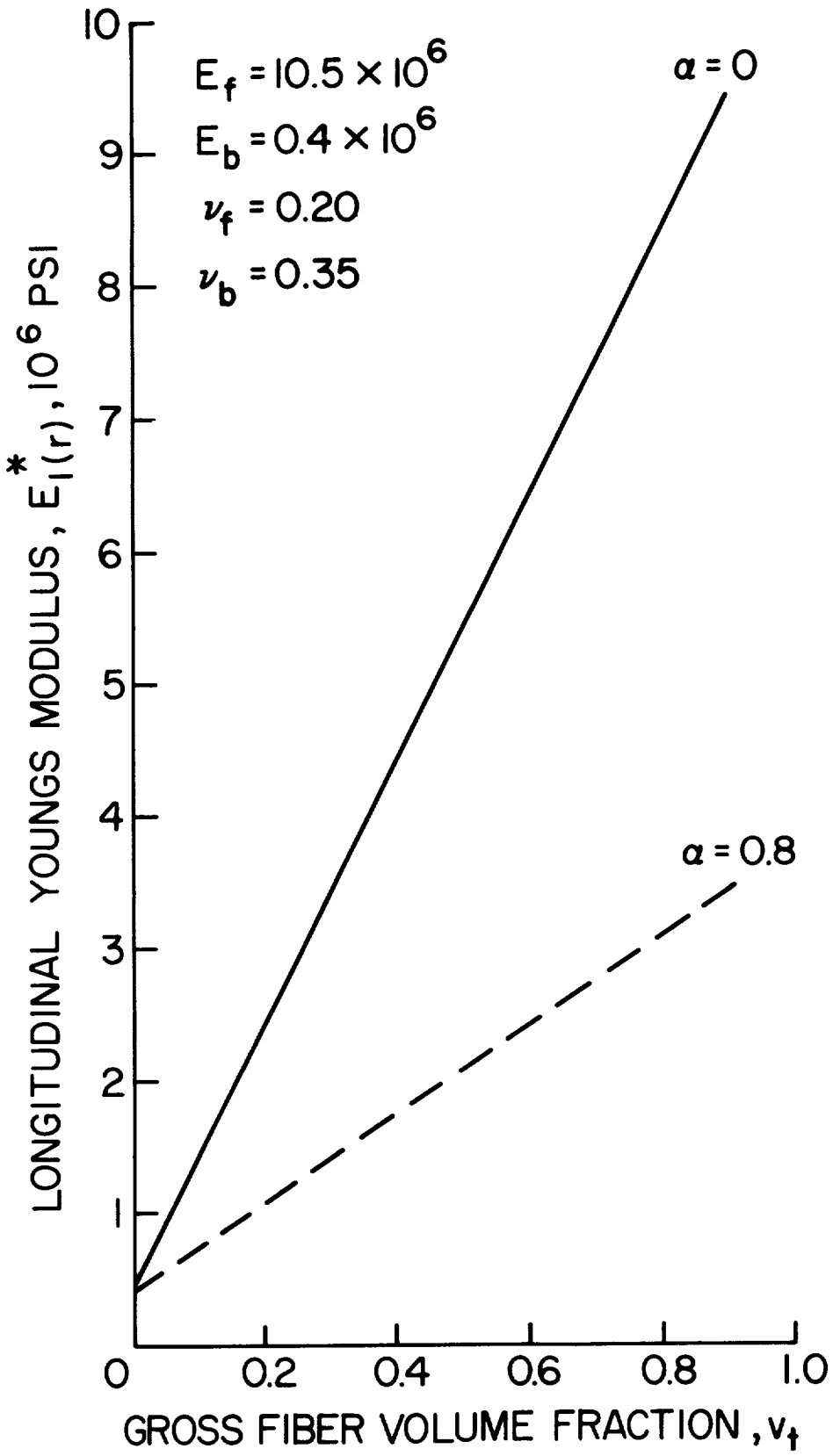

Figure 6. Effective Longitudinal Young's Modulus for Solid and Hollow Glass Fibers in a Plastic Matrix (Parallel Fibers, Random Array)

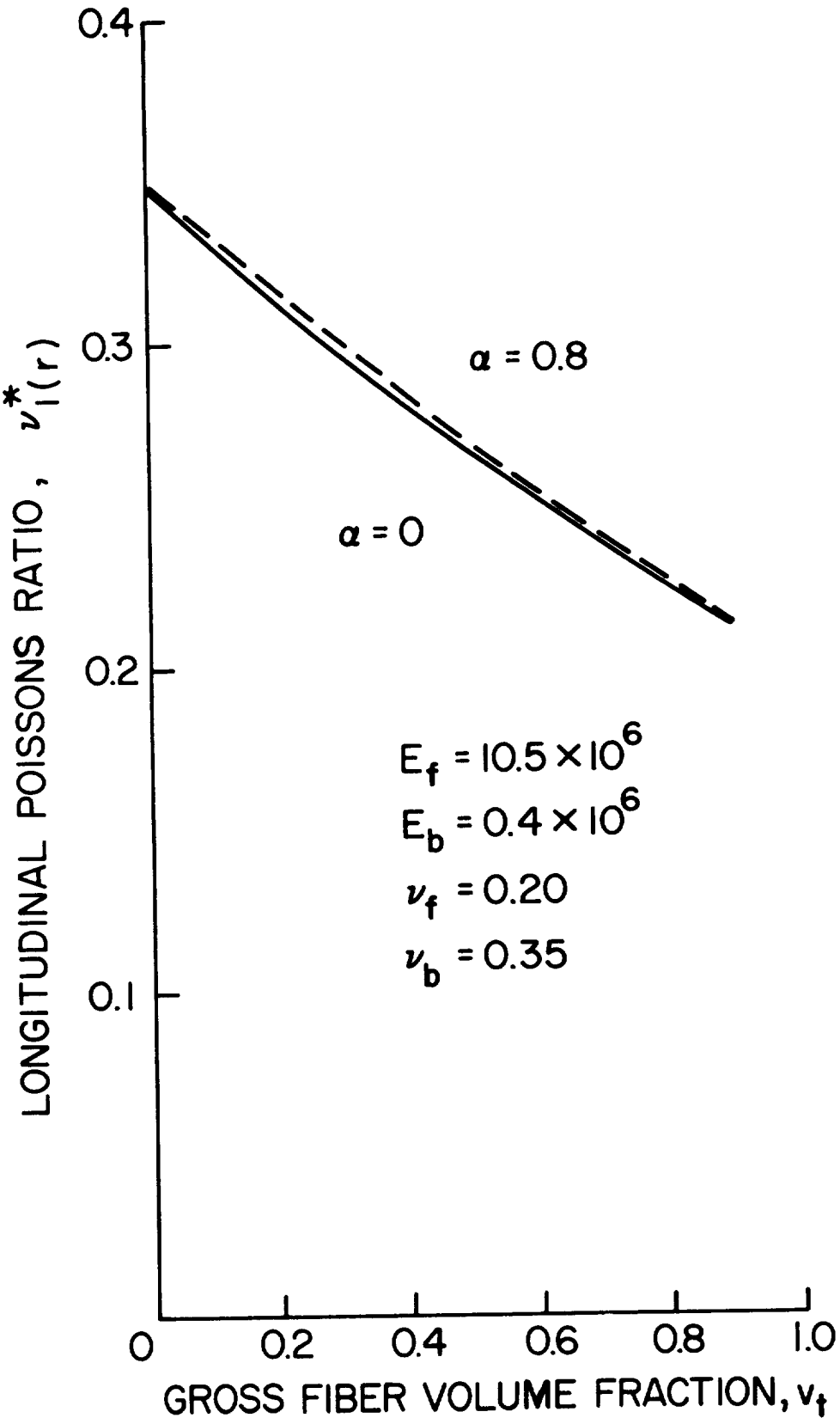

Figure 7. Effective Longitudinal Poisson's Ratio for Solid and Hollow Glass Fibers in a Plastic Matrix (Parallel Fibers, Random Array)

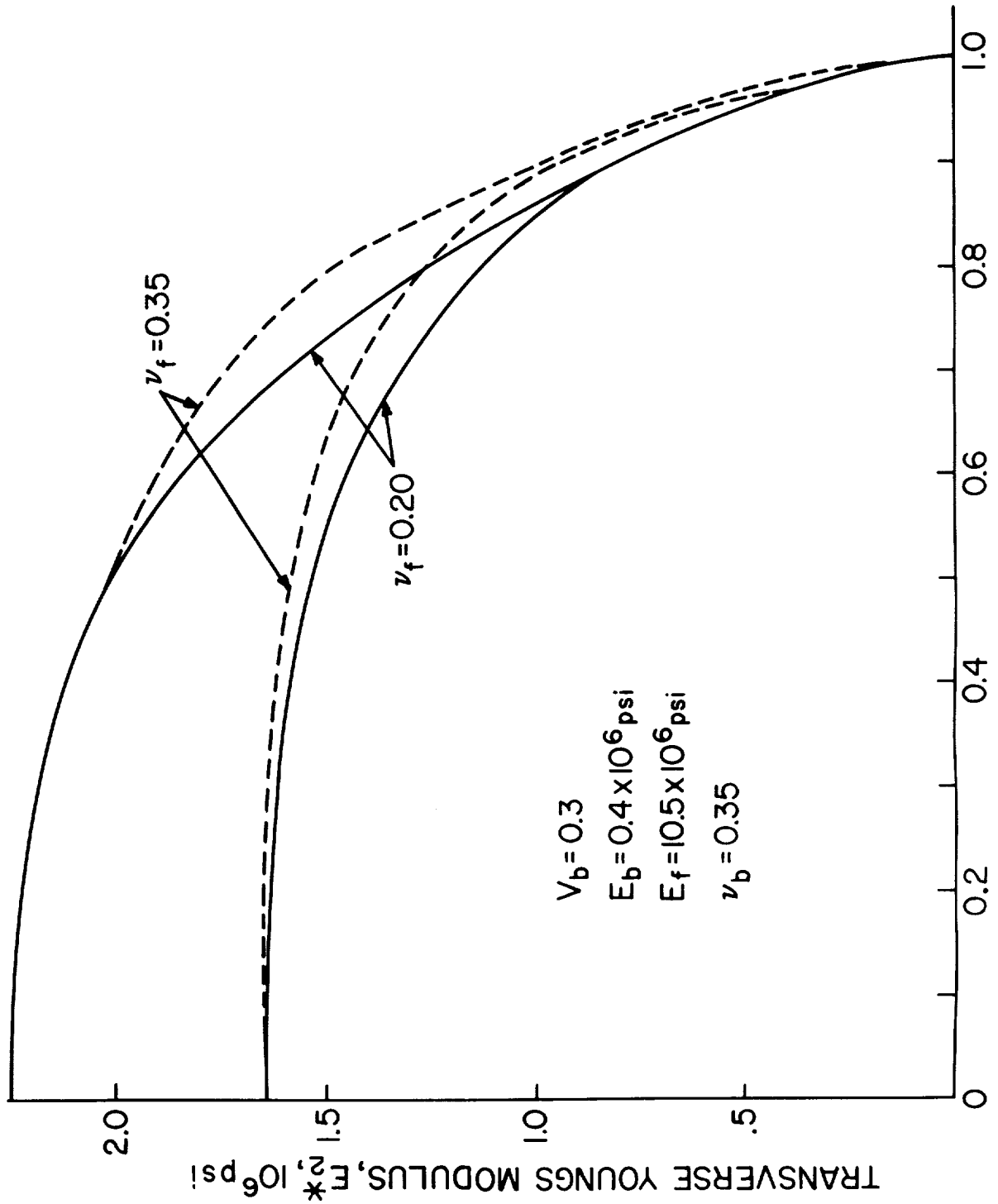

Figure 8. Bounds on the Effective Transverse Young's Modulus for Hollow Glass Fibers in a Plastic Matrix (Parallel Fibers, Random Array)

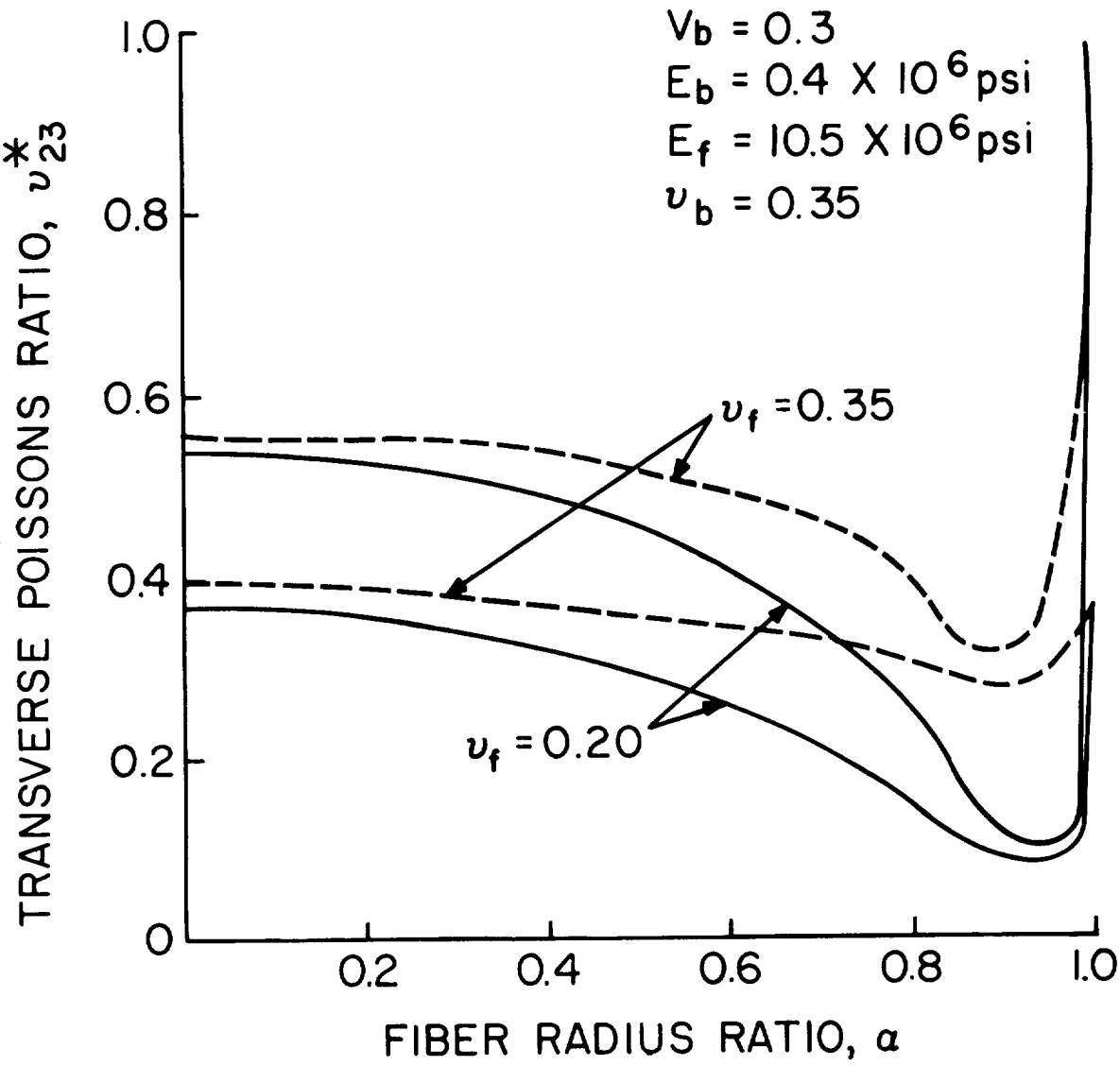

Figure 9. Bounds on the Effective Transverse Poisson's Ratio for Hollow Glass Fibers in a Plastic Matrix (Parallel Fibers, Random Array)

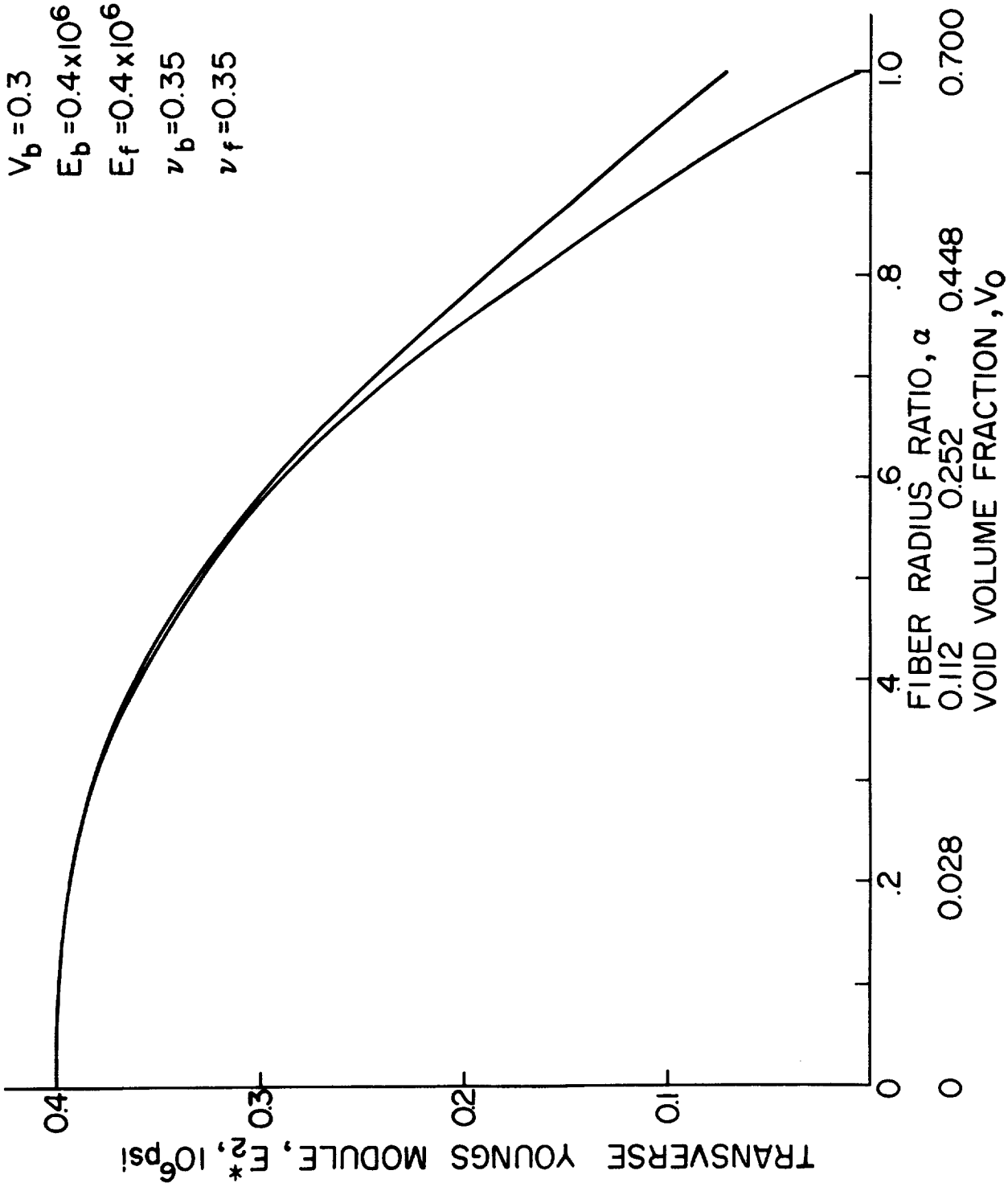

Figure 10. Bounds on the Effective Transverse Young's Modulus for a Plastic Matrix with Parallel Circular Holes

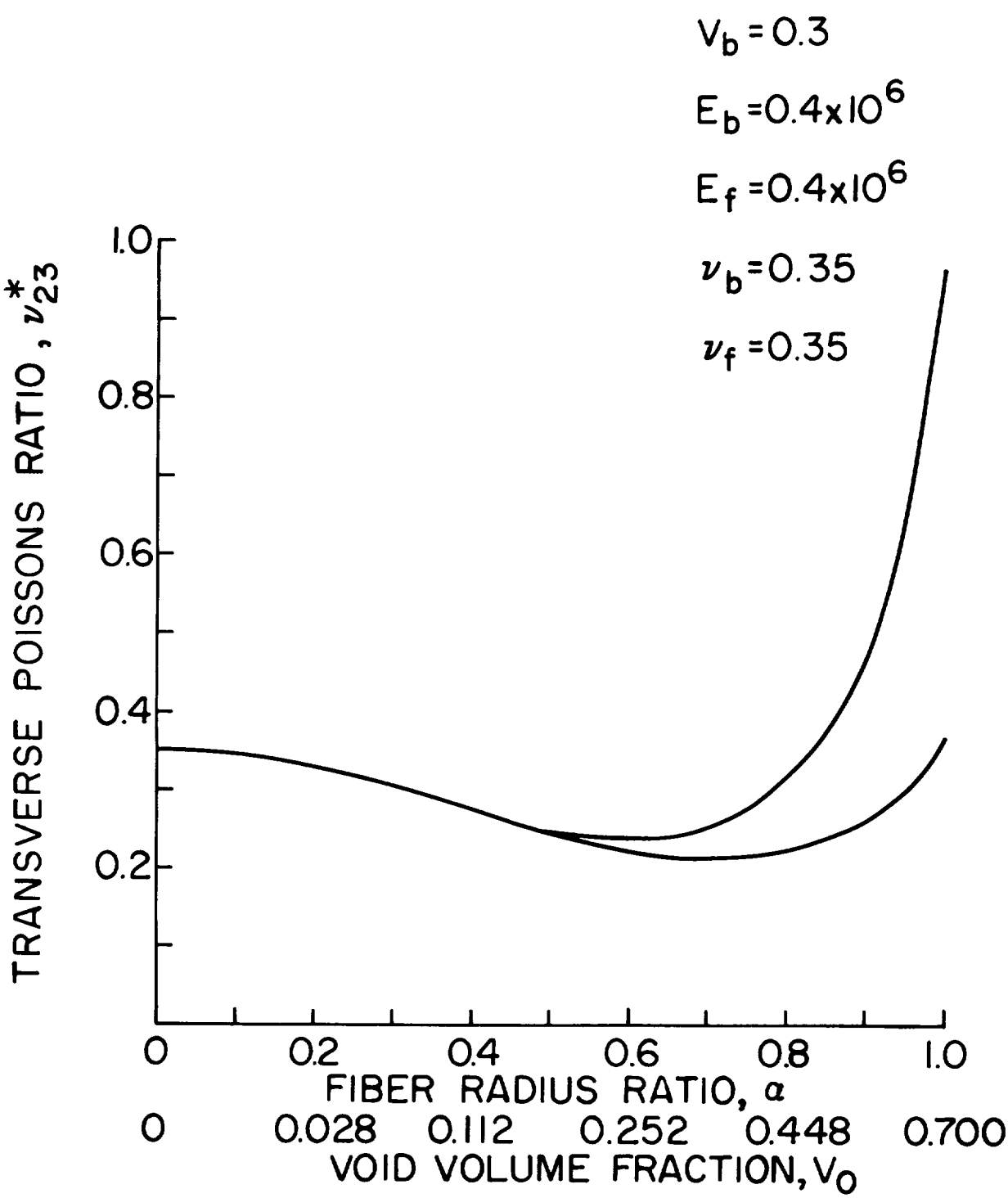

Figure 11. Bounds on the Effective Transverse Poisson's Ratio for a Plastic Matrix with Parallel Circular Holes

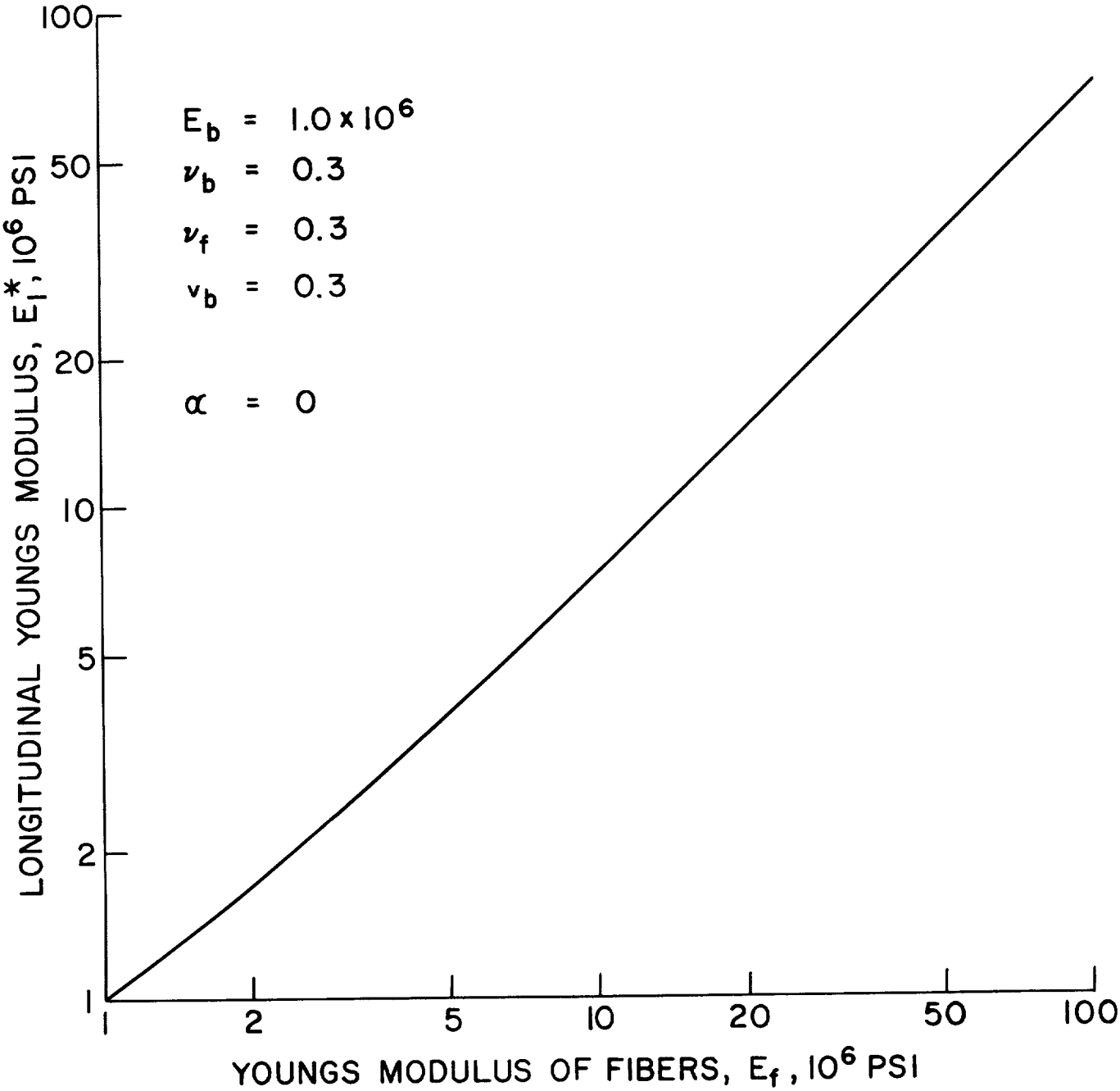

Figure 12. Effective Longitudinal Young's Modulus of a Fibrous Composite as a Function of the Young's Modulus of the Fibers

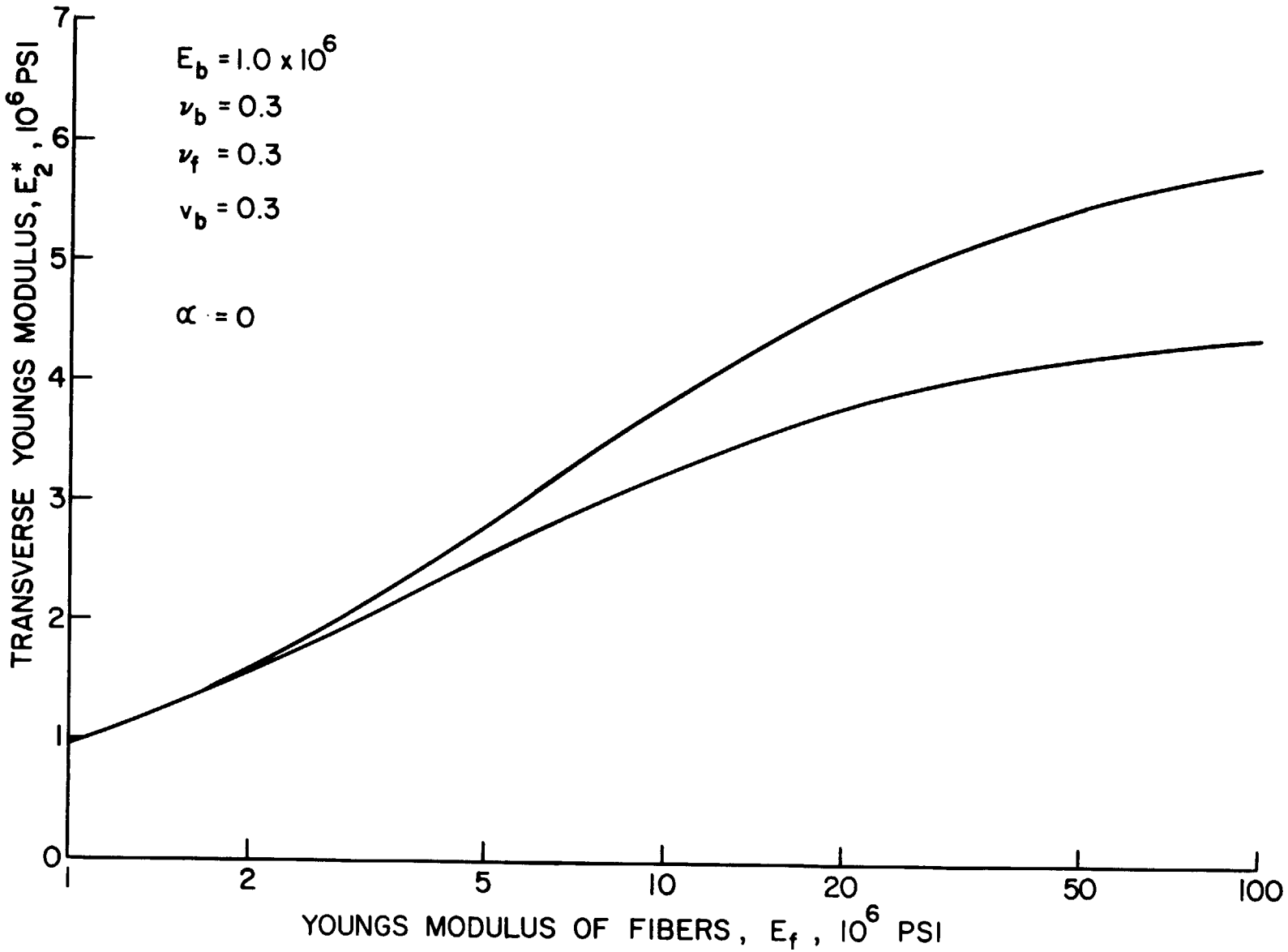

Figure 13. Bounds on the Effective Transverse Young's Modulus of a Fibrous Composite as a Function of the Young's Modulus of the Fibers

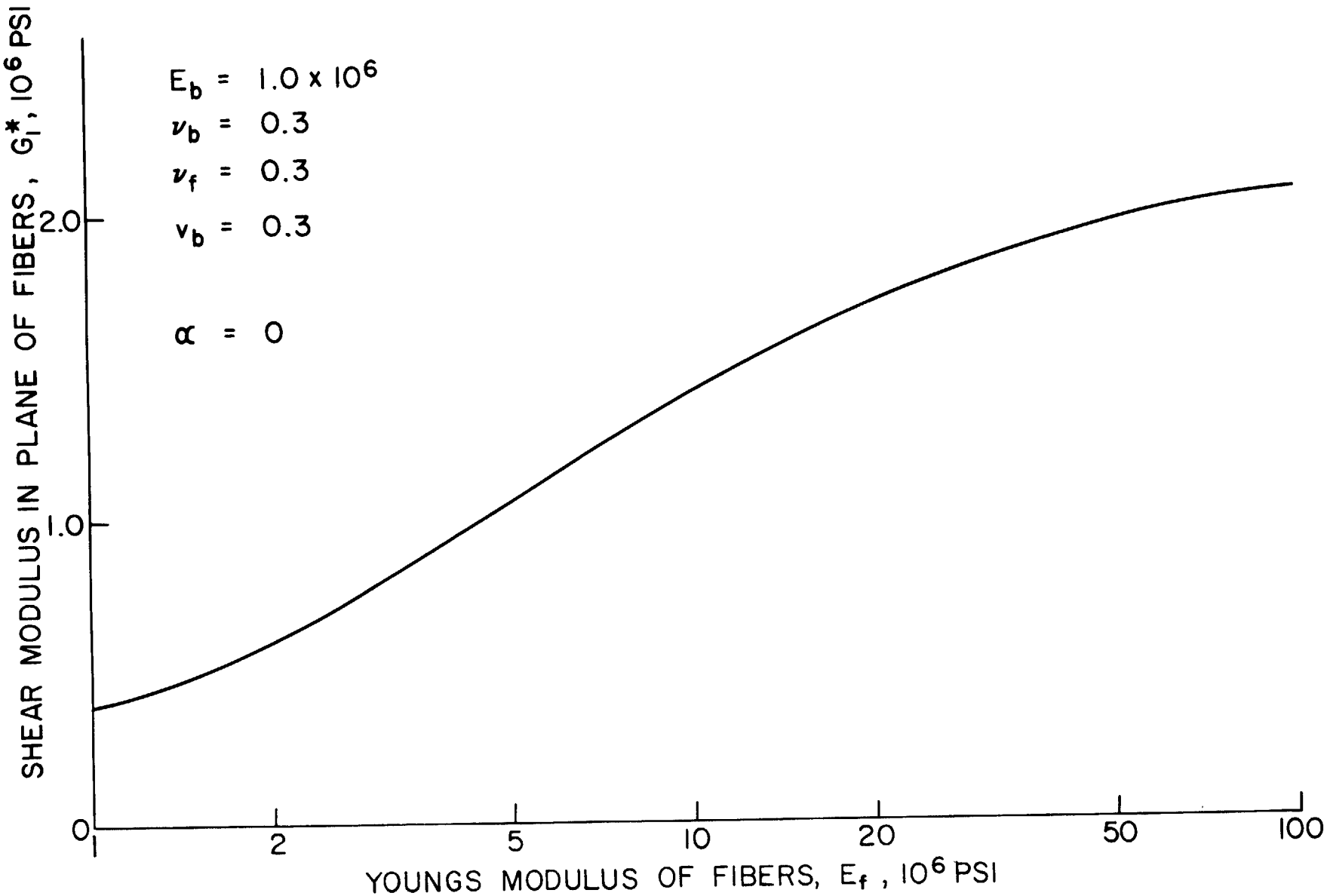

Figure 14. Effective Shear Modulus of a Fibrous Composite in the Plane of the Fibers as a Function of the Young's Modulus of the Fibers

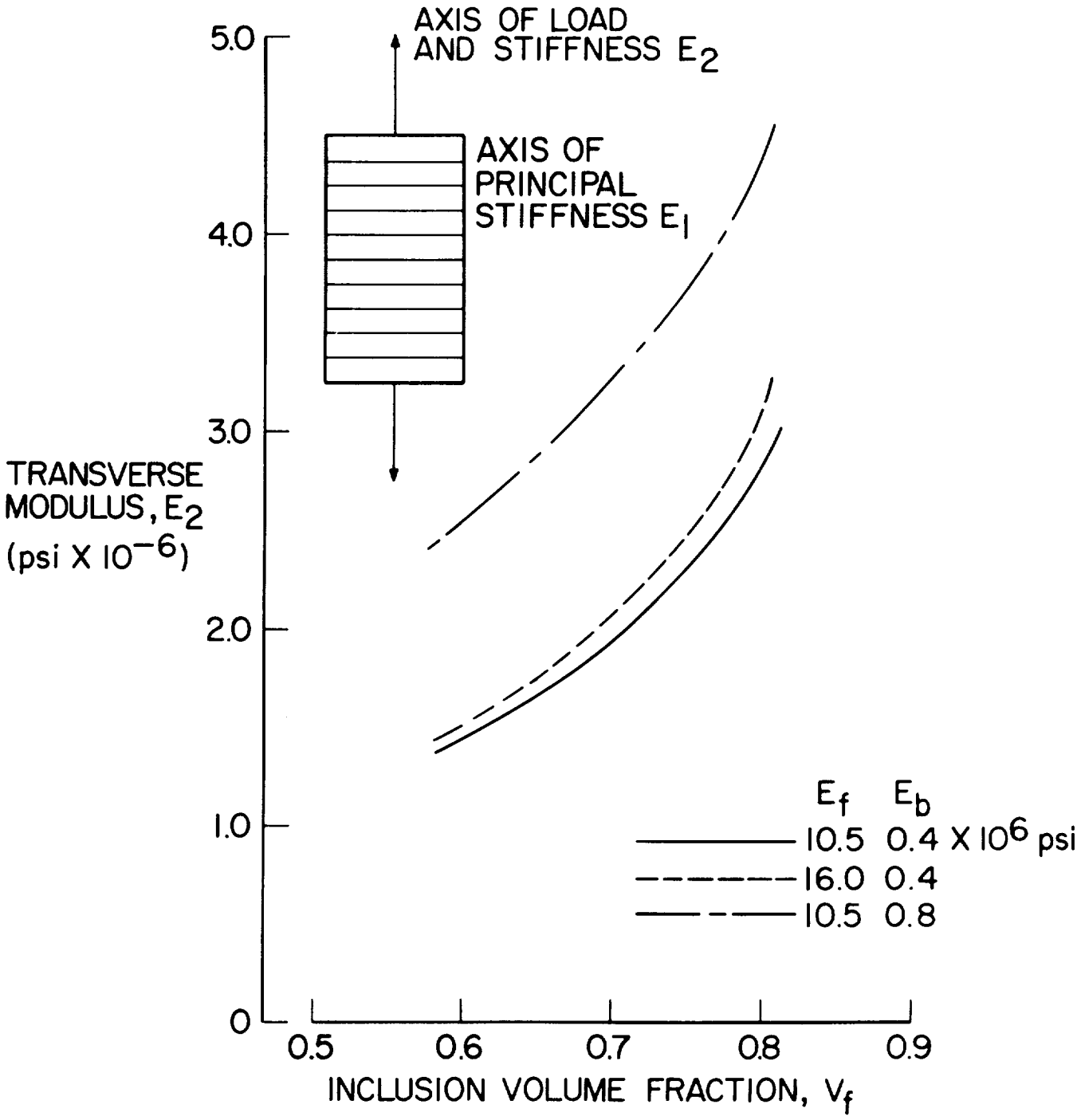

Figure 15. Effect of Transverse Cylindrical Inclusions on the Effective Young's Modulus of a Stiffened Elastic Matrix

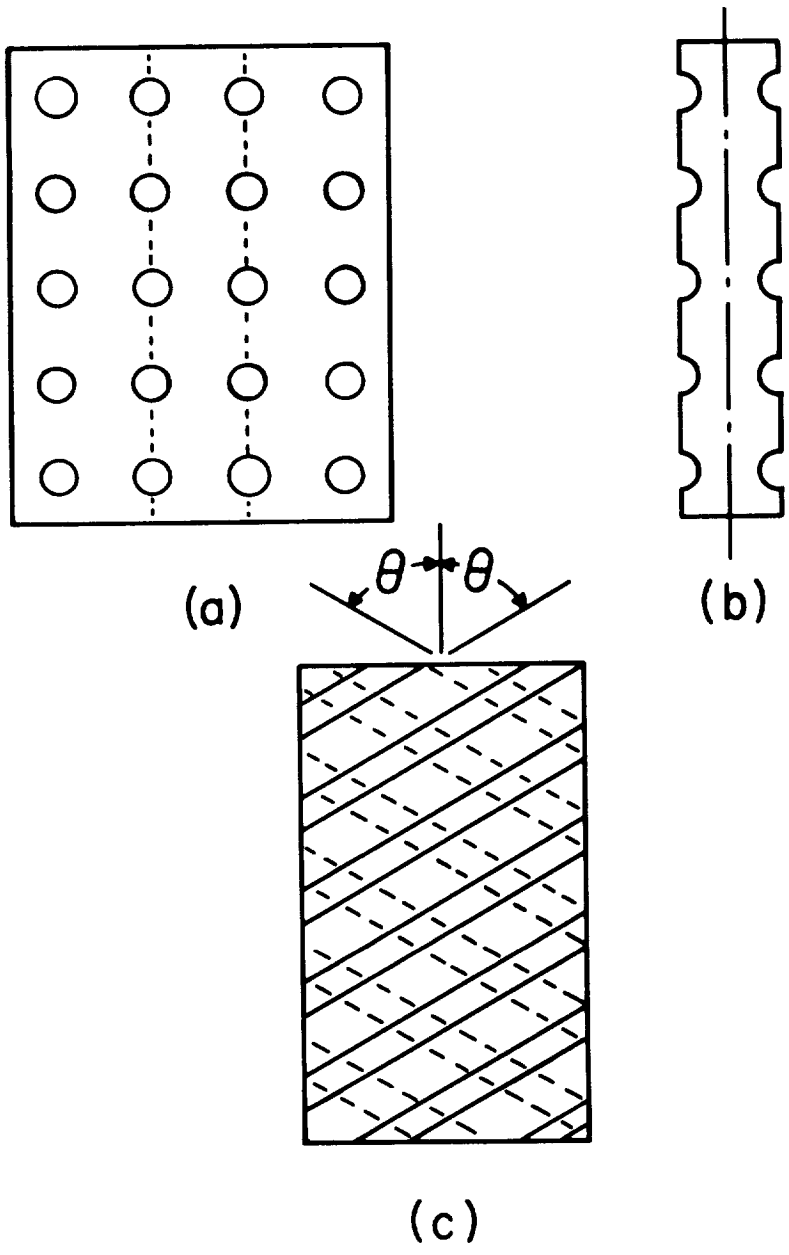

Figure 16. Model Used for Analysis of Oriented Voids

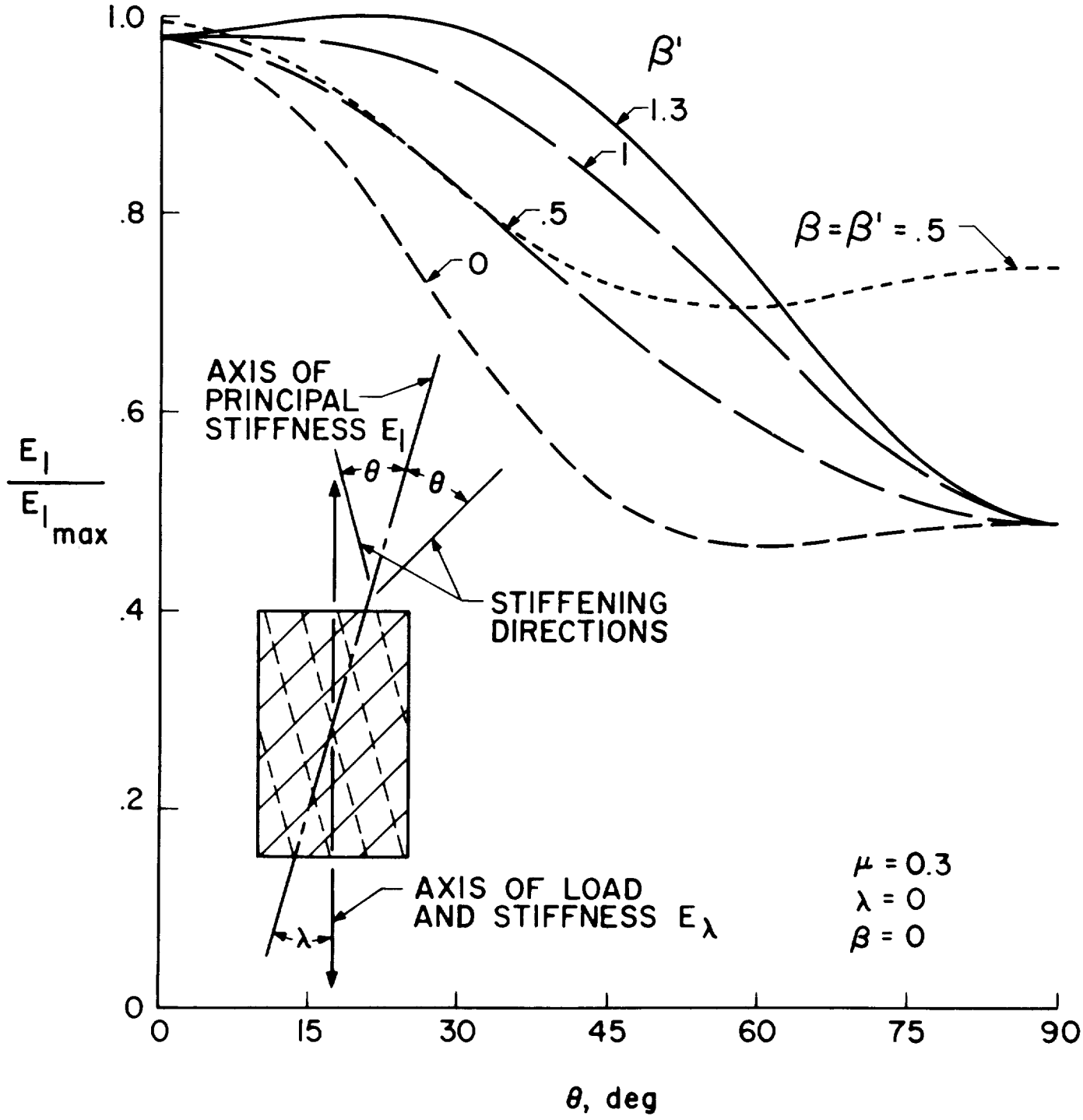

Figure 17a. Variation of Principal Stretching Stiffness with Angle of Orientation of the Holes for Various Values of Transverse Effectiveness

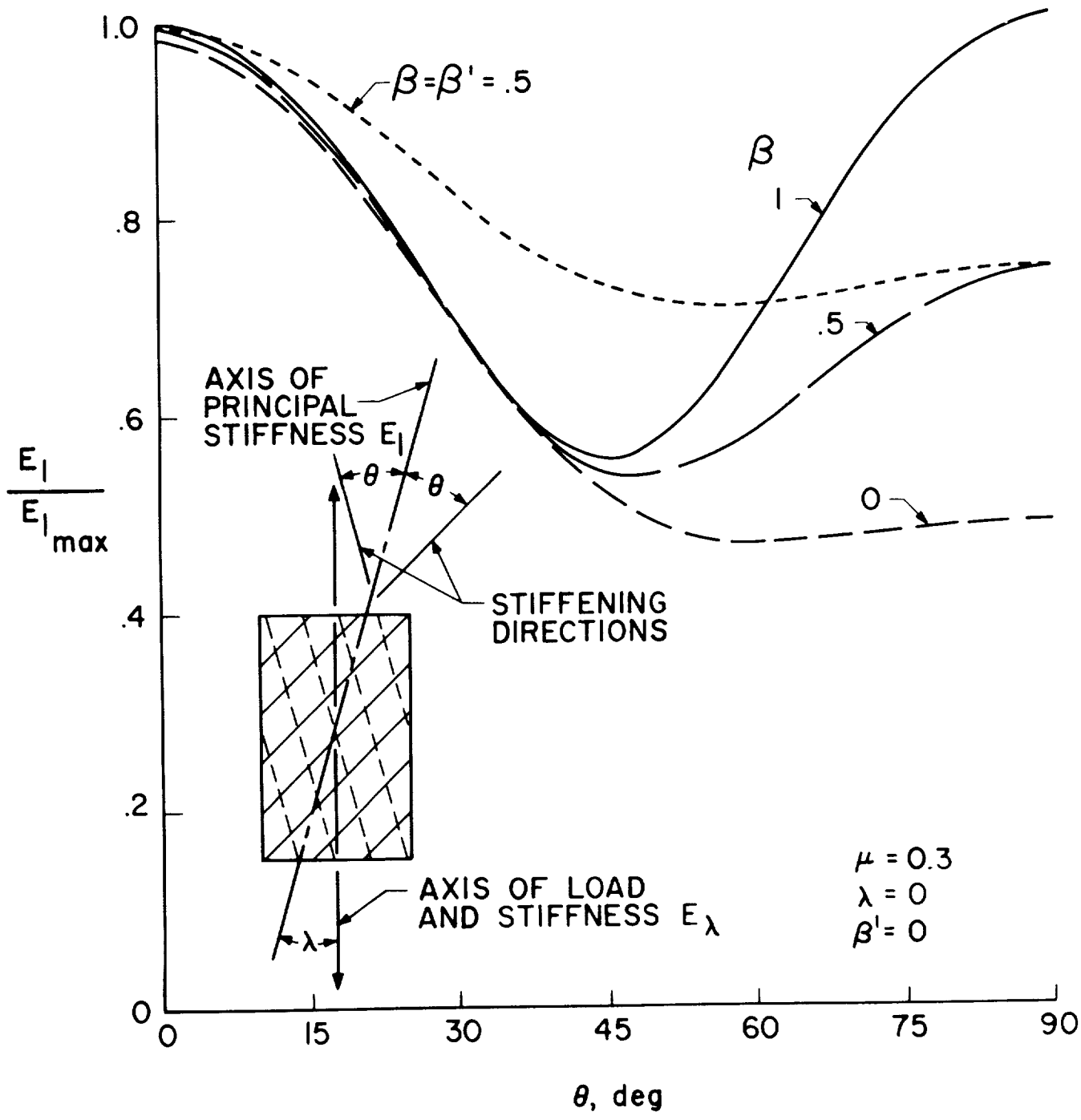

Figure 17b. Variation of Principal Stretching Stiffness with Angle of Orientation of the Holes for Various Values of Transverse Effectiveness

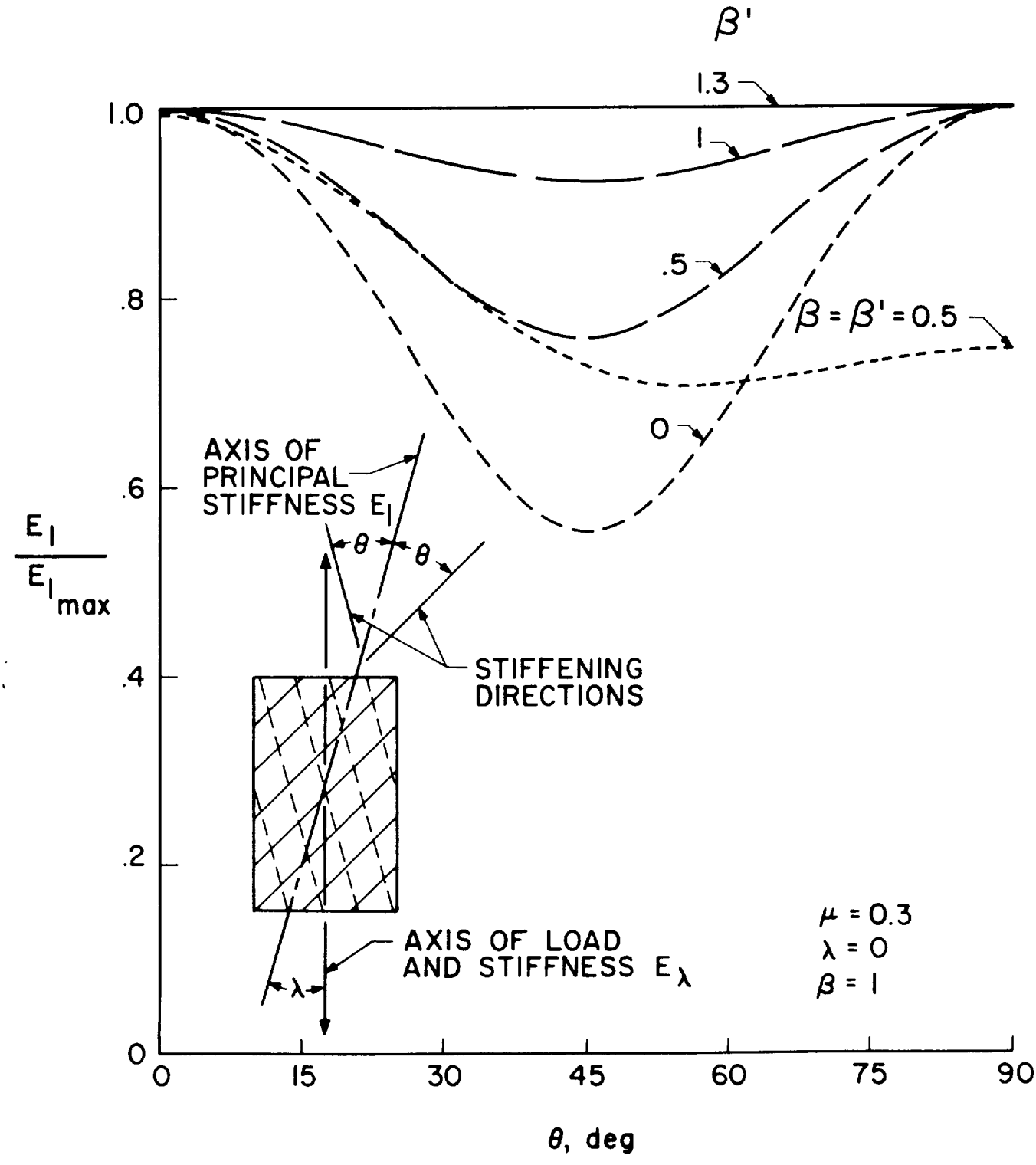

Figure 17c. Variation of Principal Stretching Stiffness with Angle of Orientation of the Holes for Various Values of Transverse Effectiveness

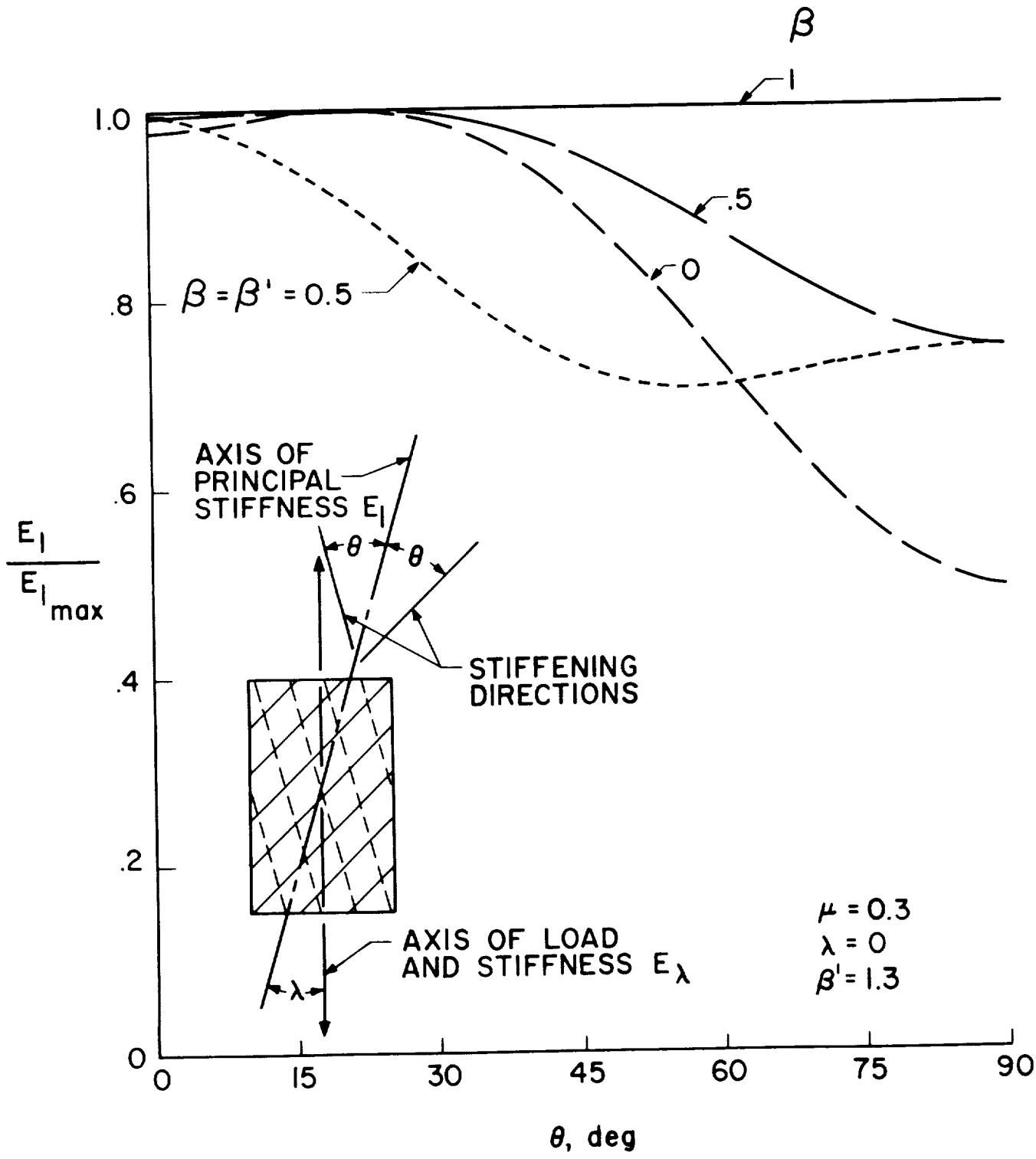

Figure 17d. Variation of Principal Stretching Stiffness with Angle or Orientation of the Holes for Various Values of Transverse Effectiveness

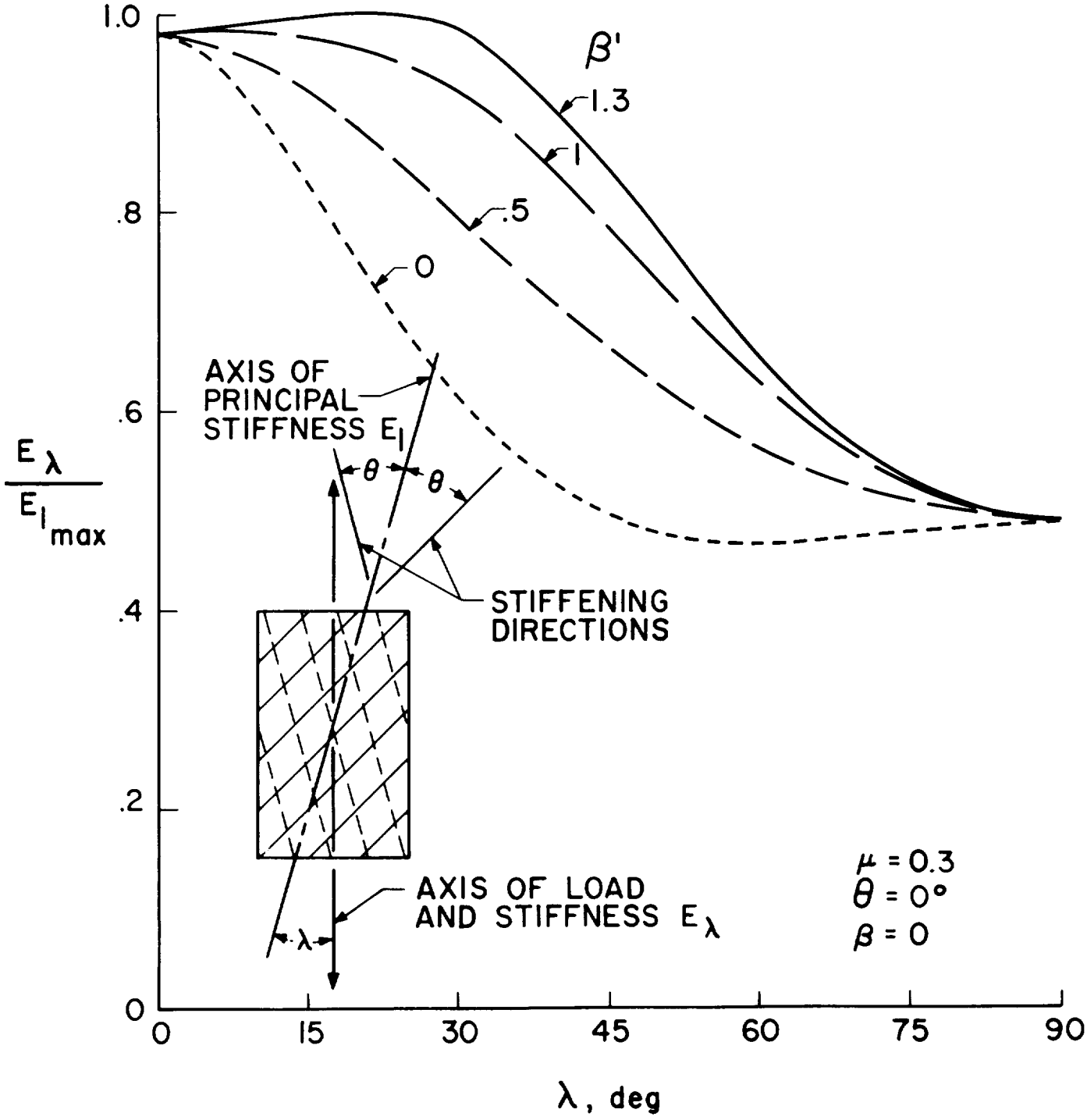

Figure 18a. Effect of Variation of Transverse Shearing Effectiveness on Stretching Stiffness

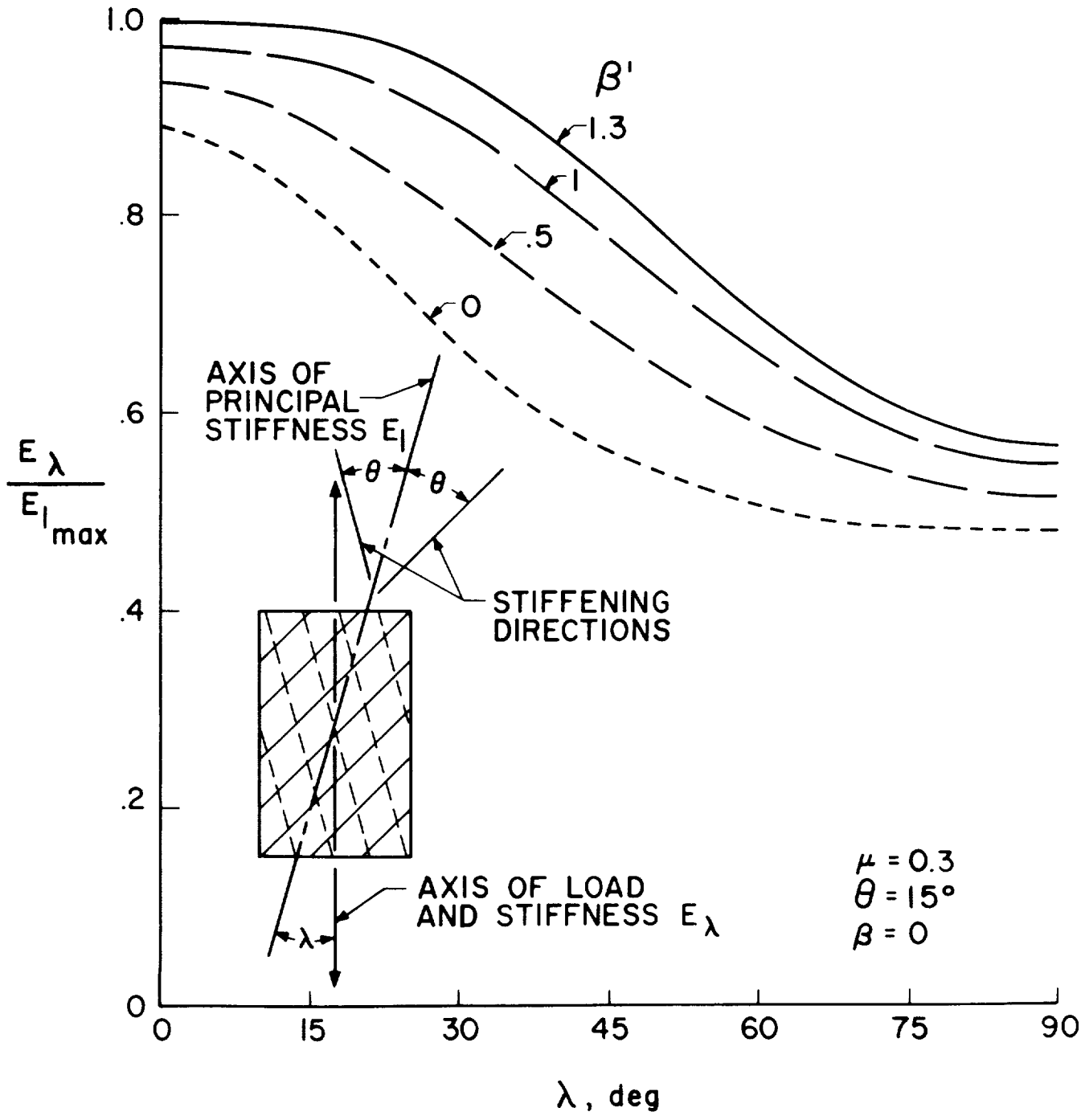

Figure 18b. Effect of Variation of Transverse Shearing Effectiveness on Stretching Stiffness

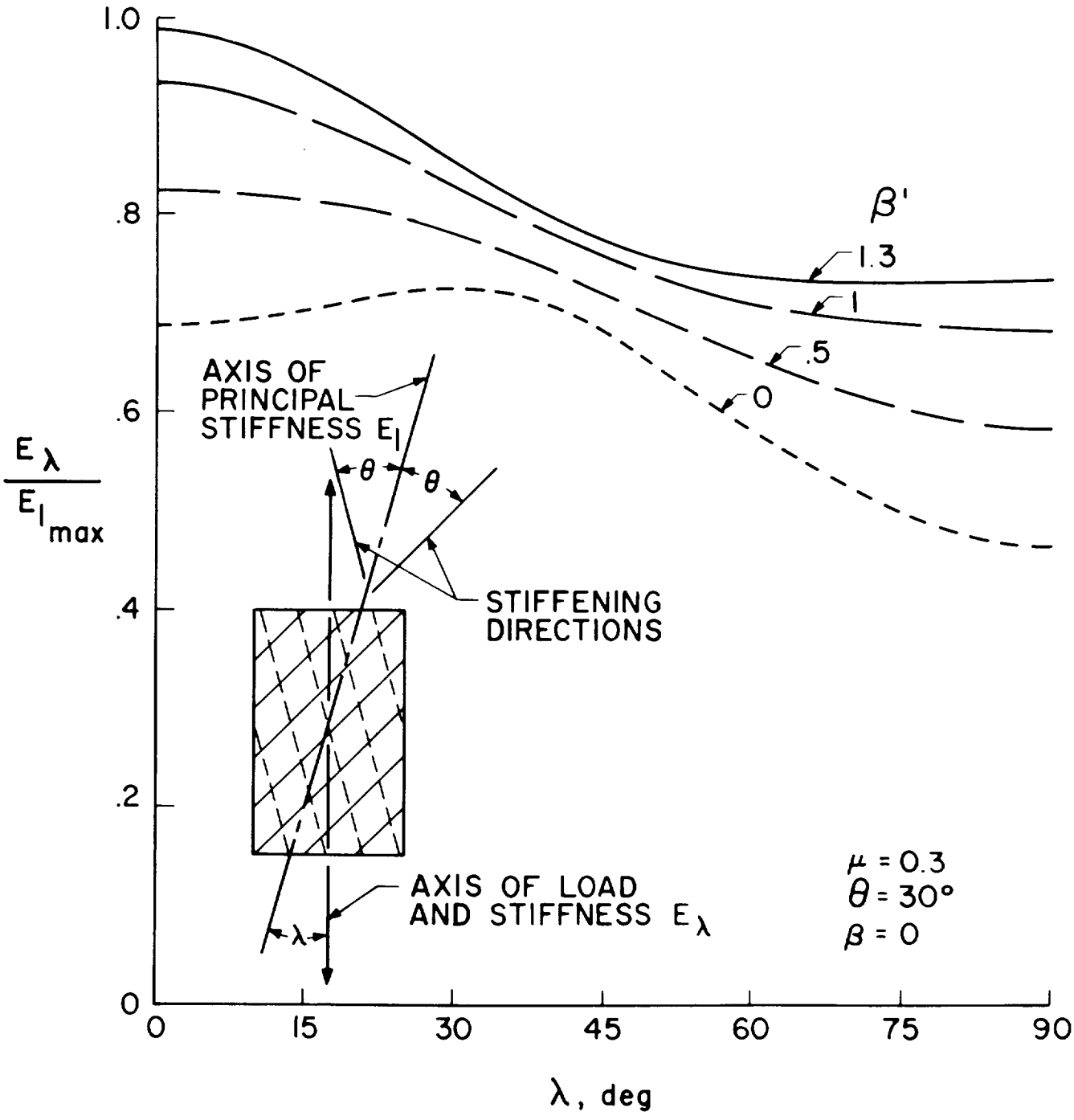

Figure 18c. Effect of Variation of Transverse Shearing Effectiveness on Stretching Stiffness

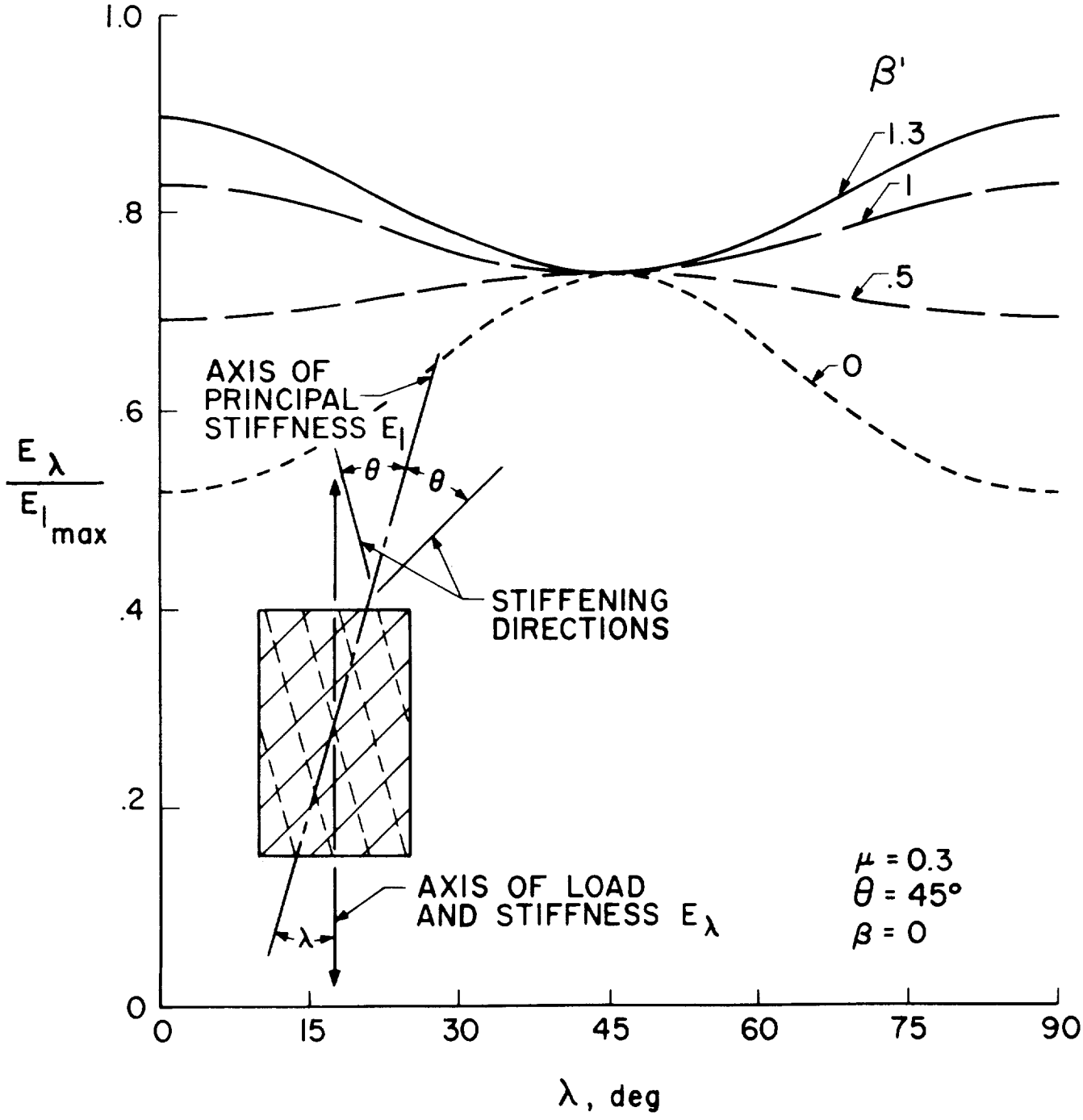

Figure 18d. Effect of Variation of Transverse Shearing Effectiveness on Stretching Stiffness

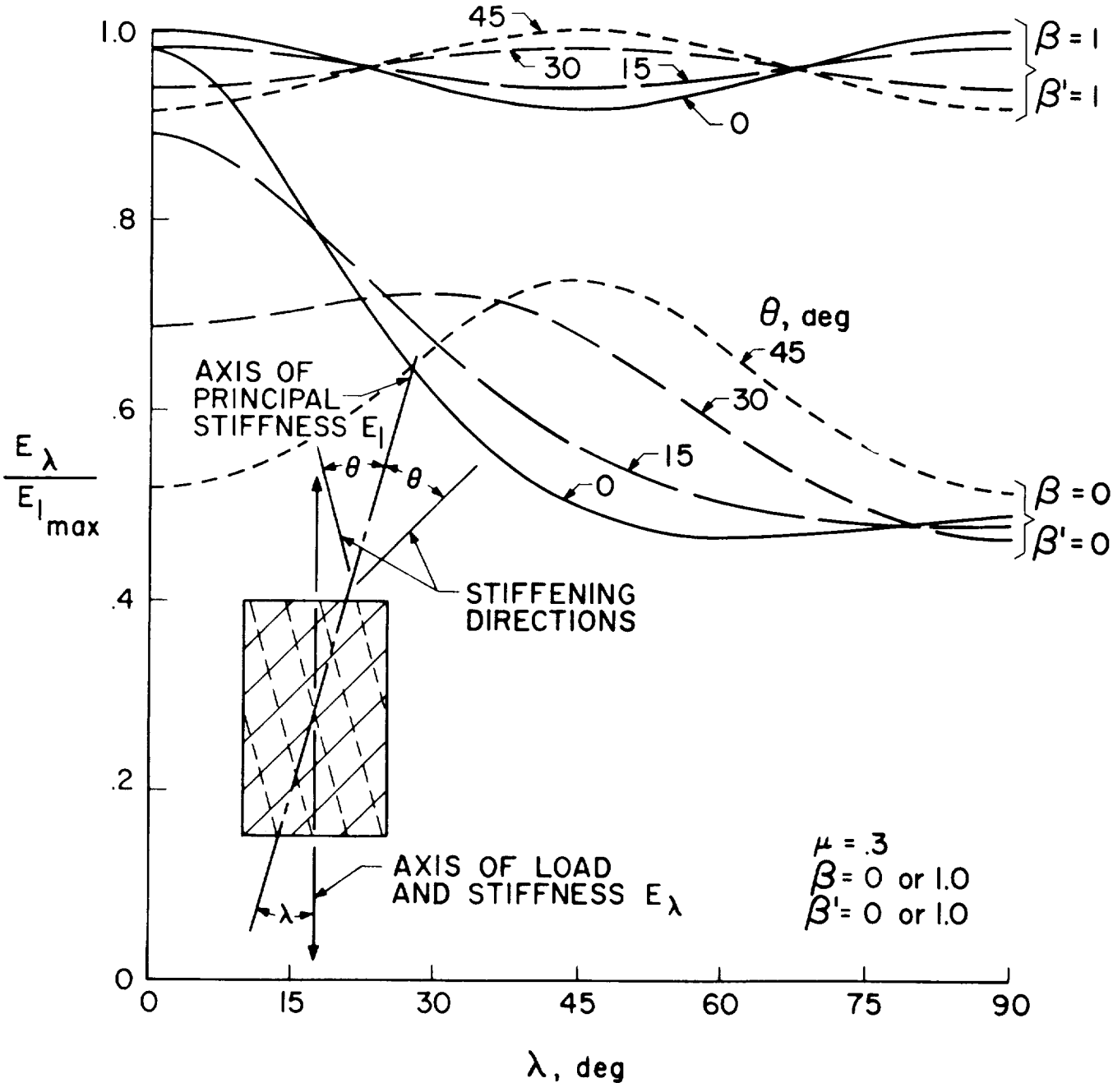

Figure 19a. Effect of Variation of Both Transverse Shearing and Stretching Stiffness on Stretching Stiffness

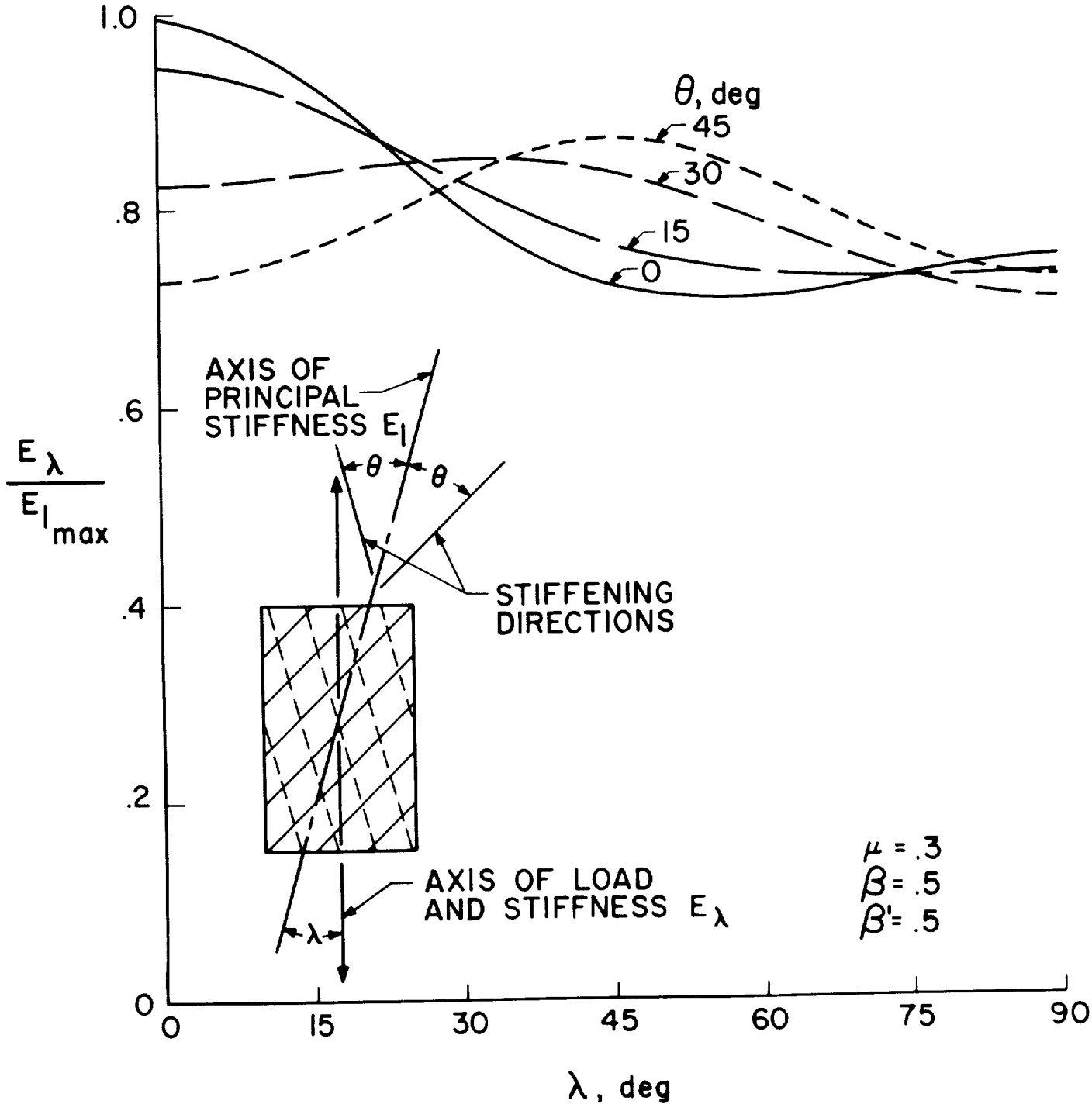

Figure 19b. Effect of Variation of Both Transverse Shearing and Stretching Stiffness on Stretching Stiffness

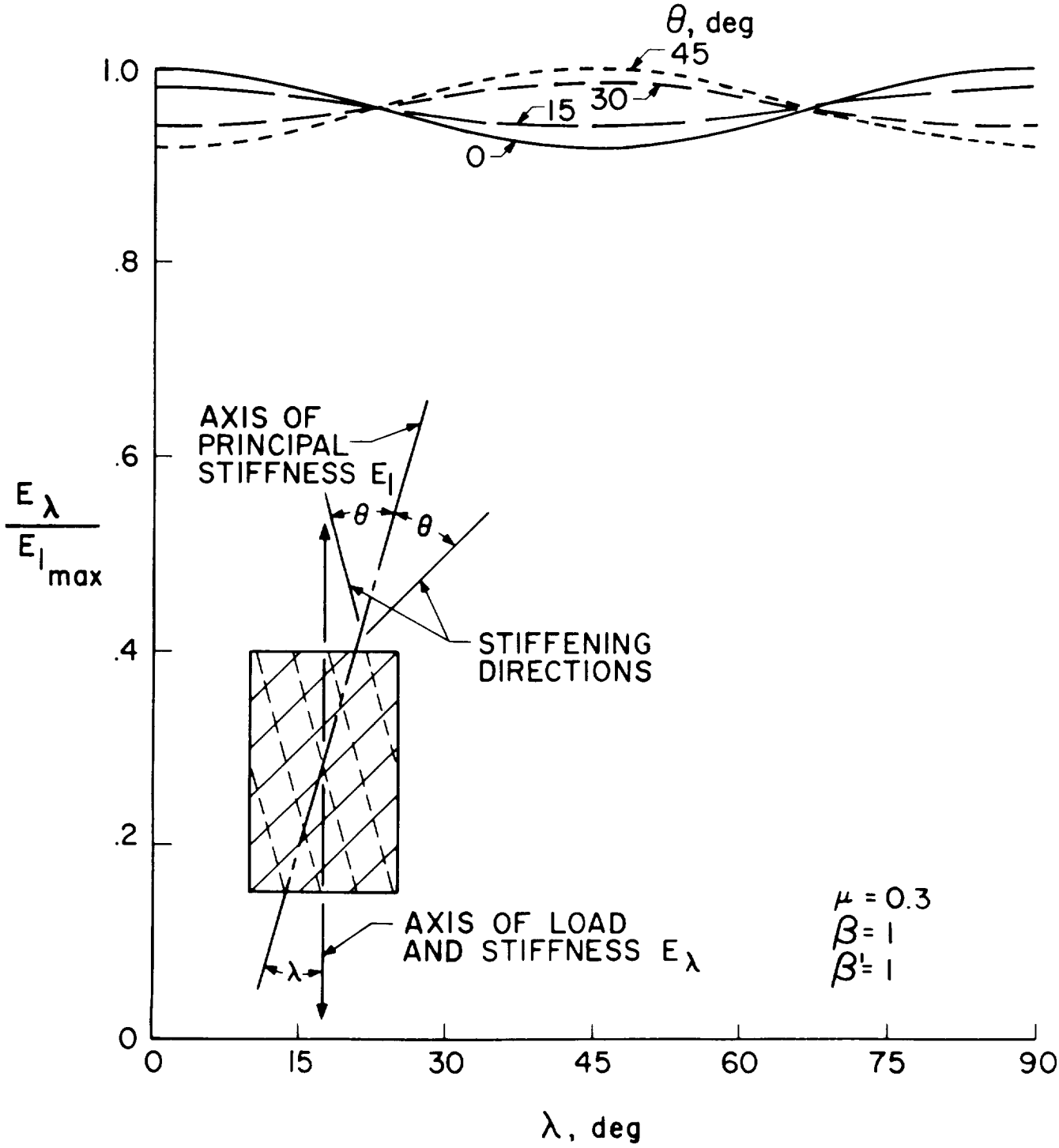

Figure 19c. Effect of Variation of Both Transverse Shearing and Stretching Stiffness on Stretching Stiffness

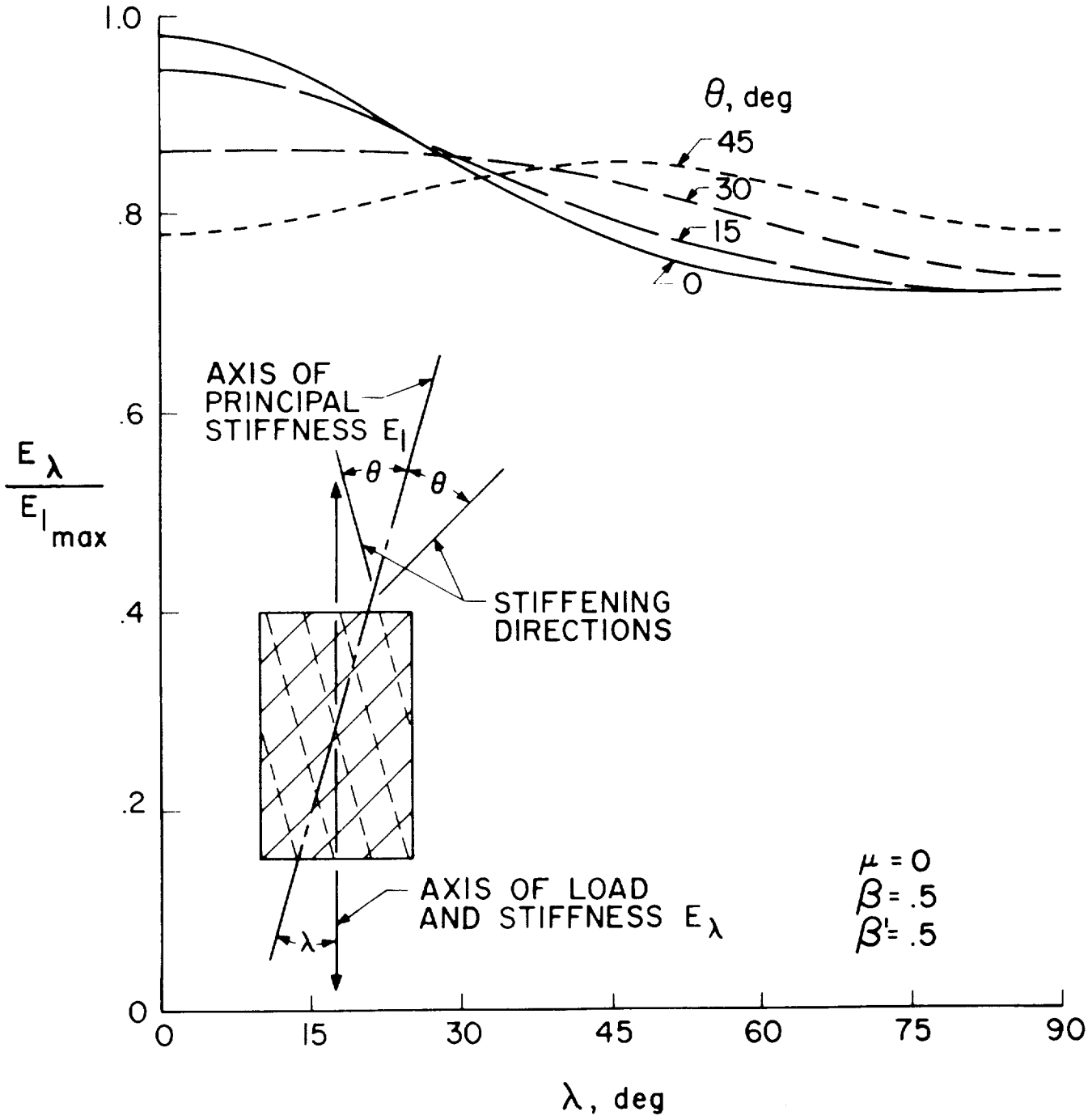

Figure 20a. Effects of Variations in Poisson's Ratio on Stretching Stiffness

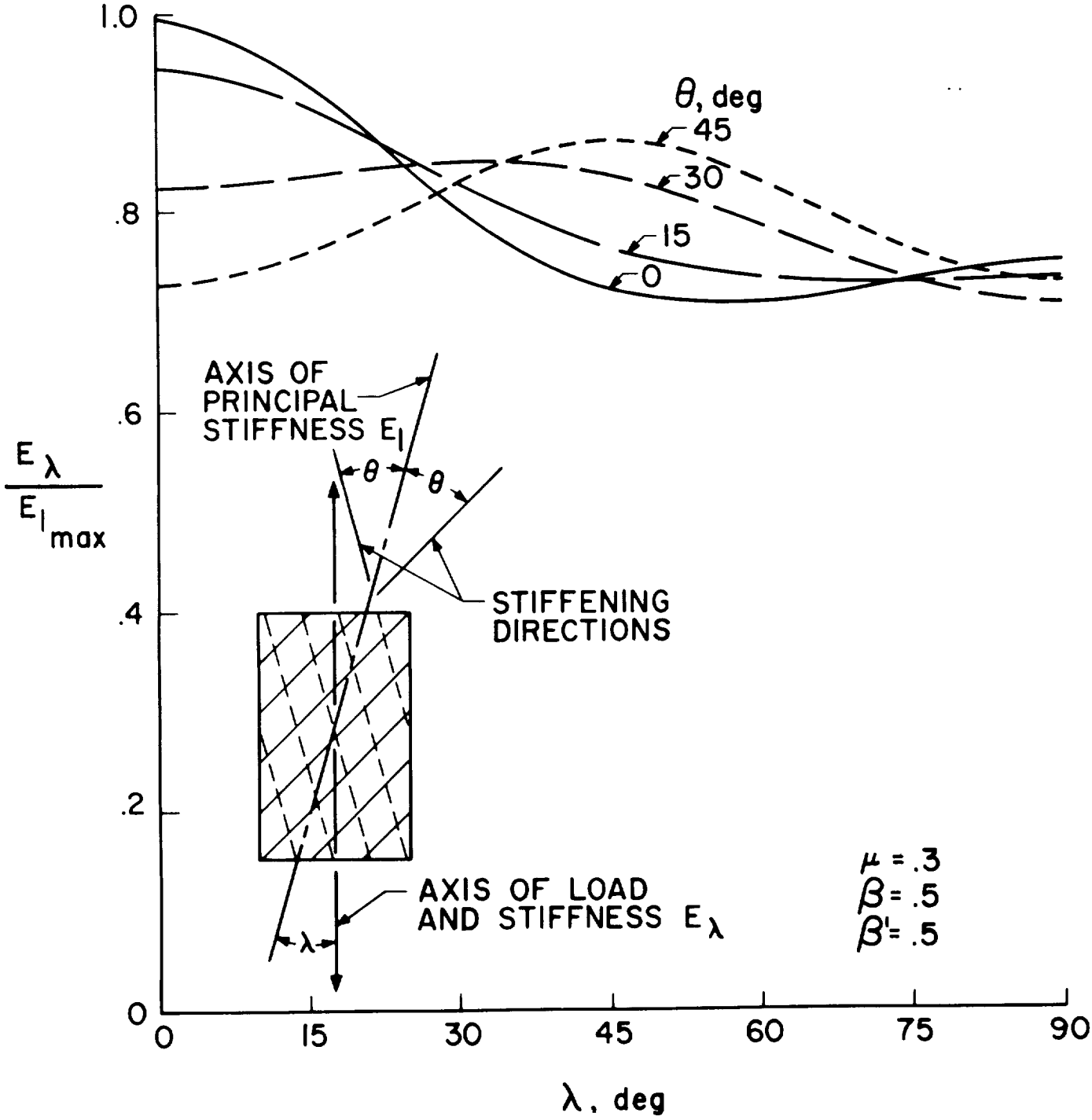

Figure 20b. Effect of Variation of Both Transverse Shearing and Stretching Stiffness on Stretching Stiffness

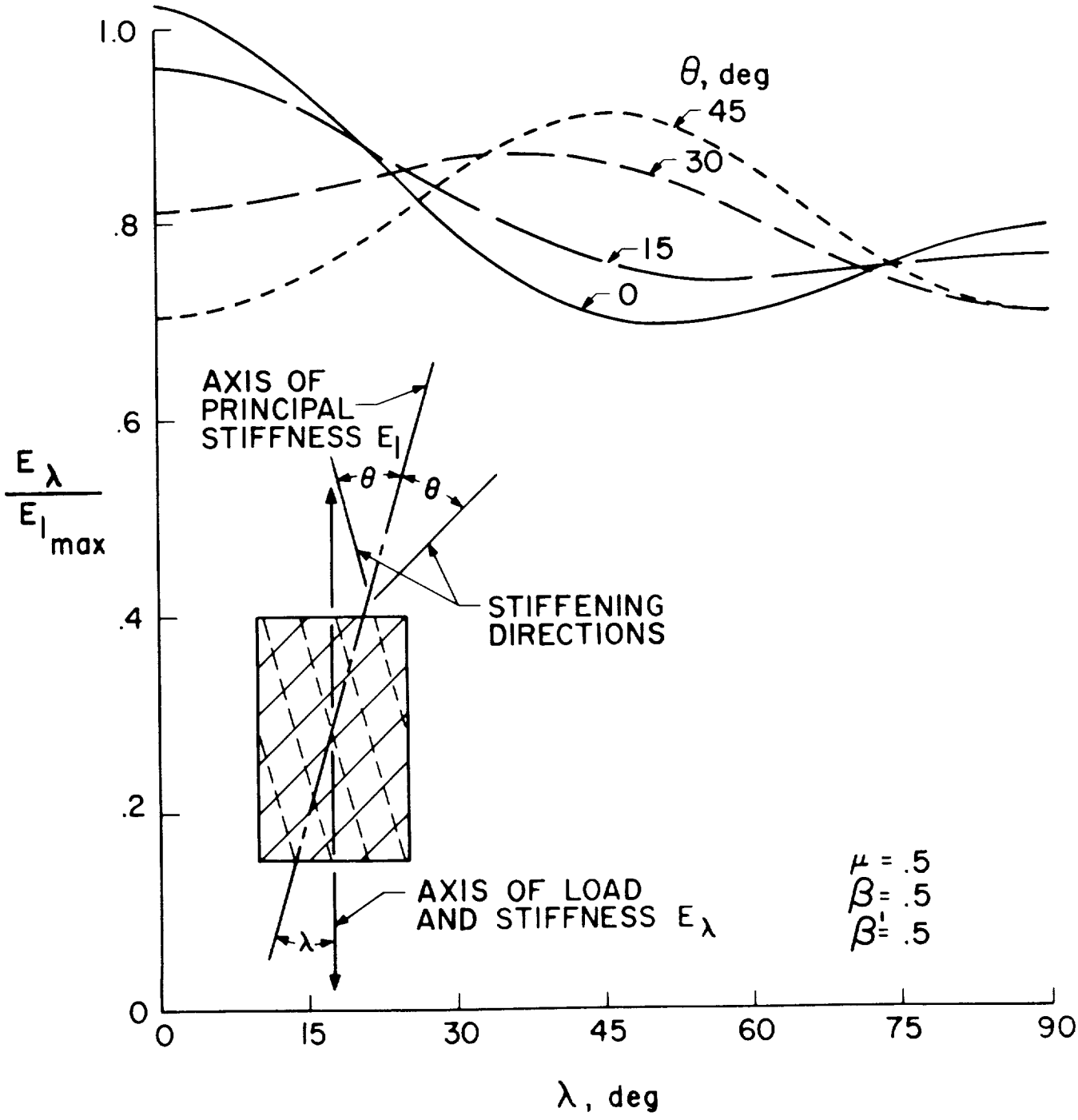

Figure 20c. Effects of Variations in Poisson's Ratio on Stretching Stiffness

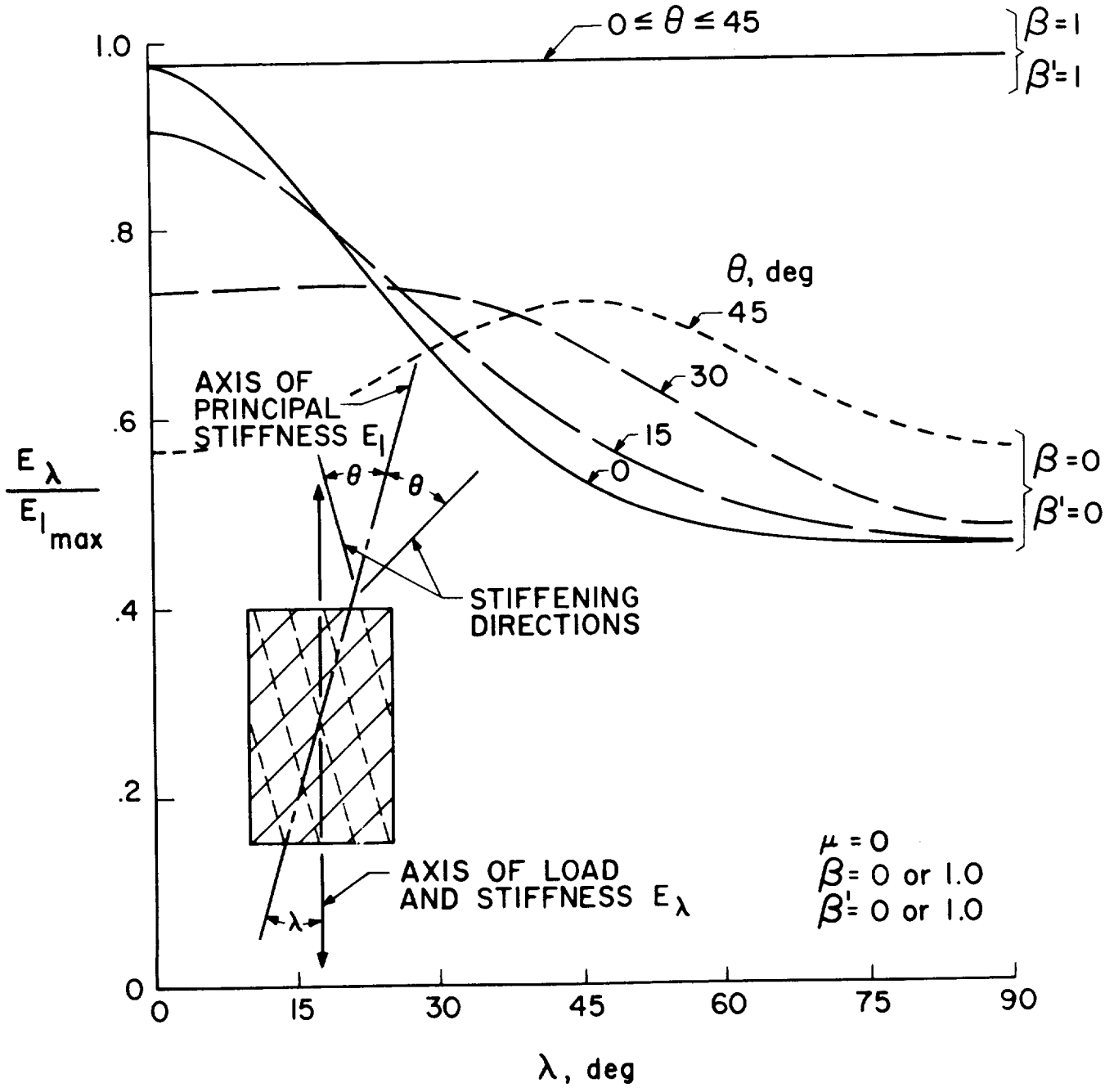

Figure 21a. Combined Effects of Variations in Angles of Orientation of Holes, Transverse Effectiveness, and Poisson's Ratio on Stretching Stiffness

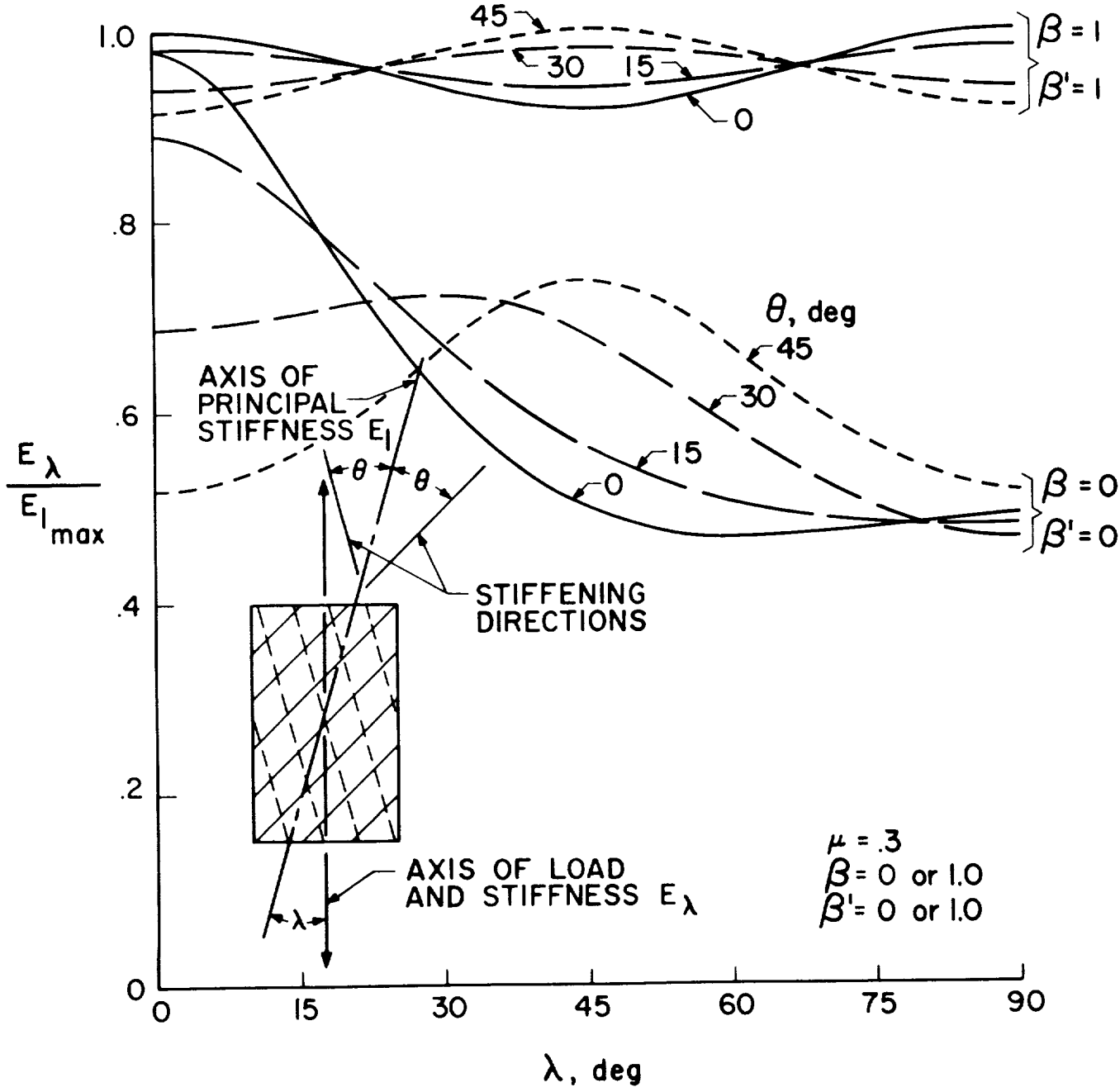

Figure 21b. Effect of Variation of Both Transverse Shearing and Stretching Stiffness on Stretching Stiffness

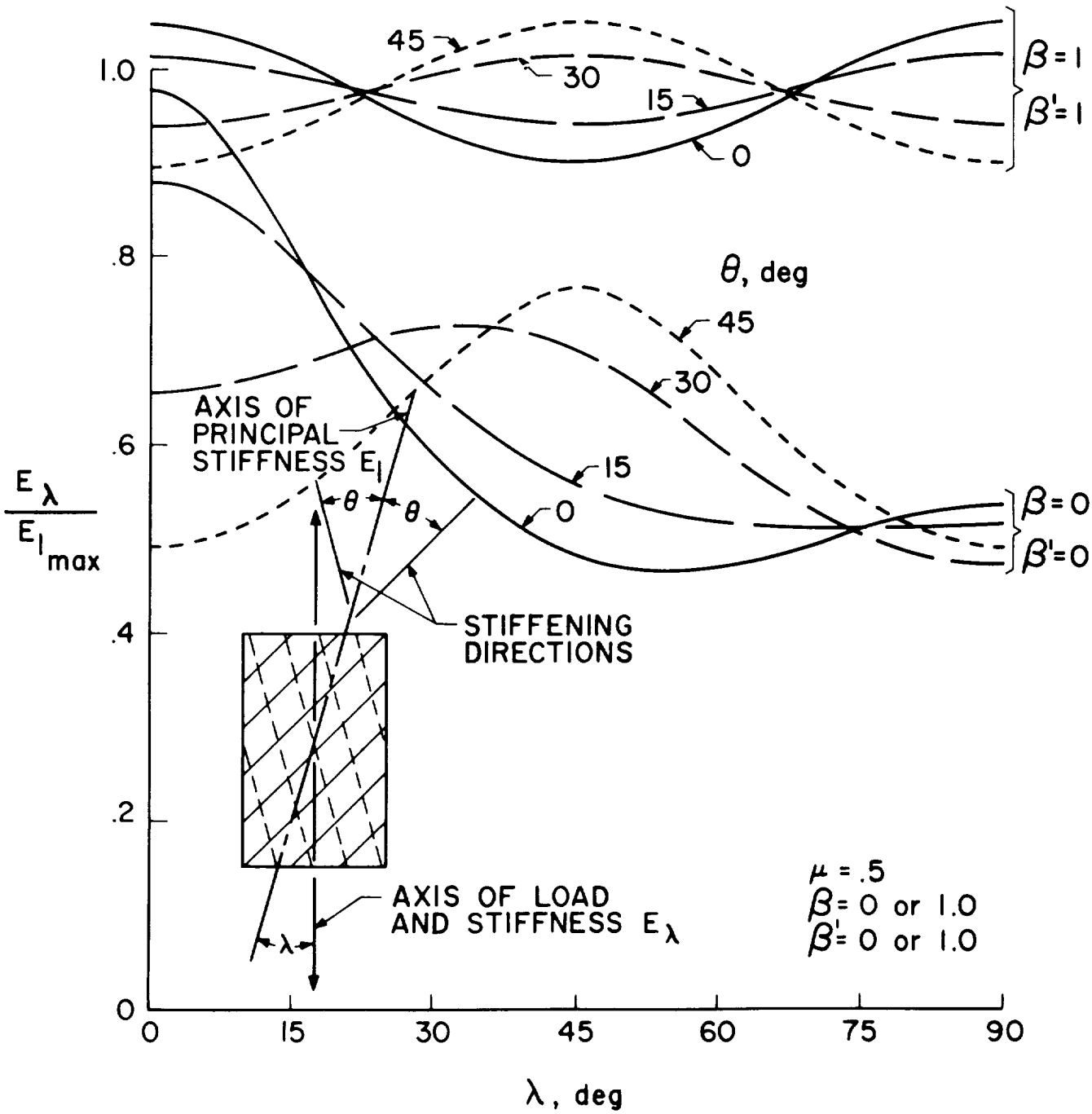

Figure 21c. Combined Effects of Variations in Angles of Orientation of Holes, Transverse Effectiveness, and Poisson's Ratio on Stretching Stiffness

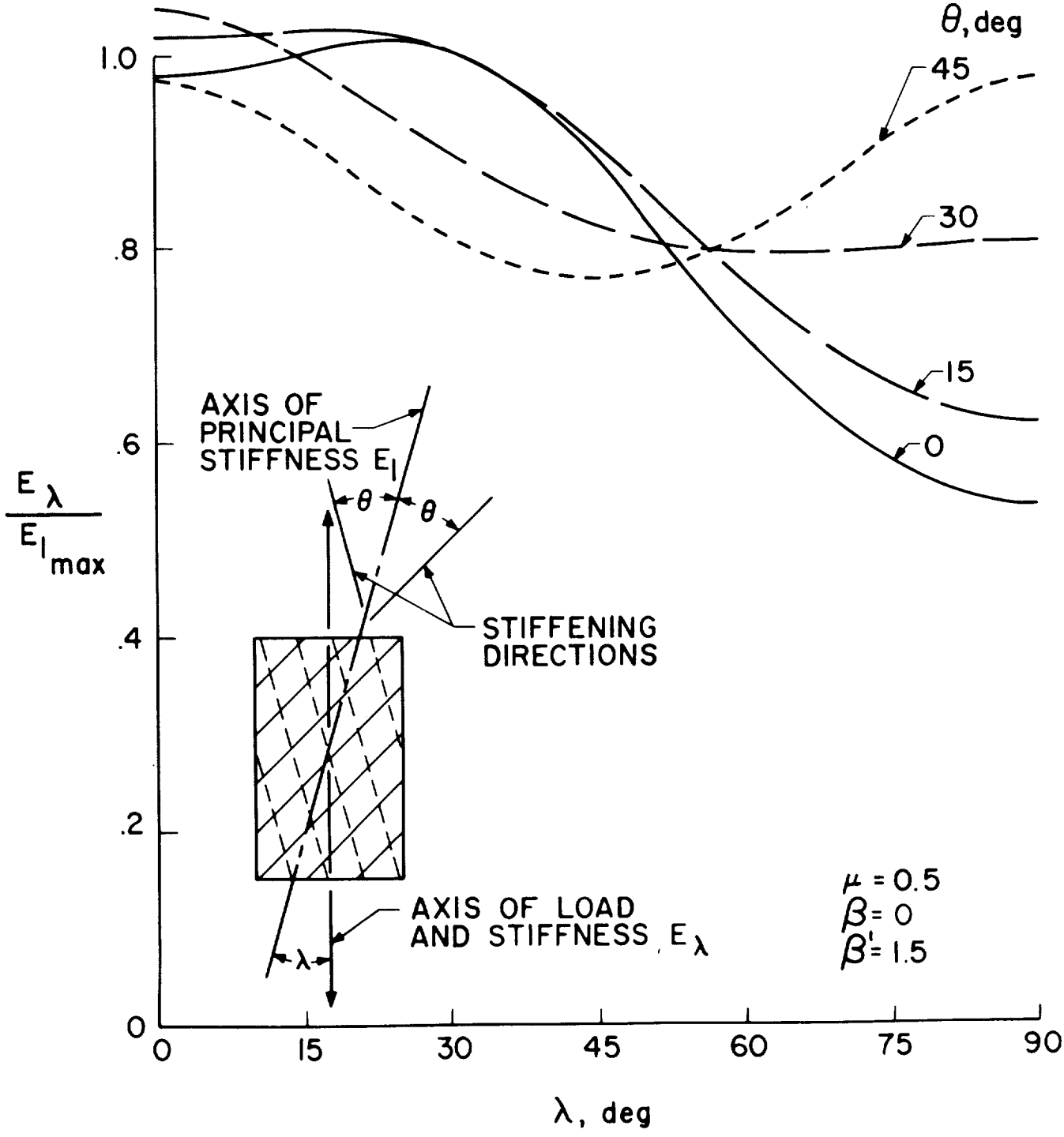

Figure 21d. Combined Effects of Variations in Angles of Orientation of Holes, Transverse Effectiveness, and Poisson's Ratio on Stretching Stiffness

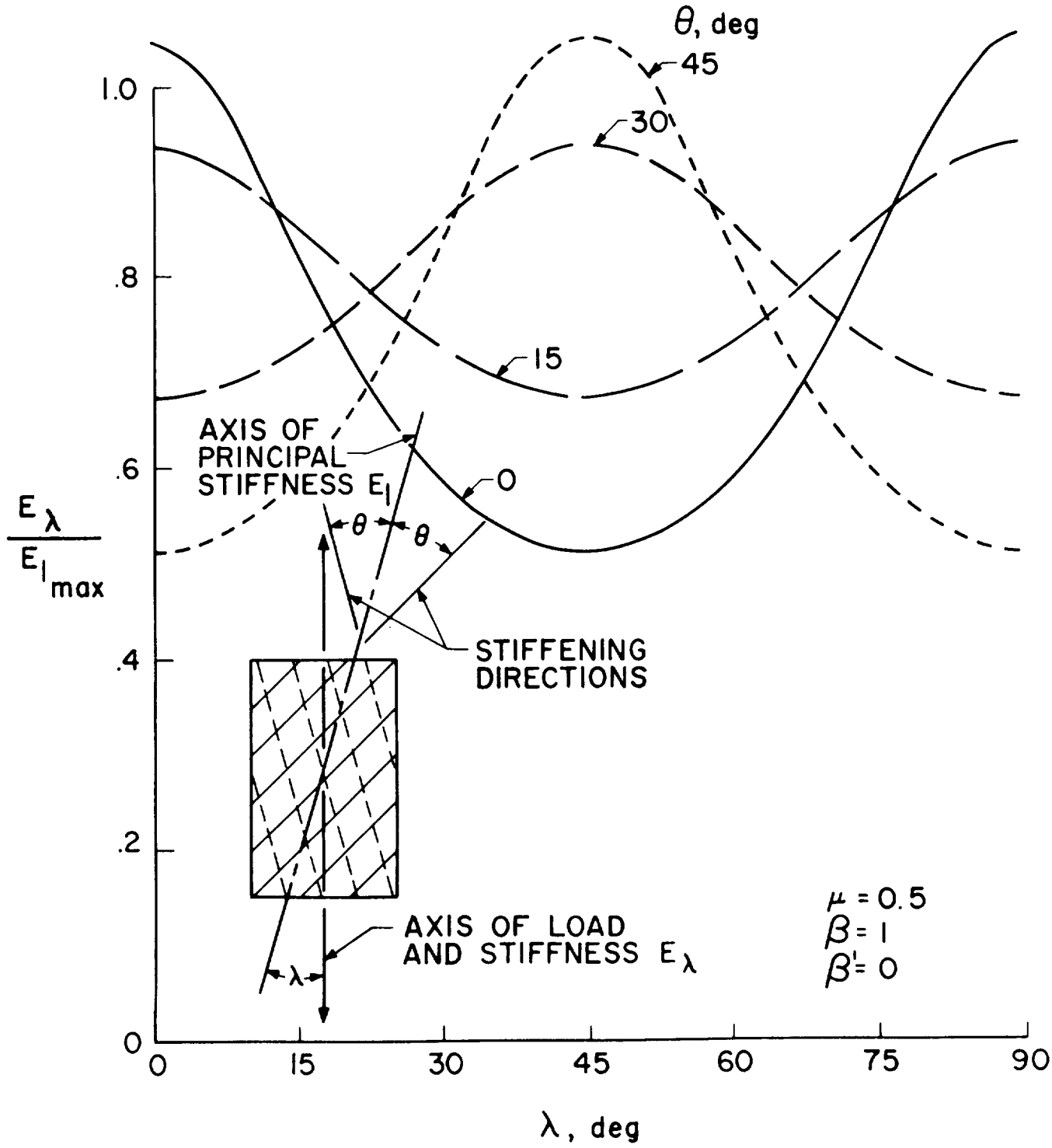

Figure 21e. Combined Effects of Variations in Angles of Orientation of Holes, Transverse Effectiveness, and Poisson's Ratio on Stretching Stiffness

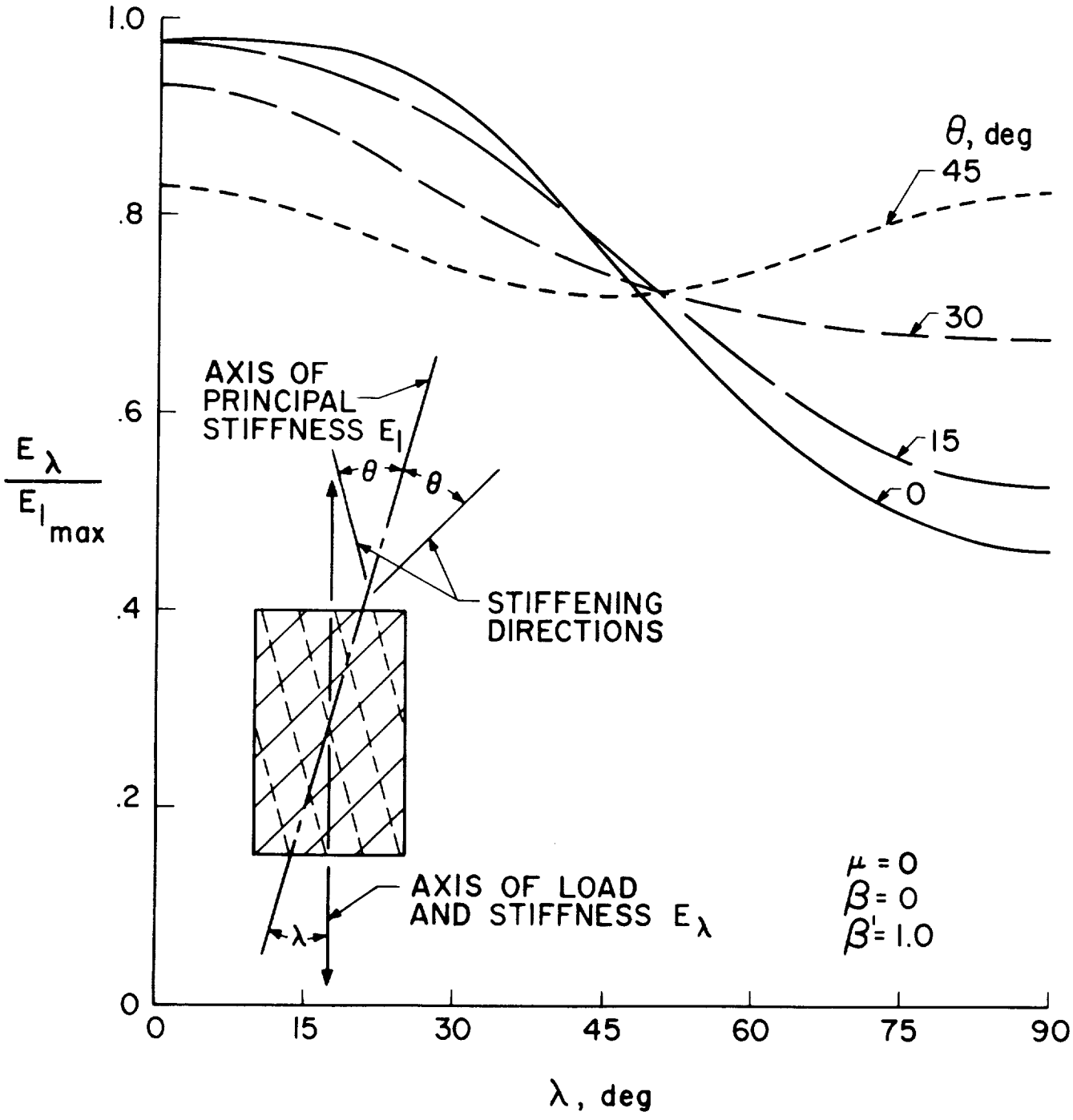

Figure 21f. Combined Effects of Variations in Angles of Orientation of Holes, Transverse Effectiveness, and Poisson's Ratio on Stretching Stiffness

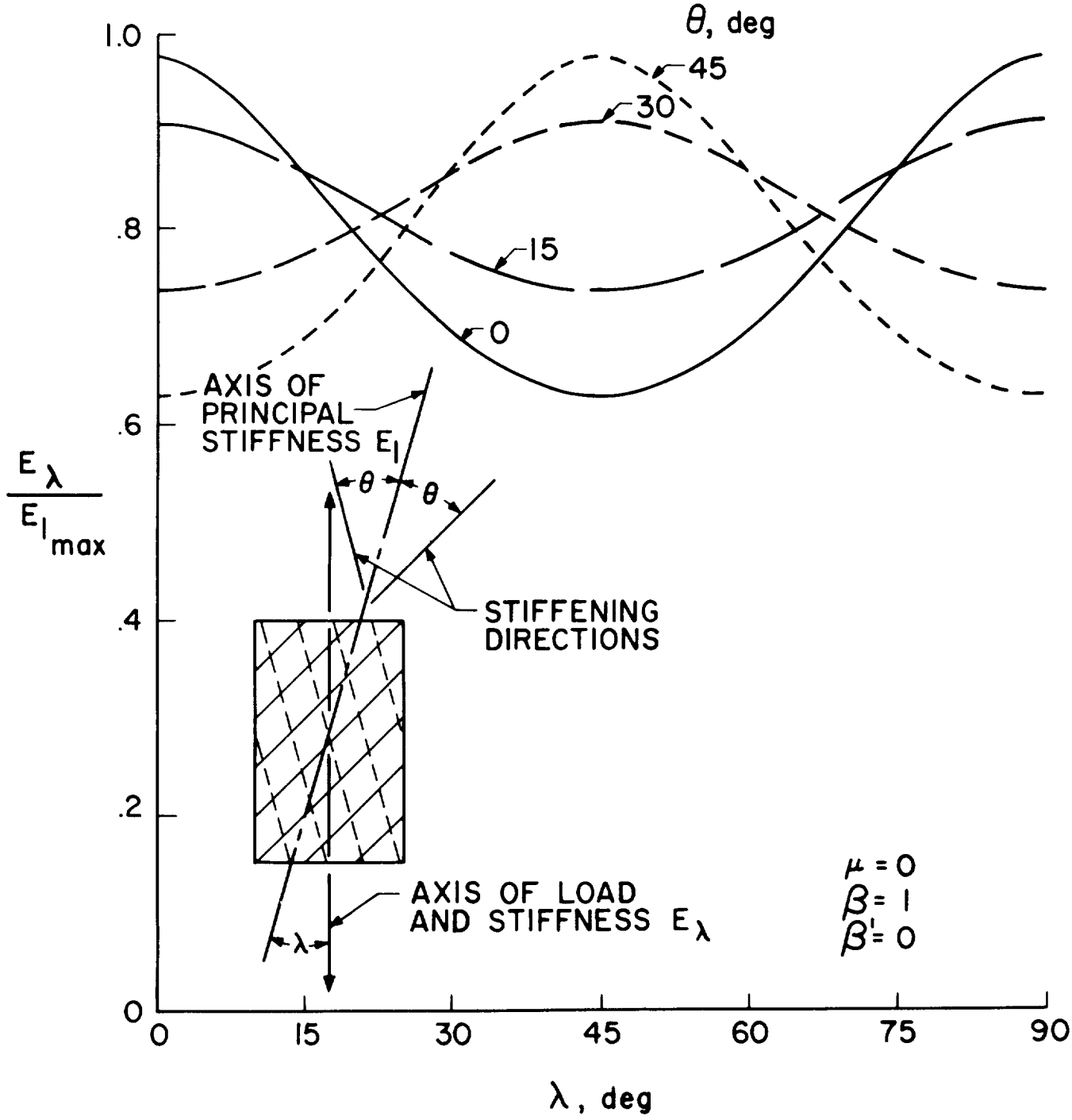

Figure 21g. Combined Effects of Variations in Angles of Orientation of Holes, Transverse Effectiveness, and Poisson's Ratio on Stretching Stiffness

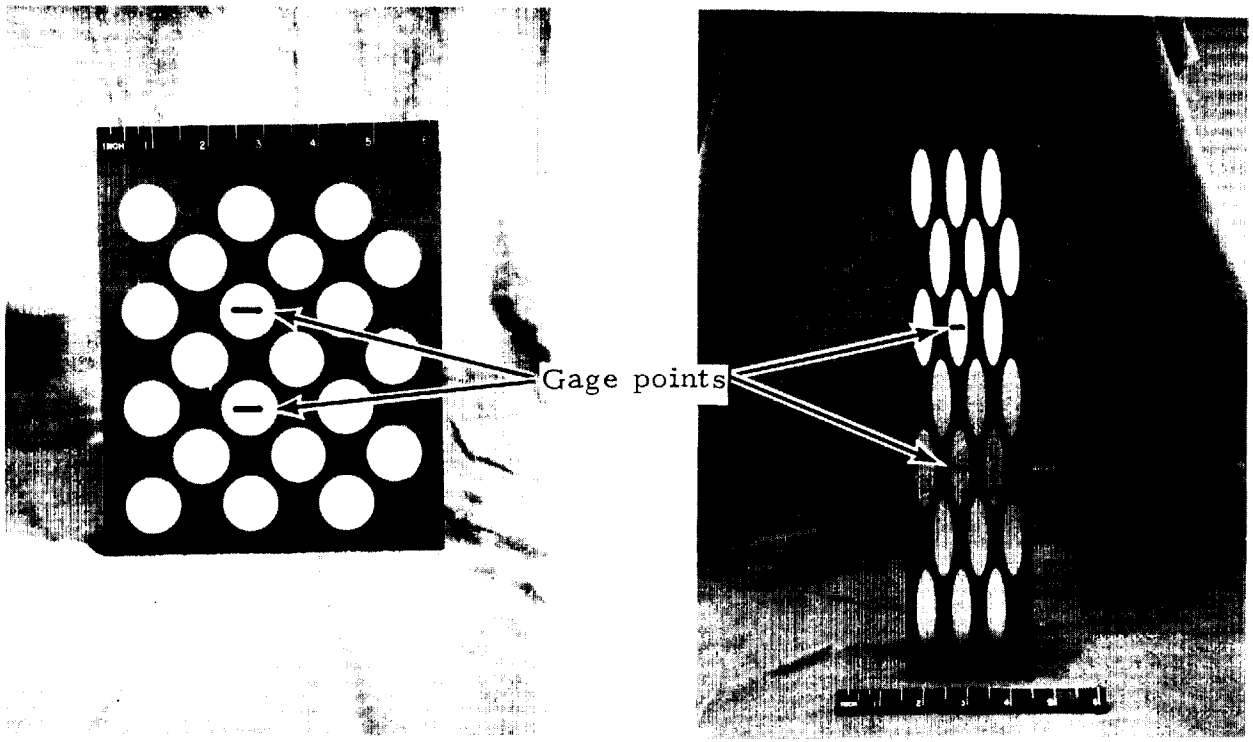

Inclusion Aspect Ratio = 1

Young's Modulus = 0.98×10^6 psi

Inclusion Aspect Ratio = 4

Young's Modulus = 1.77×10^6 psi

Figure 22. Test Specimens for Influences of Fiber Shape on the Effective Transverse Composite Modulus

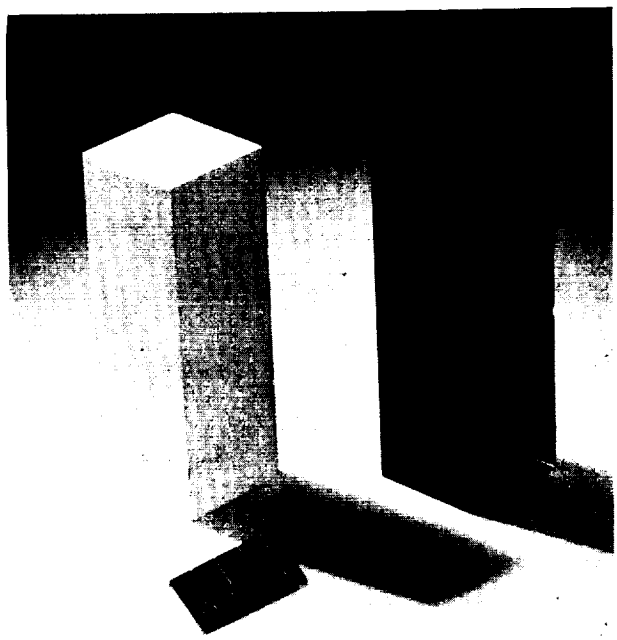

Figure 23. Experimental Solid Alumina Particle-Epoxy Composites for Young's Modulus Measurement

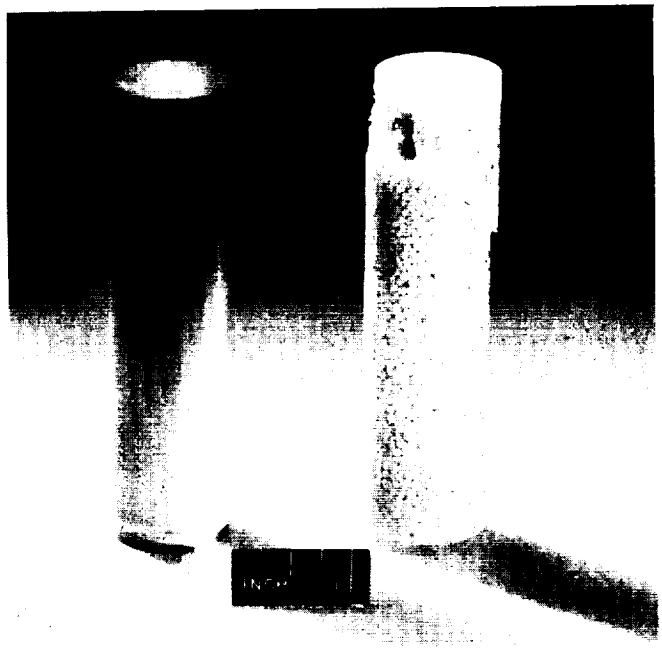

Figure 24. Experimental Hollow Alumina Particle-Epoxy Composites for Young's Modulus Measurement

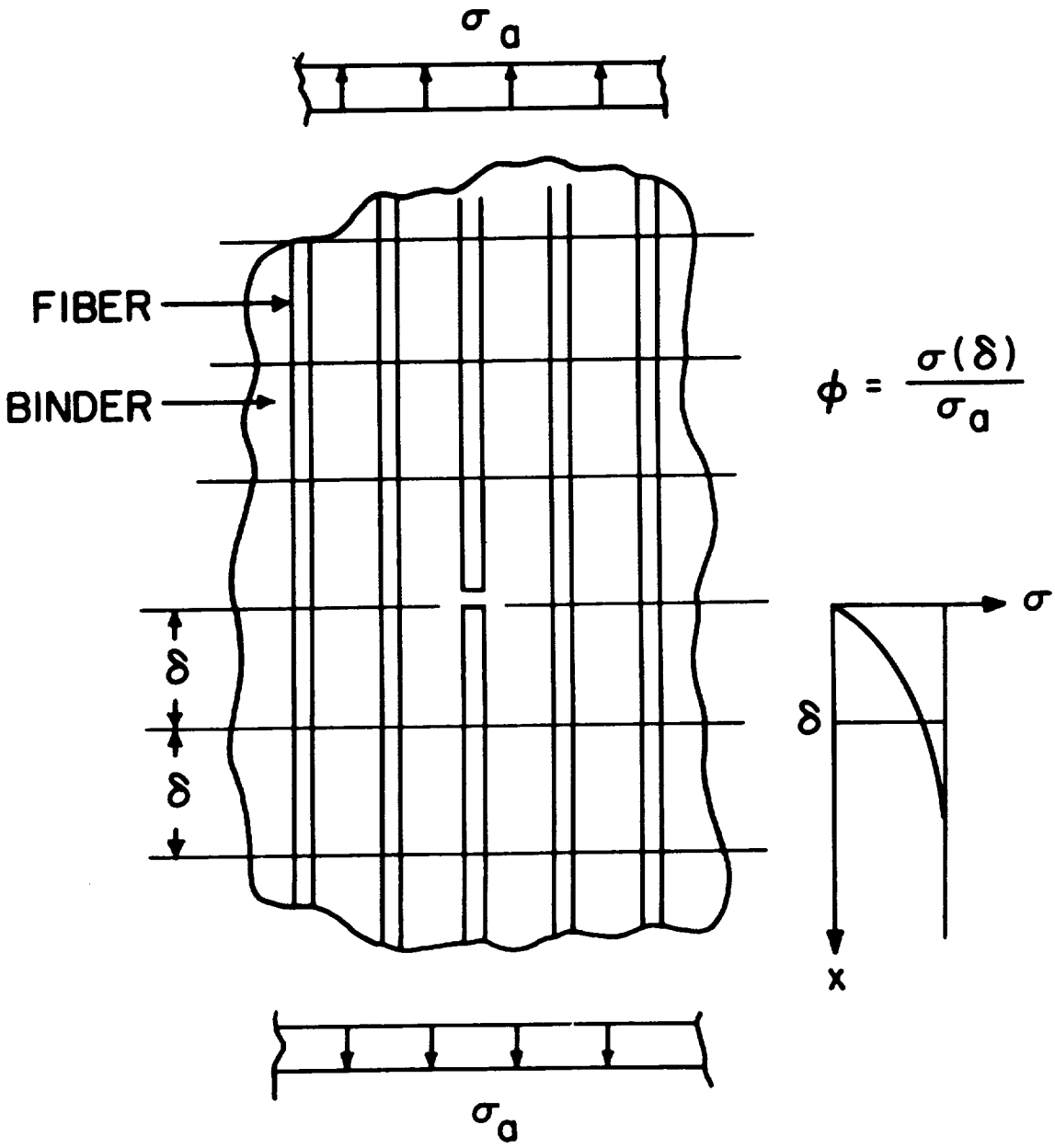

Figure 25. Fiber Reinforced Composite - Failure Model

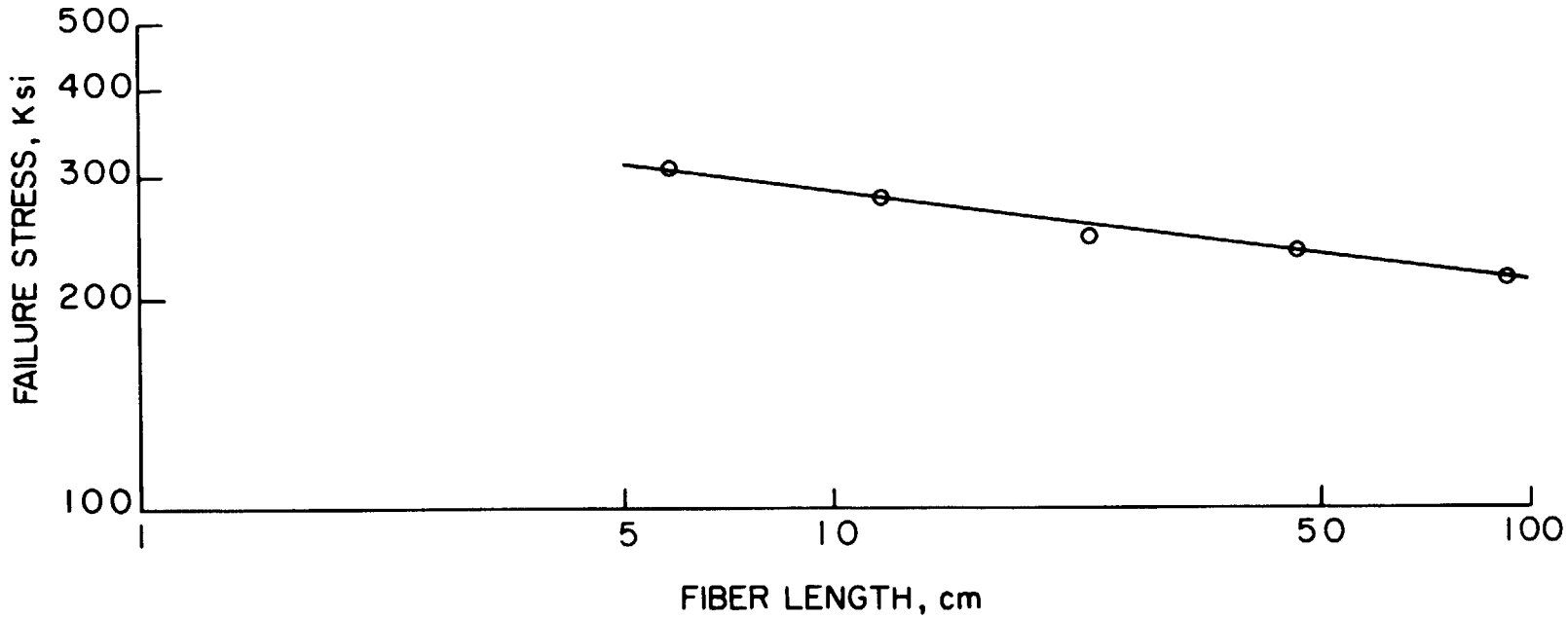

Figure 26. Effect of Length on Mean Fiber Strength [From Data of (21)]

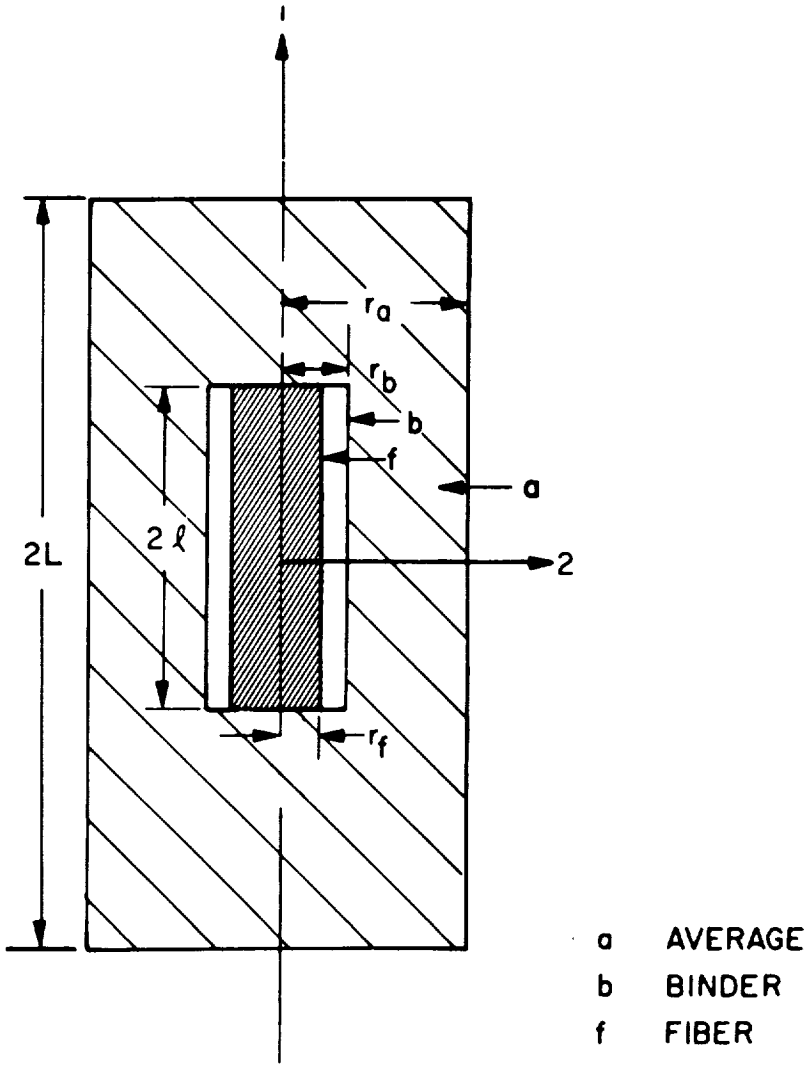

Figure 27. Model for Evaluation of Stresses at Fiber Ends

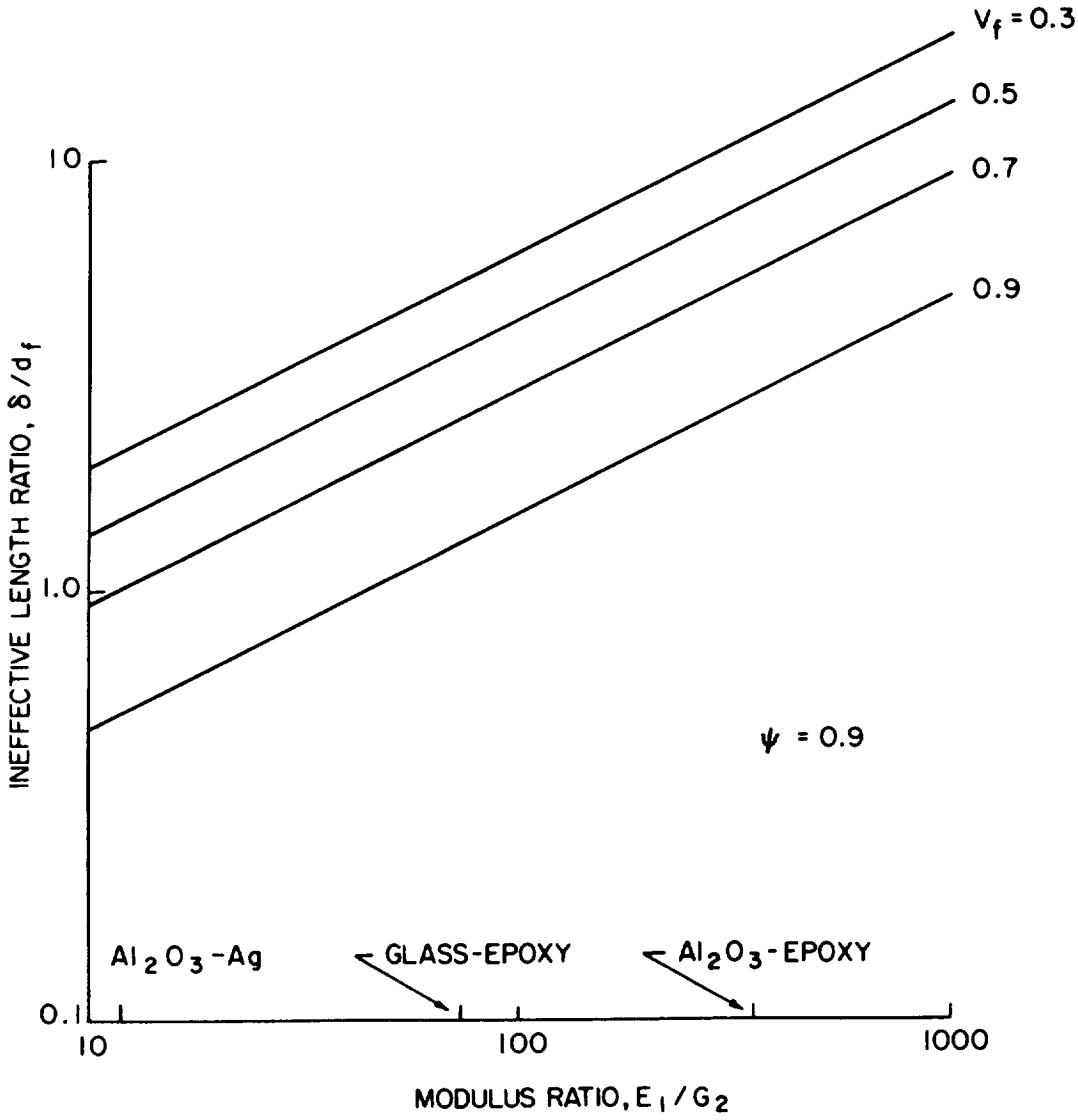

Figure 28. Ineffective Length of Fibers in Composites

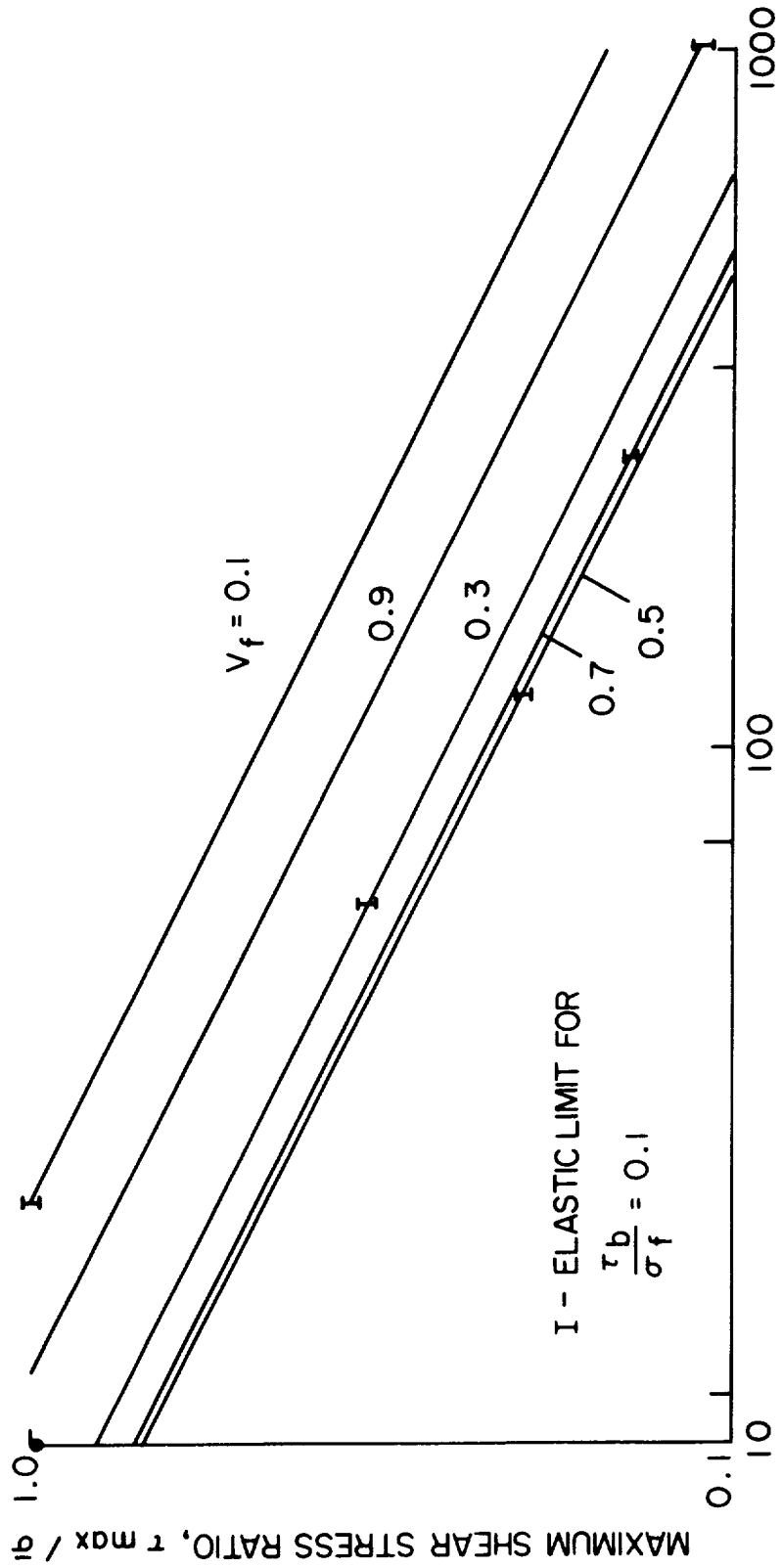

Figure 29. Maximum Fiber-Matrix Interface Shear Stress

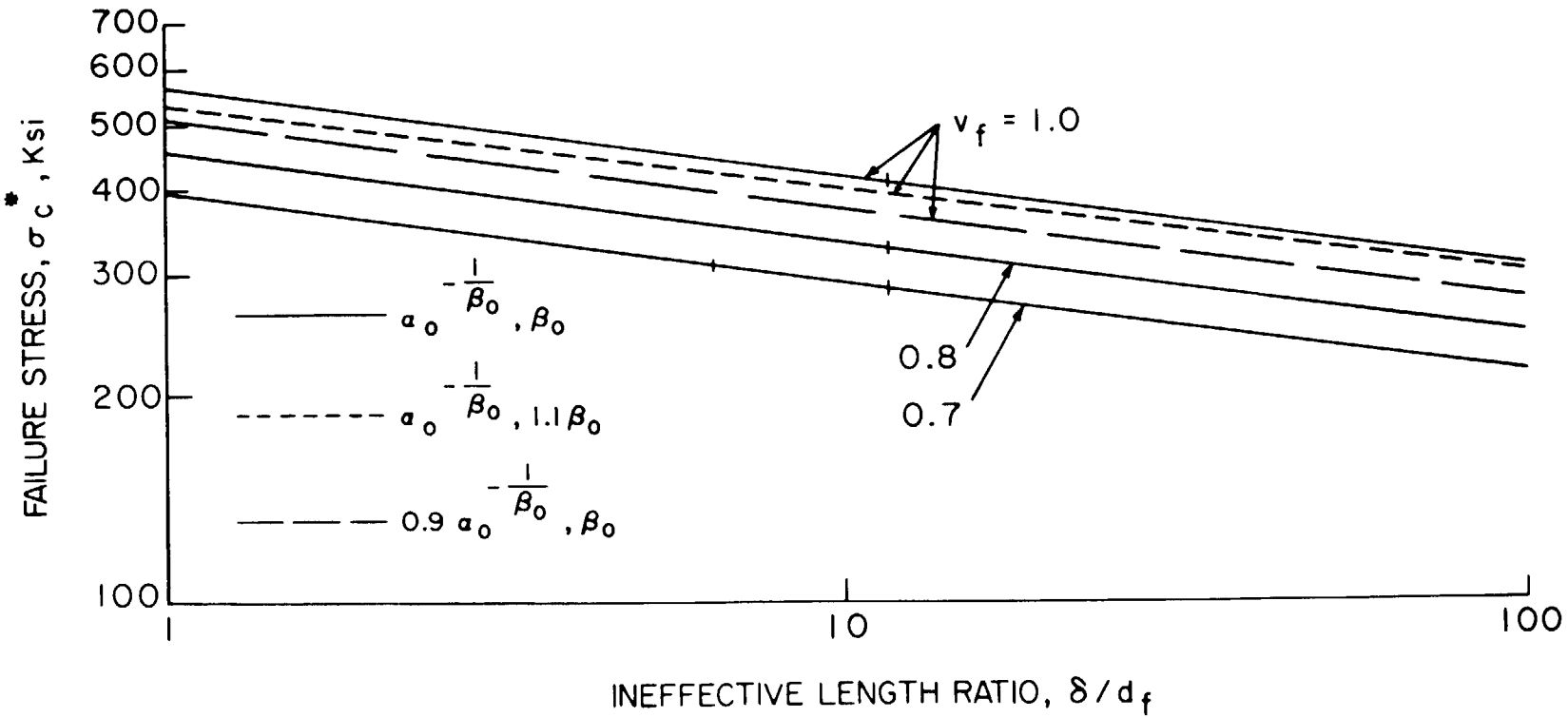

Figure 30. Statistical Mode of Glass Fiber-Plastic Composite Failure Stress

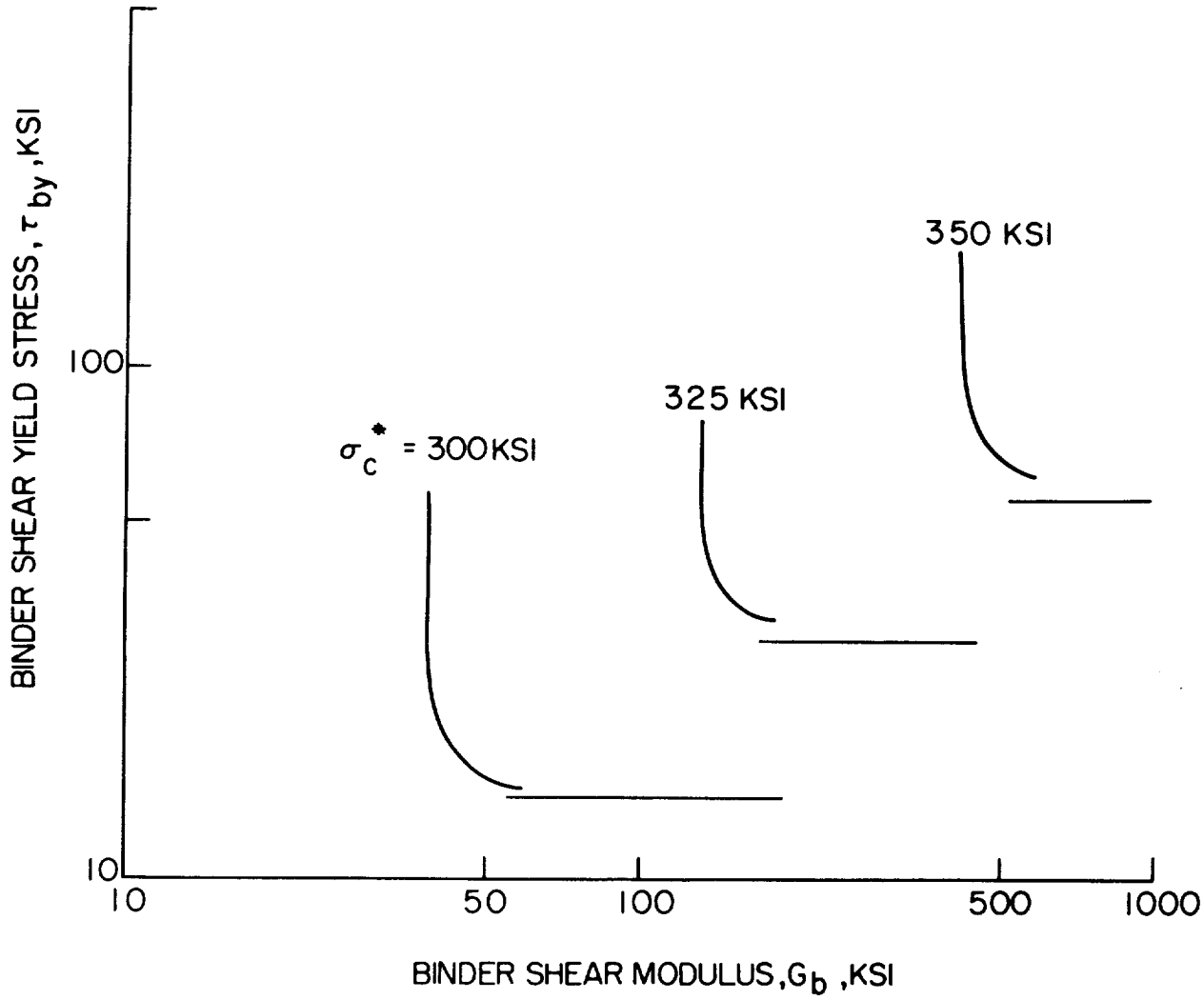

Figure 31. Influence of the Shear Modulus and Shear Yield Stress of an Elastic-Plastic Binder Upon the Strength of a Glass-Fiber Reinforced Composite

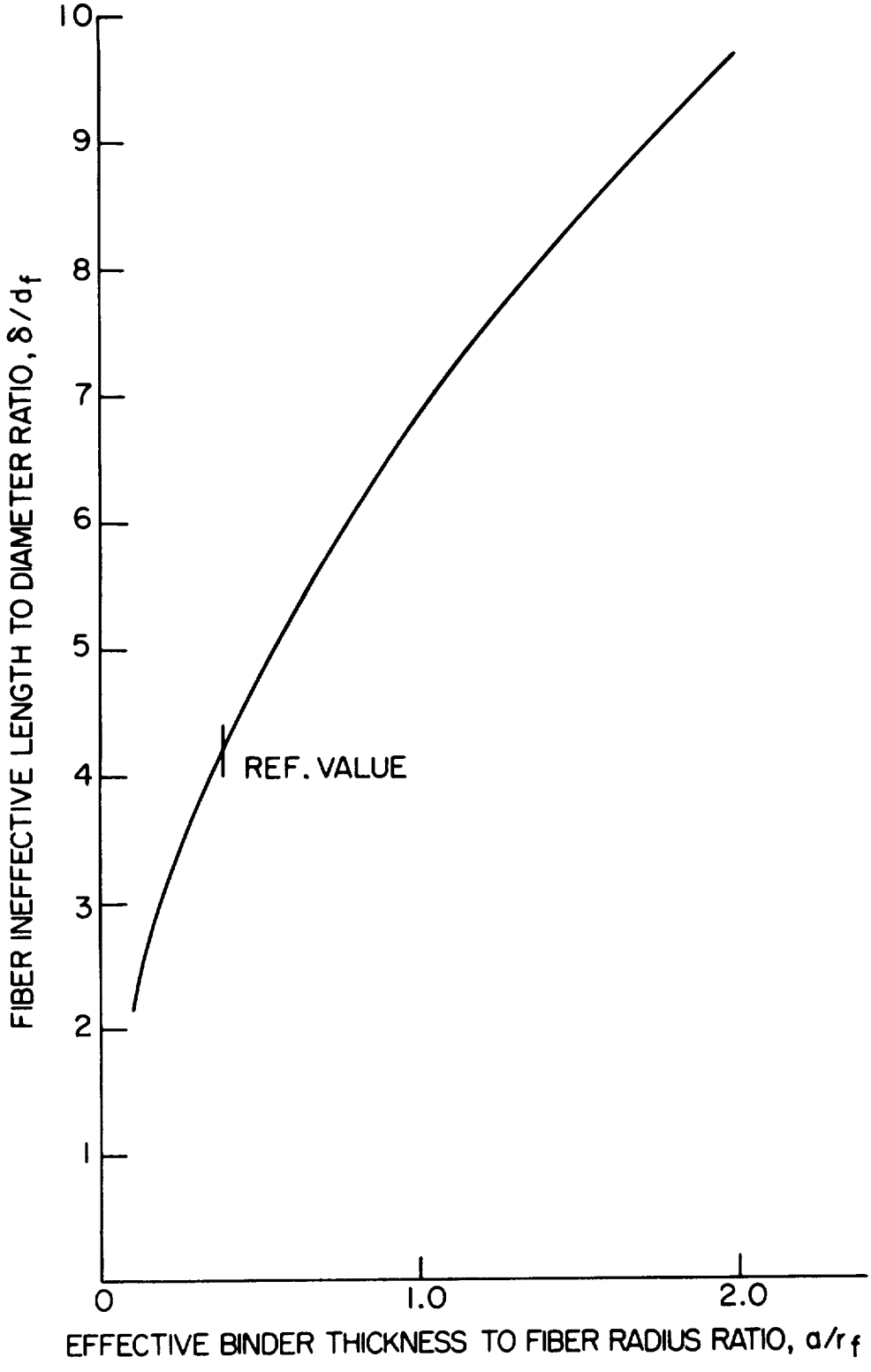

Figure 32. Effect of Volume of Binder Assumed Acting with a Fiber Upon the Fiber Ineffective Length

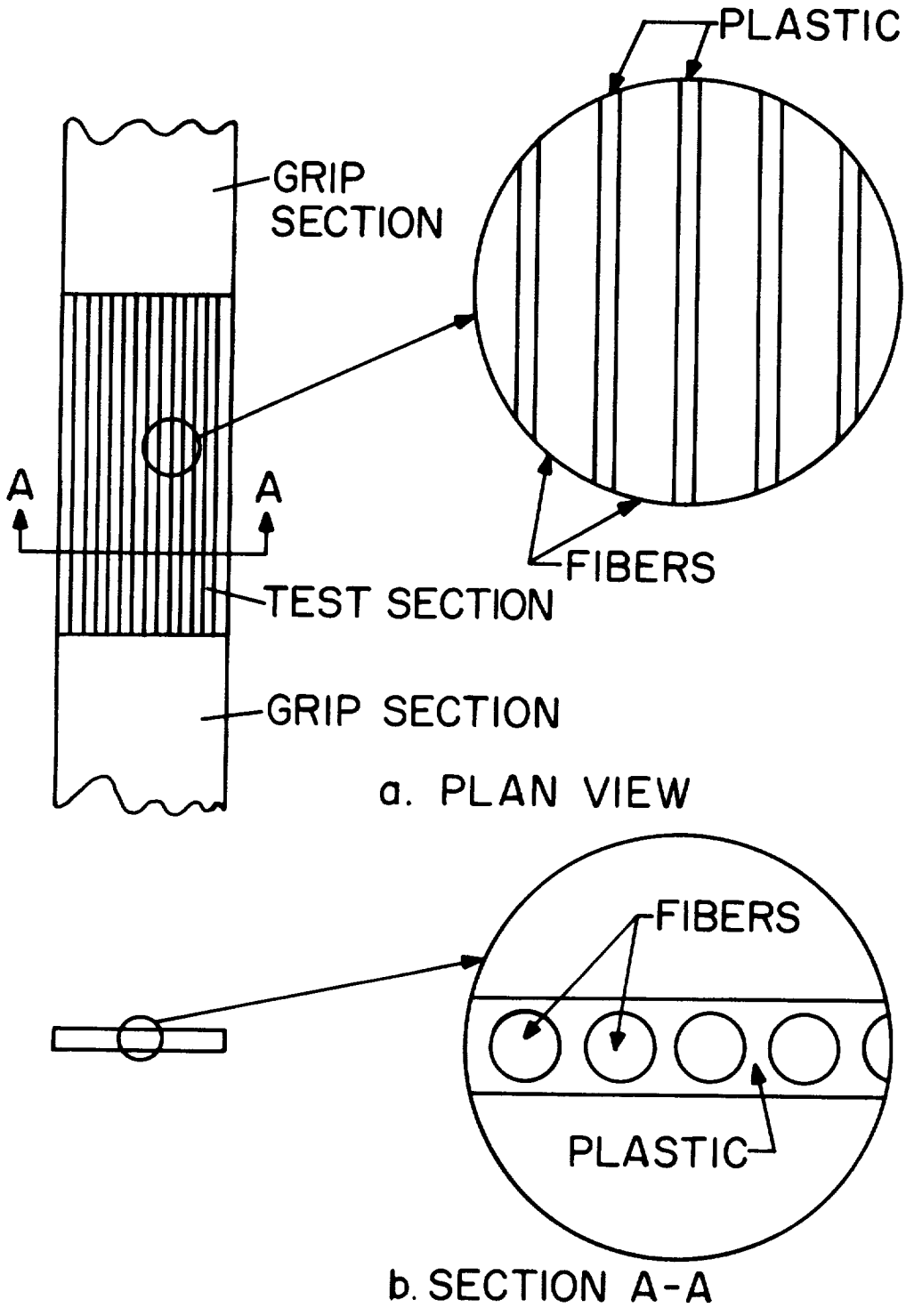

Figure 33. Tensile Failure Test Specimen

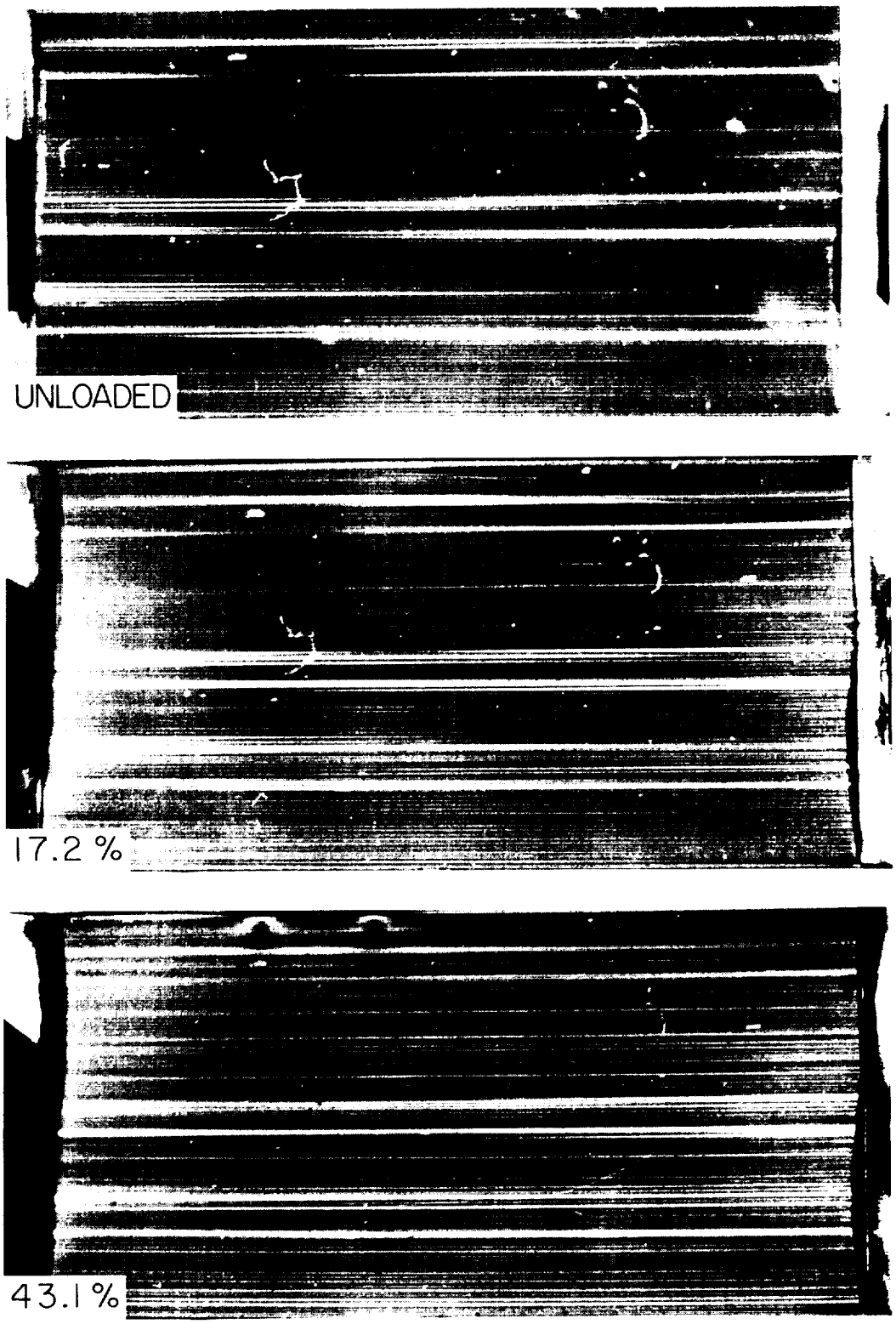

Figure 34a. Typical Sequence of Photographs of Tensile Failure Specimen Showing Distribution of Fiber Breaks Prior to Failure (Specimen A-7)

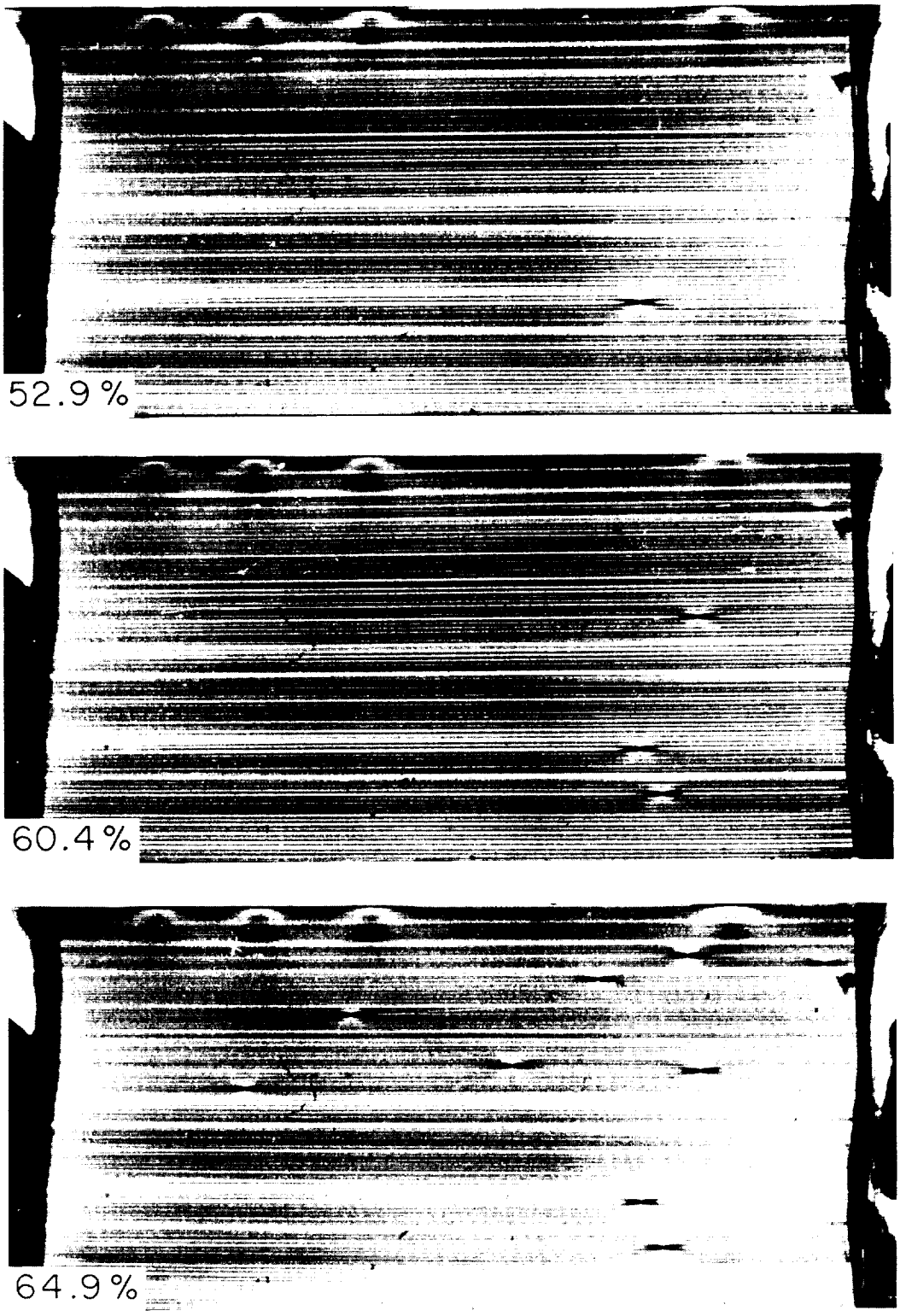

Figure 34b. Typical Sequence of Photographs of Tensile Failure Specimen Showing Distribution of Fiber Breaks Prior to Failure (Specimen A-7)

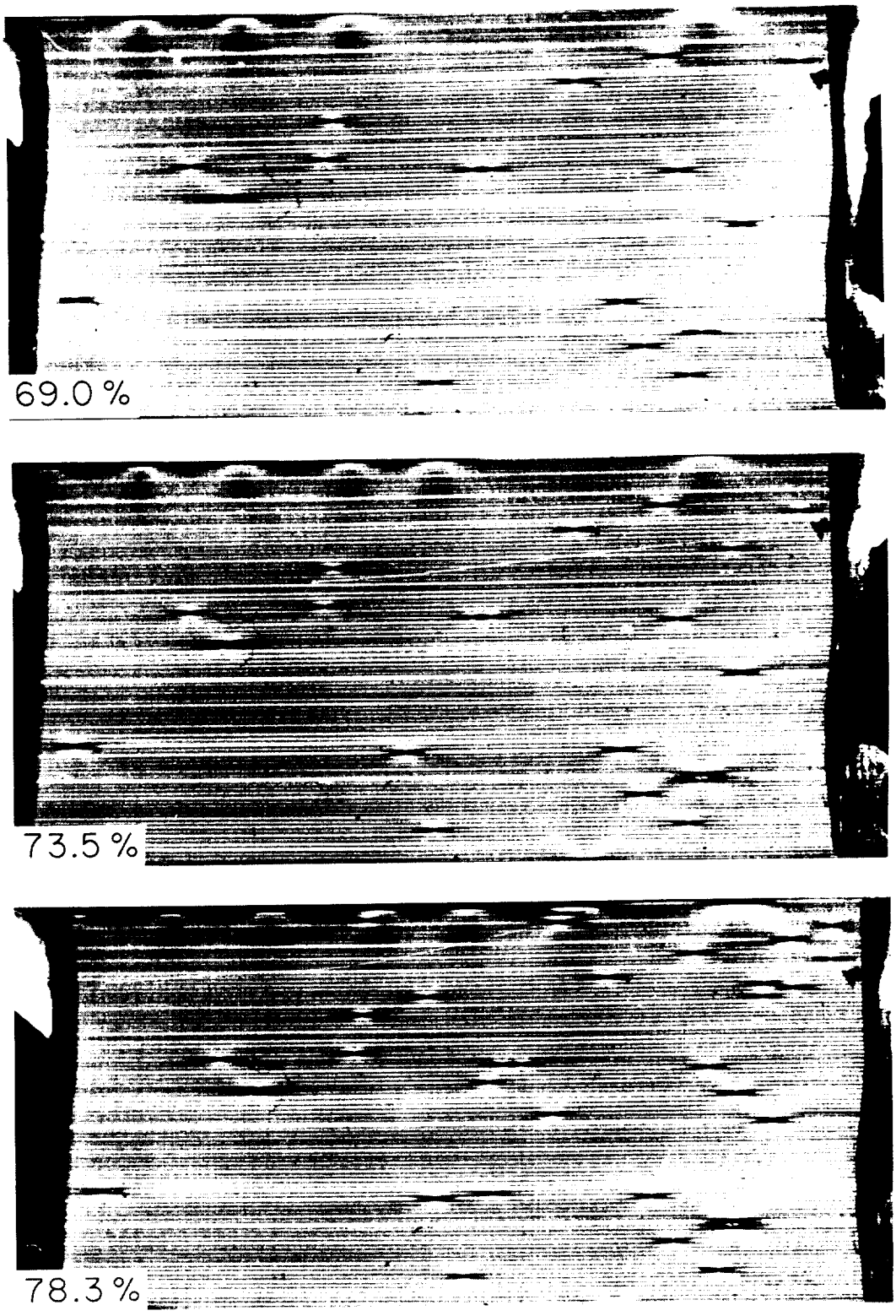

Figure 34c. Typical Sequence of Photographs of Tensile Failure Specimen Showing Distribution of Fiber Breaks Prior to Failure (Specimen A-7)

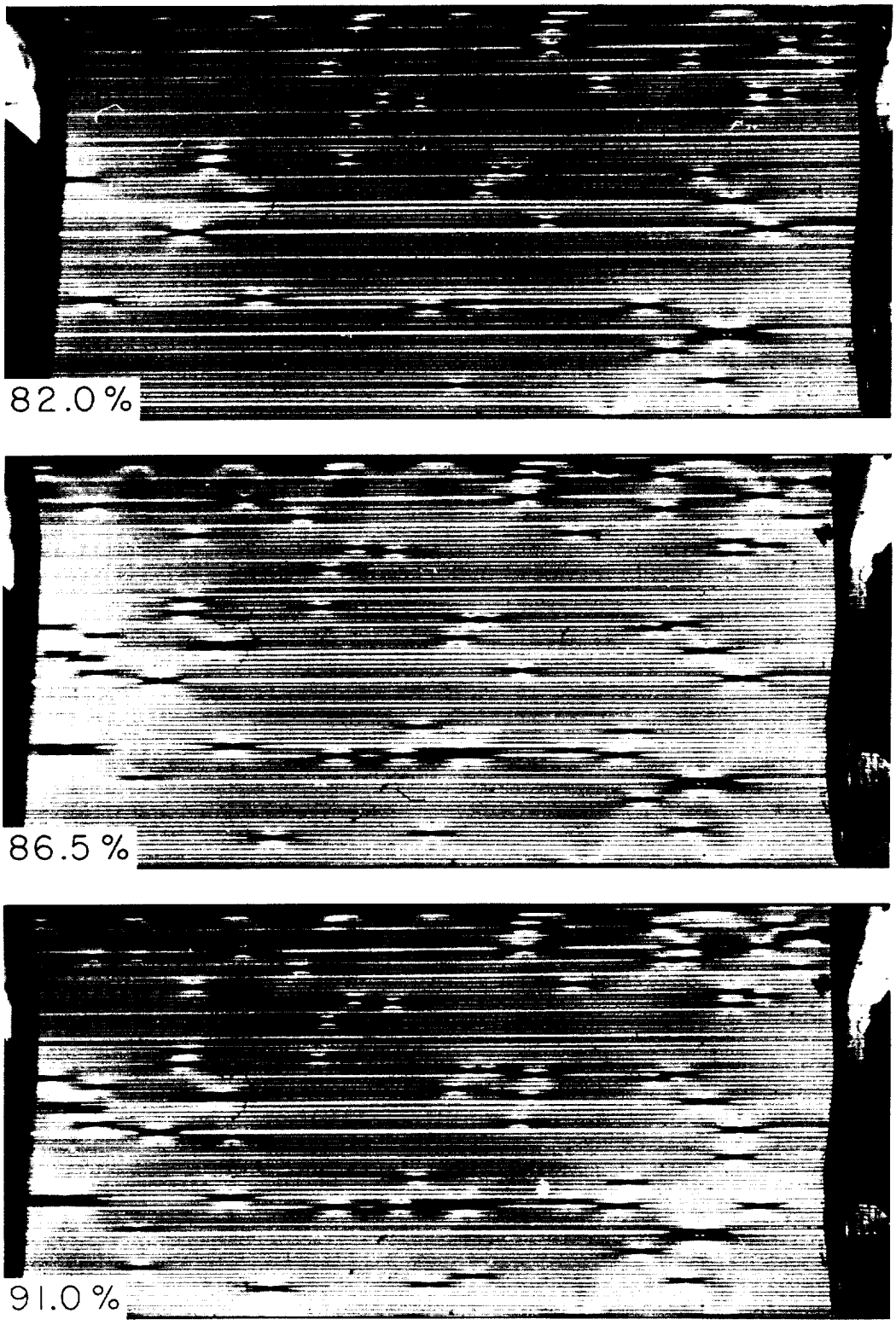

Figure 34d. Typical Sequence of Photographs of Tensile Failure Specimen Showing Distribution of Fiber Breaks Prior to Failure (Specimen A-7)

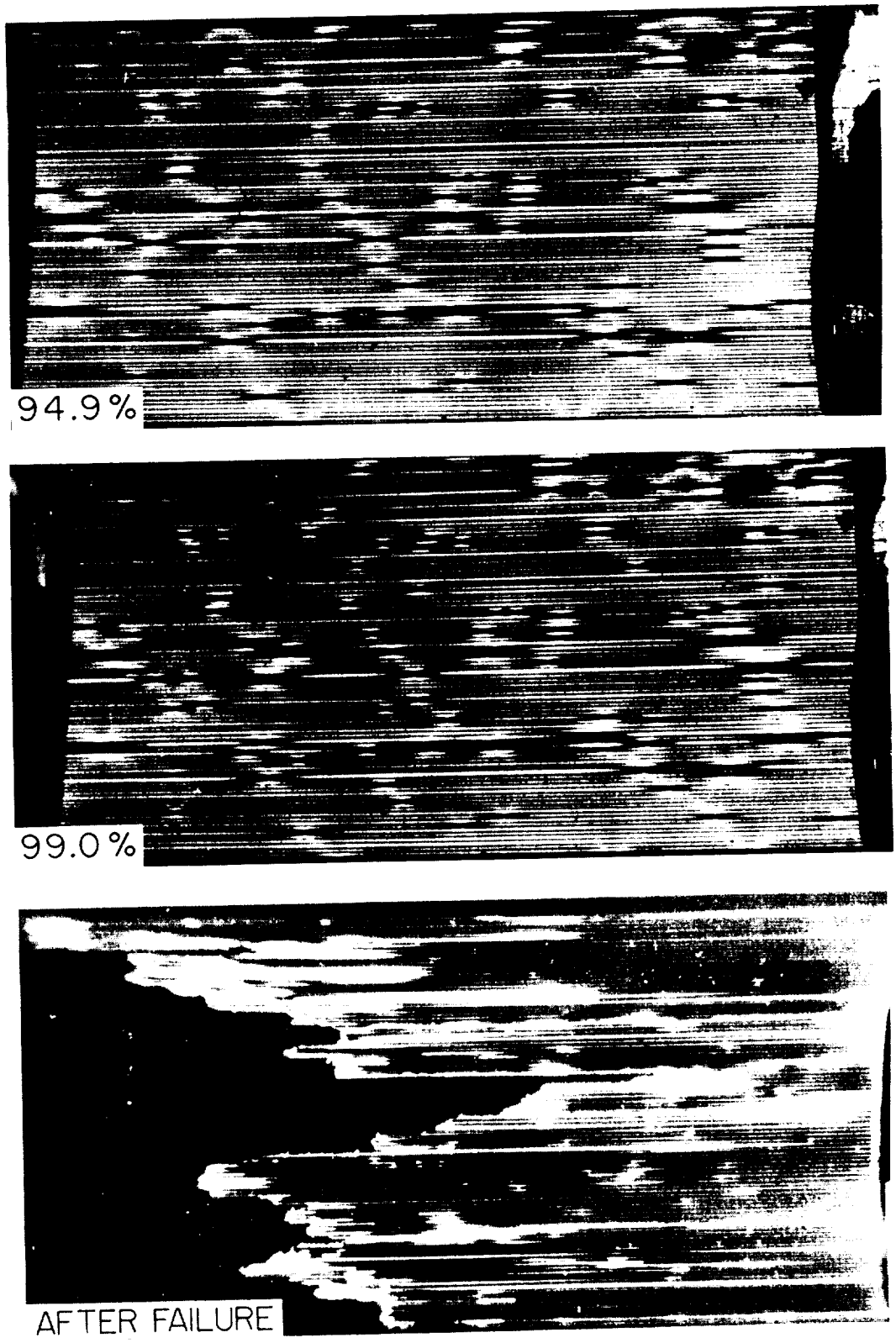

Figure 34e. Typical Sequence of Photographs of Tensile Failure Specimen Showing Distribution of Fiber Breaks Prior to Failure (Specimen A-7)

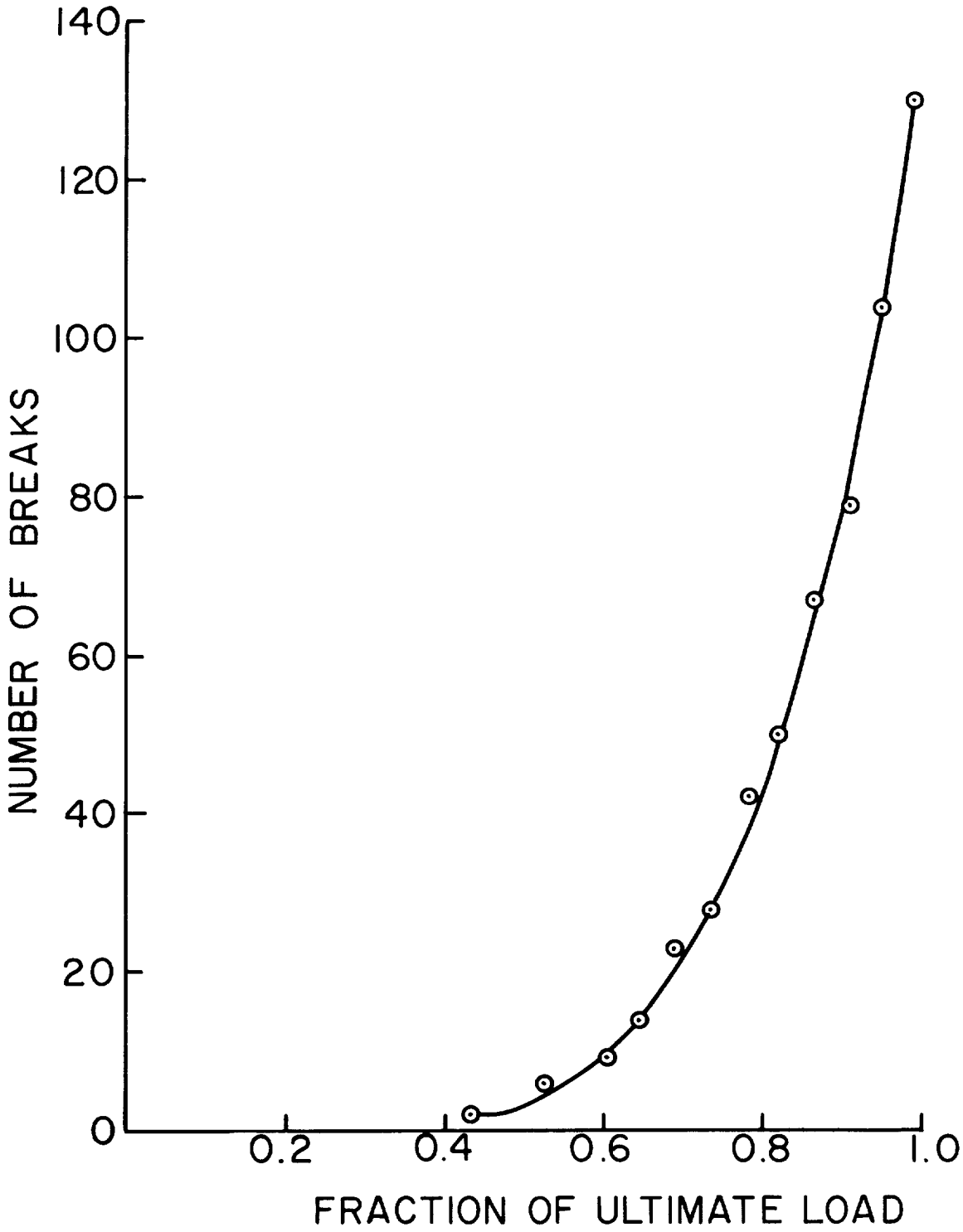

Figure 35. Number of Fiber Breaks in Specimen A-7 as a Function of Applied Load

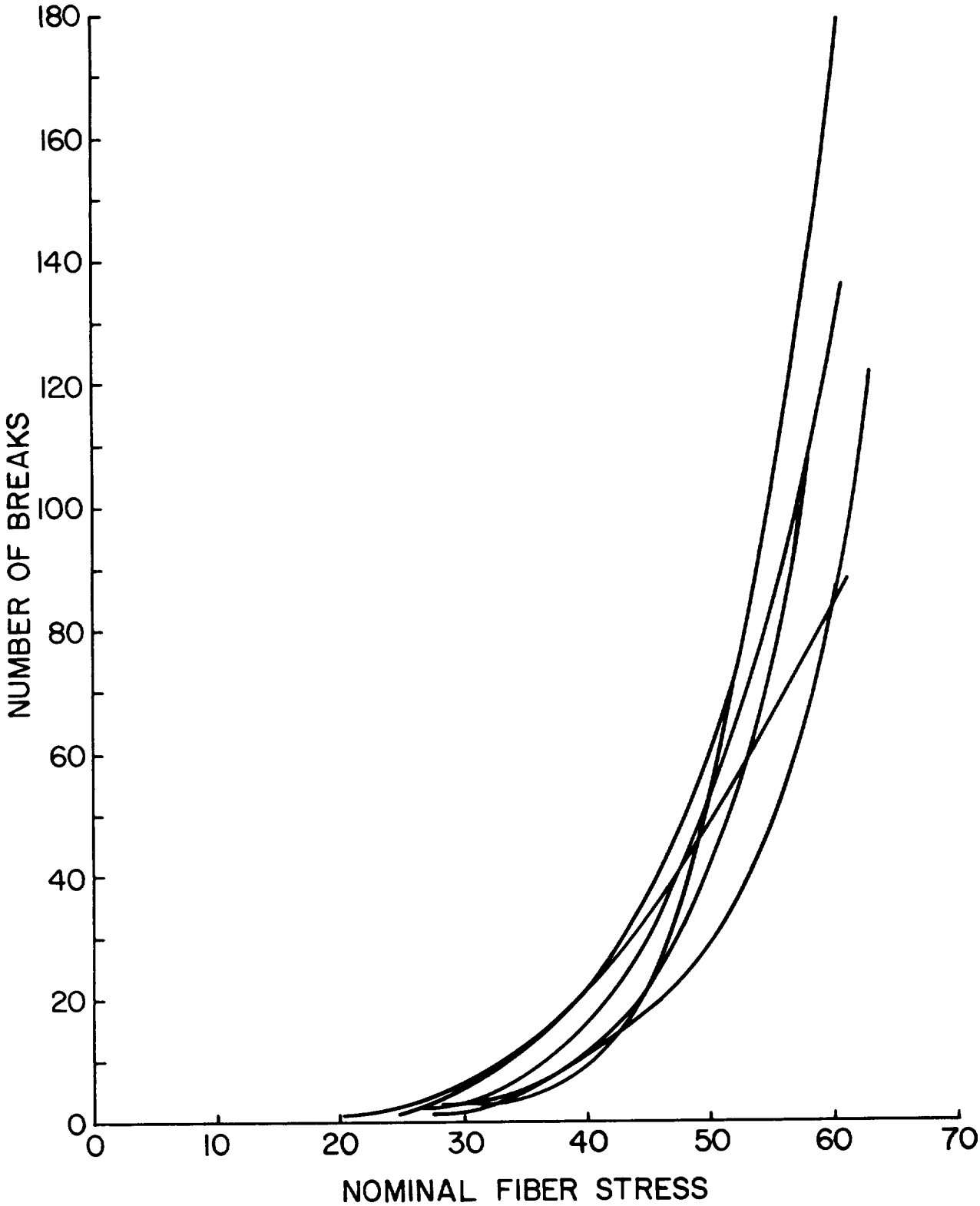

Figure 36. Number of Fiber Breaks as a Function of Nominal Fiber Stress for Series A Specimens

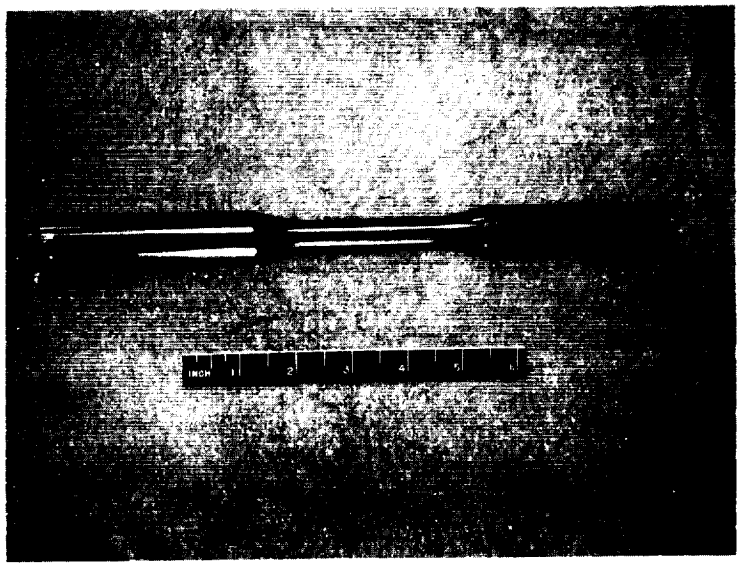

a. Epoxy

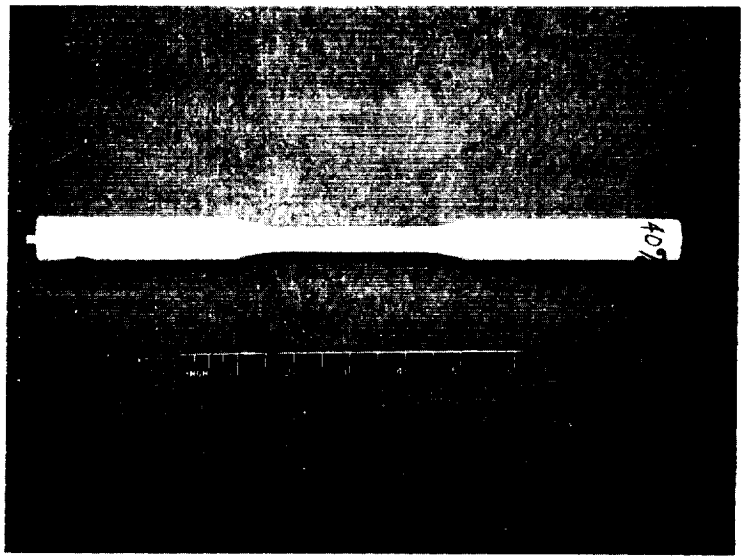

b. Epoxy with alumina particles

Figure 37. Experimental Alumina Particle Tensile Test Specimens

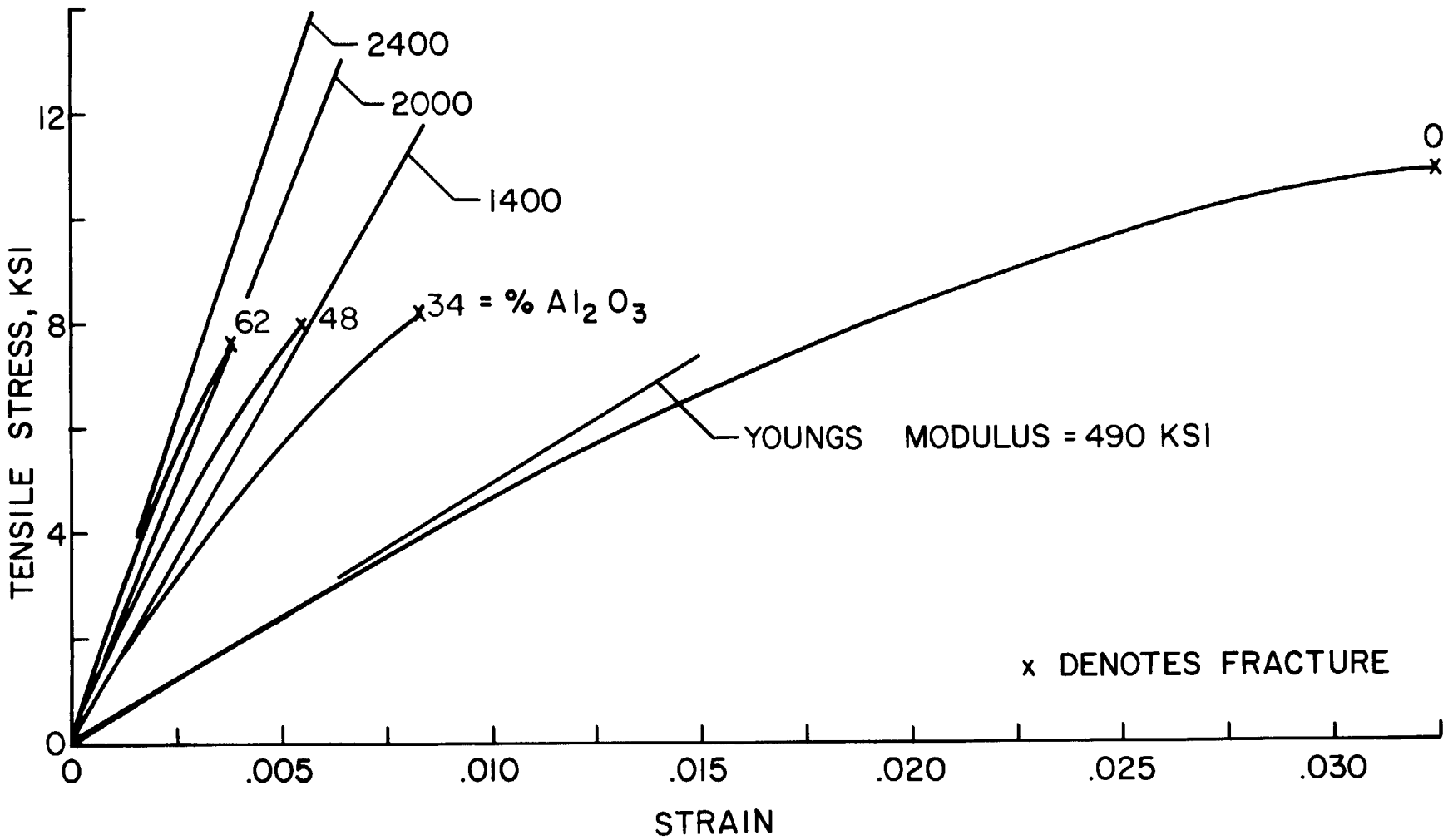

Figure 38. Stress-Strain Characteristics of Epoxy Resin Filled With Various Percentages of Al_2O_3 Powder

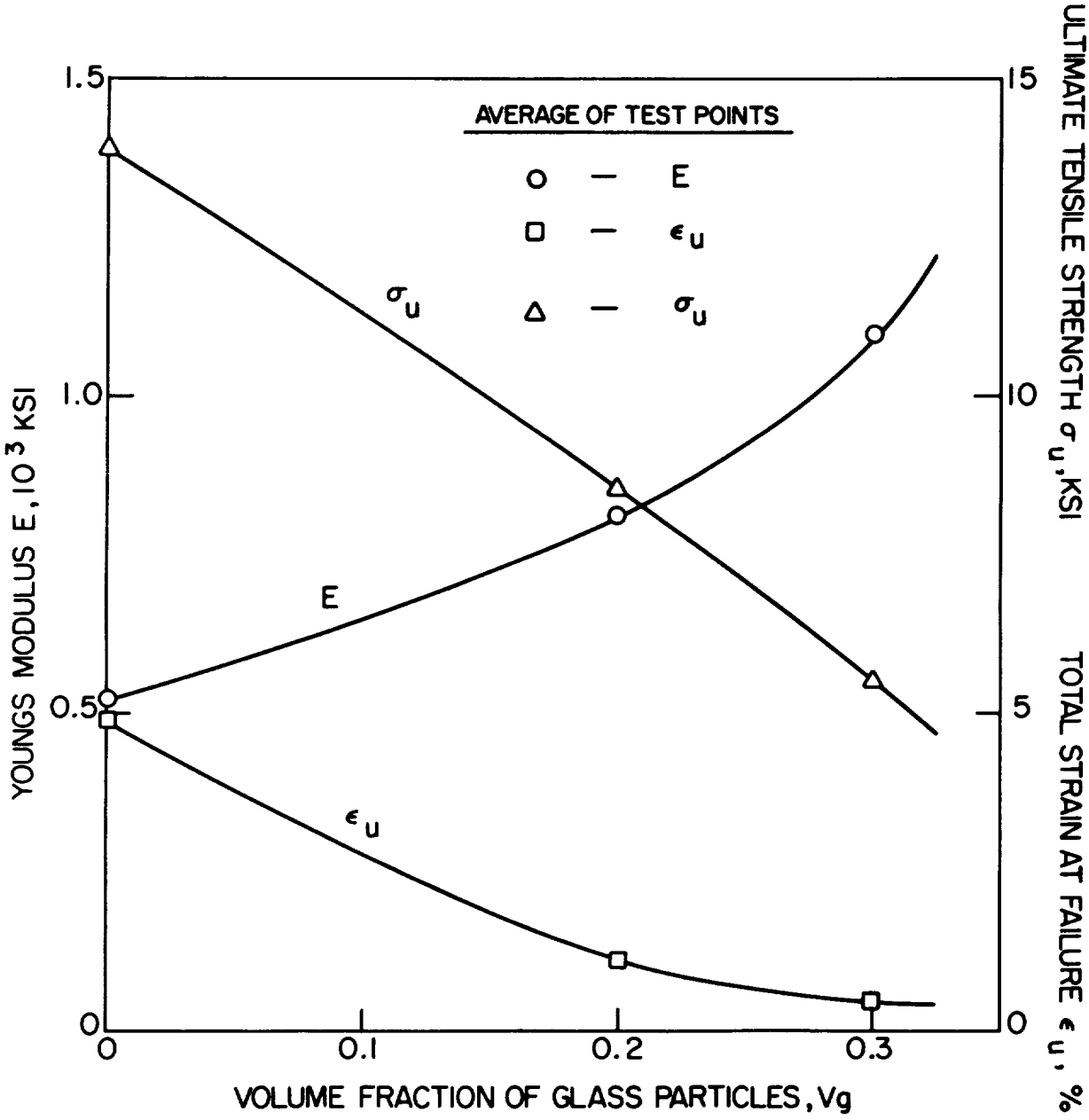

Figure 39. Tensile Properties of Glass Particle Reinforced Plastic Composites

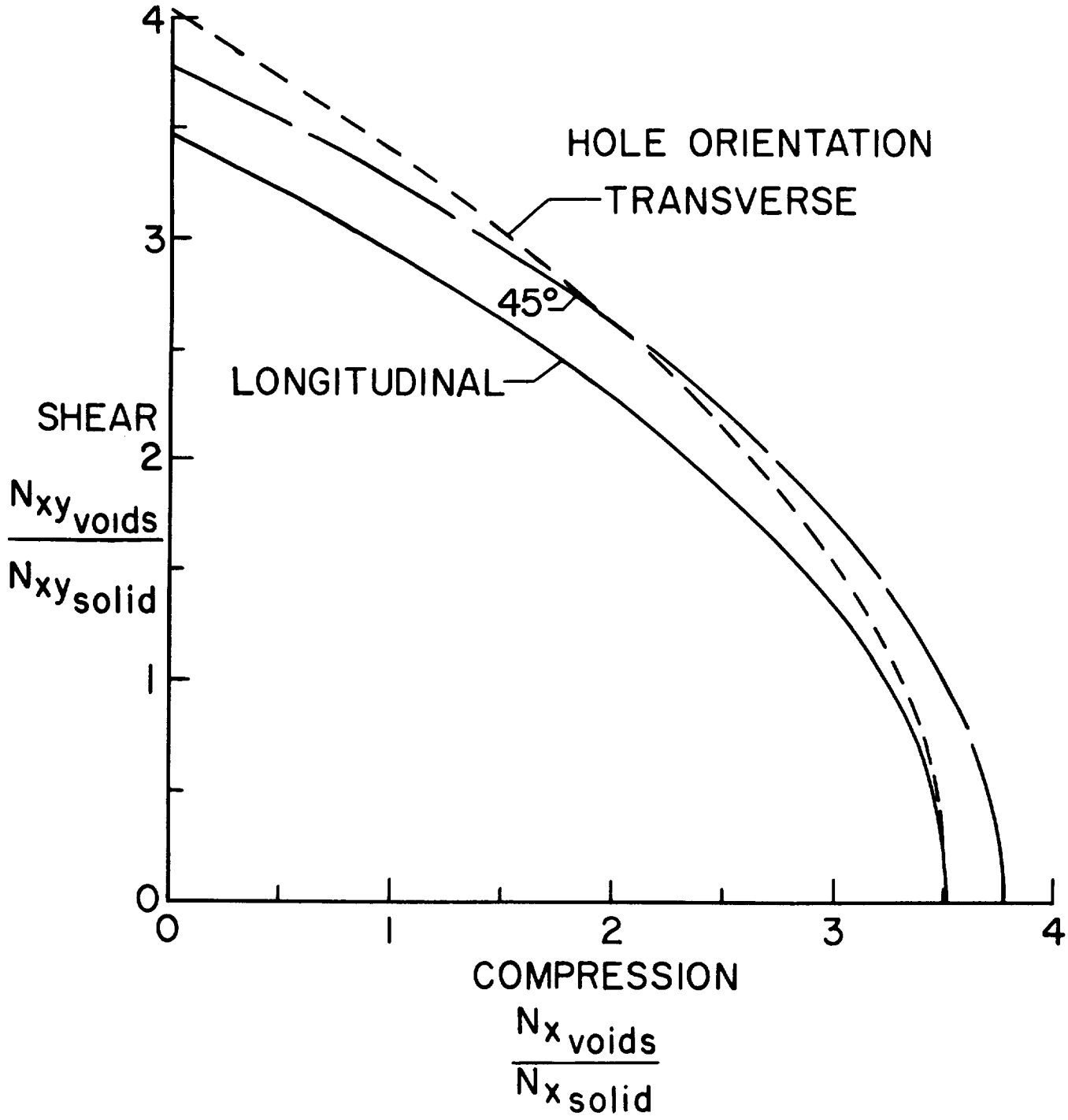

Figure 40. Normalized Interaction Curves for Buckling of Infinitely Long, Simply Supported Flat Plates of 40% Oriented Voids Under Combined Compressions and Shear

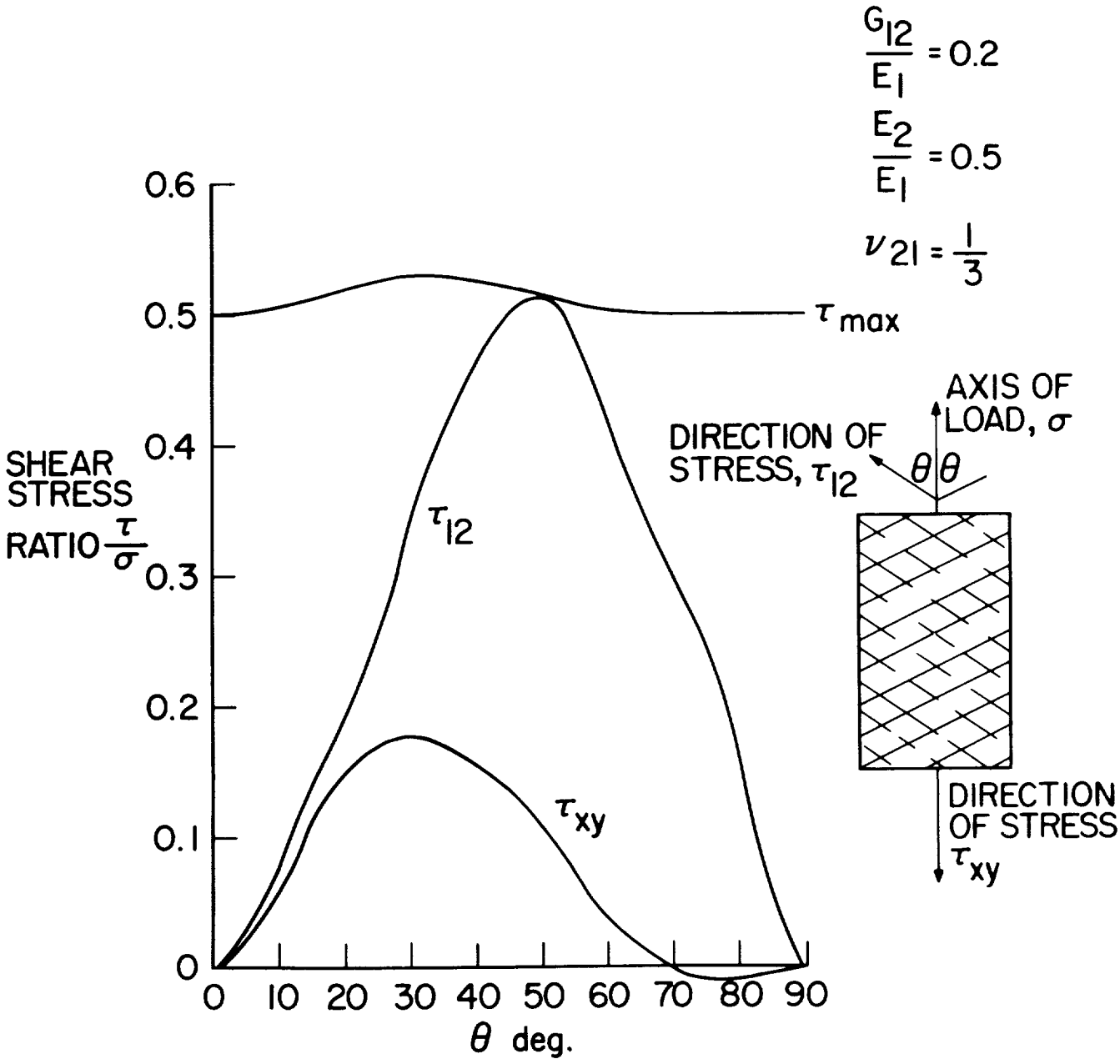

Figure 41. Shear Stresses in Biaxially Stiffened, Filament-Matrix Composites

a. Effect of geometry

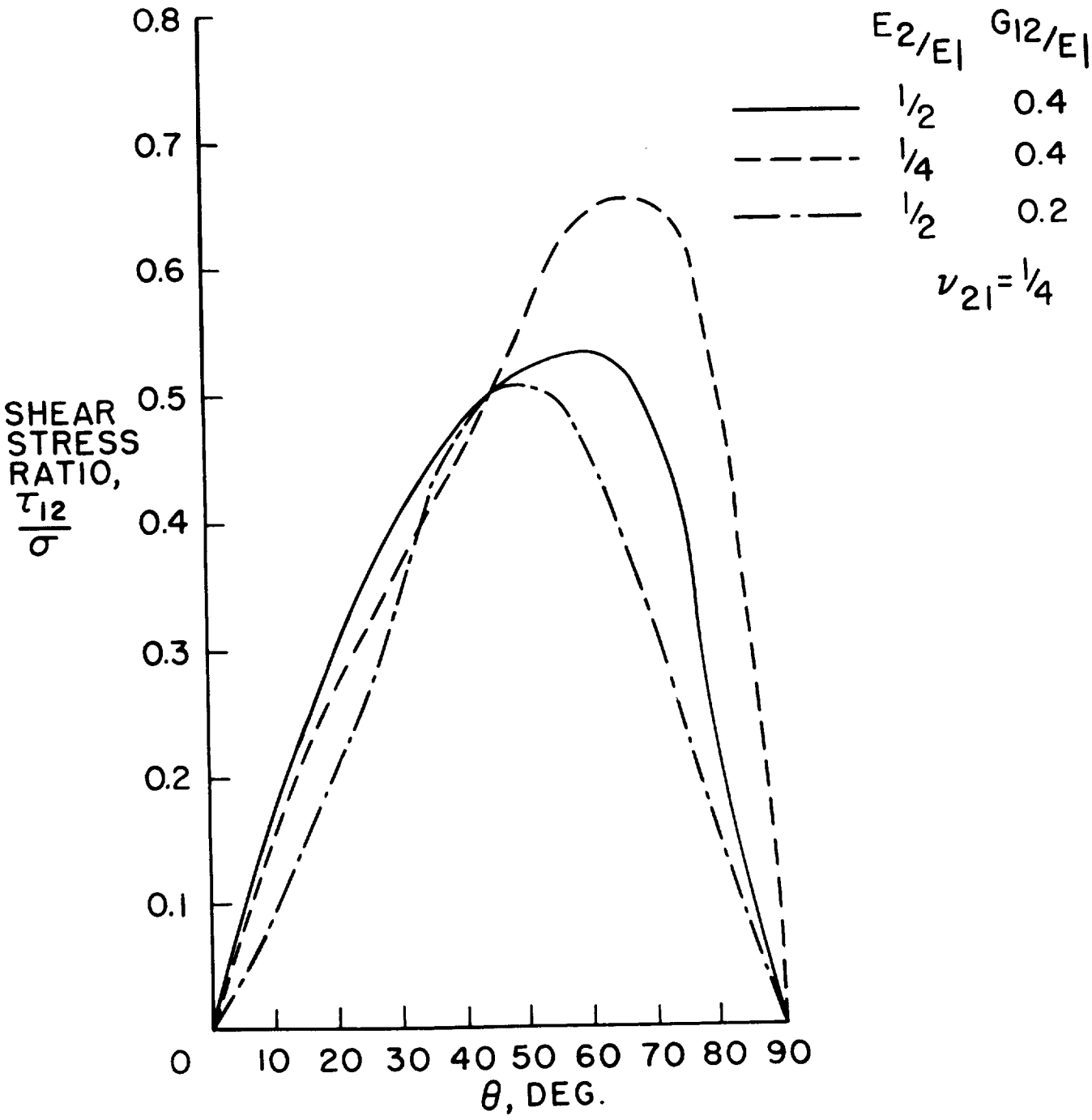

Figure 41. Shear Stresses in Biaxially Stiffened, Filament-Matrix Composites

b. Effect of lamina properties